Management of Natural Resources
in the Coastal Zone of Soc Trang Province

Current and Erosion Modelling Survey

Thorsten Albers and Nicole von Lieberman

giz
COOPERATION
FEDERAL REPUBLIC OF GERMANY
SOCIALIST REPUBLIC OF VIETNAM
Soc Trang Provincial
People's Committee

Published by
Deutsche Gesellschaft für
Internationale Zusammenarbeit (GIZ) GmbH
Management of Natural Resources in the Coastal Zone
of Soc Trang Province

Authors
Thorsten Albers and Nicole von Lieberman

Cover photo
Erosion in Vinh Tan, K. Schmitt 2010

Current and Erosion Modelling Survey

Thorsten Albers and Nicole von Lieberman

January 2011

About GIZ

Broad-based expertise for sustainable development – under one roof

Working efficiently, effectively and in a spirit of partnership, we support people and societies in developing, transition and industrialised countries in shaping their own futures and improving living conditions. This is what the Deutsche Gesellschaft für Internationale Zusammenarbeit (GIZ) is all about. Established on 1 January 2011, it brings together under one roof the long-standing expertise of the Deutscher Entwicklungsdienst (DED) gGmbH (German development service), the Deutsche Gesellschaft für Technische Zusammenarbeit (GTZ) GmbH (German technical cooperation) and InWEnt – Capacity Building International, Germany. As a federally owned enterprise, we support the German Government in achieving its objectives in the field of international cooperation for sustainable development. We are also engaged in international education work around the globe.

Making development effective

Our partners want to take responsibility for achieving their own long-term development goals. We support them by offering demand-driven, tailor-made and effective services for sustainable development. We apply a holistic and value-based approach to ensure the participation of all stakeholders. In doing so, we are always guided by our concept of sustainable development. We take account of political, economic, social and ecological dimensions as we support our partners at local, regional, national and international level in negotiating solutions in the broader social context. This is how we drive development.

GIZ operates in many fields, including economic development and employment; governance and democracy; security, reconstruction, peace building and civil conflict transformation; food security, health and basic education; and environmental protection, resource conservation and climate change mitigation. We also provide management and logistical services to help our partners perform their development tasks. In crises we carry out refugee and emergency aid programmes. As part of our development services, we also second technical advisors to partner countries.

We advise our clients and partners on drawing up plans and strategies, place integrated experts and returning experts in partner countries, and promote networking and dialogue among international cooperation actors. Capacity building for partner-country experts is a key component of our services, and we offer our programme participants diverse opportunities to use the contacts they have made. We also give young people a chance to gain professional experience around the world – exchange programmes for young professionals lay the foundations for successful careers in national and international markets.

Who we work for

Most of our activities are commissioned by the German Federal Ministry for Economic Cooperation and Development (BMZ). GIZ also operates on behalf of other German ministries – in particular the Federal Foreign Office, the Federal Environment Ministry and the Federal Ministry of Education and Research – as well as German federal states and municipalities, and public and private sector clients both in Germany and abroad. These include the governments of other countries, the European Commission, the United Nations and the World Bank. We work closely with the private sector and promote results-oriented interaction between the development and foreign trade sectors. Our considerable experience with alliances in partner countries and in Germany is a key factor for successful international cooperation, not only in the business, academic and cultural spheres but also in civil society.

The company at a glance

GIZ operates in more than 130 countries worldwide. In Germany we maintain a presence in nearly all the federal states. Our registered offices are in Bonn and Eschborn. GIZ employs approximately 17,000 staff members worldwide, more than 60 % of whom are local personnel. In addition, there are 1,135 technical advisors, 750 integrated and 324 returning experts, 700 local experts in partner organisations and 850 ‘weltwärts’ volunteers. With an estimated turnover of EUR 1.9 billion as at December 2010, GIZ can look to the future with confidence.

Foreword

Shoreline changes along the coast of Soc Trang Province (Mekong Delta, Viet Nam) are the result of natural processes of erosion and accretion. In some areas, loss of land as a result of erosion of up to 30 m per year has been recorded, while in other areas land created through accretion can grow by more than 60 m per year.

Since 1993 more than 3,000 ha of mangroves have been planted along the coast of Soc Trang with the aim of protecting the sea dyke and coast from erosion, and the land from storms. But in areas of high erosion energy, some of the forests have been completely destroyed. As a result, the earth dyke, which protects the hinterland from flooding, is endangered in several places by severe erosion, which in turn endangers the people and farmland directly behind the dyke.

Mangroves grow along sheltered tropical and sub-tropical coastlines. They do not grow naturally on sites with strong erosion. In such sites where bioshields (a protective mangrove forest belt) are not feasible or sufficiently effective, other forms of coastal protection, including hard solutions and a combination of hard and 'soft' solutions must be put in place.

The project "Management of Natural Resources in the Coastal Zone of Soc Trang Province" has therefore decided to set up an erosion control model, which combines breakwaters and mangroves (i.e. hard and 'soft' solutions). The area selected is in Vinh Tan Commune, on a site subjected to more than 20 m of erosion per year.

Along such a highly dynamic coastline with strong long-shore currents it is essential to understand that, if erosion control measures are inappropriate; improperly designed, built, or maintained; or if the effects on adjacent shores are not carefully evaluated, such measures will worsen rather than improve the erosion problem.

The GIZ project has therefore commissioned a study to design wave-breaking barriers according to computer-based current and erosion modelling with the aim of reducing erosion and stimulating sedimentation in the target site and, as far as possible, avoid downdrift erosion.

This study was carried out by the Institute of River and Coastal Engineering (Hamburg University of Technology, Germany) and the Southern Institute of Water Resources Research (Ho Chi Minh City, Viet Nam). The results of the modelling and the recommendations for the erosion control measures in Vinh Tan are presented in this report.

This model for coastal erosion protection and climate change adaptation in erosion sites is suitable for wider application in the Mekong Delta and along other sites in Viet Nam where mangroves occur naturally.

Klaus Schmitt

Chief Technical Advisor

Table of contents

List of figures

List of tables

1 Introduction

A dynamic process of accretion and erosion occurs along the coastline of Soc Trang Province, influenced by interaction between the discharge regime of the Mekong Delta, the tidal regime of the South China Sea (called East Sea in Vietnam), and the monsoon weather patterns of Southeast Asia. In some areas, such as the focus area of Vinh Tan Commune, severe erosion endangers dykes and, consequently, the people and farmland located behind those dykes.

The causes of erosion in the focus area of Vinh Tan have not been completely analysed yet.

However, the interaction between the following factors is known to affect the shoreline:

- Low sediment supply
- Exposed coastline with a dominating long-shore component, especially during the northeast monsoon
- Erosion by tidal currents and waves
- Past anthropogenic influences

Once the equilibrium of a coastal section is disturbed and erosion has started, it is very difficult to stop the progress without any appropriate countermeasures. Within the project framework, the coastal processes in the investigation area were examined, and specific erosion protection measures were developed for the focus area.

In collaboration with the Southern Institute of Water Resources Research (SIWRR), available data with relevance to the coast of Soc Trang were researched and analysed. Although data on the bathymetry, water levels, river discharges and sediment freights were available, essential data about the erosion site, especially about the wave climate, were missing. Therefore, a concept was developed to close this gap and build the foundation for sophisticated and effective erosion protection measures.

The available and generated database was used to setup, calibrate and verify different numerical models. Shoreline changes were computed considering various erosion protection measures. Besides conventional techniques, an alternative approach using local materials was investigated.

Figure 1 shows the design process of the erosion protection, which is based on wave modelling and morphodynamic modelling, as well as data analysis of available data and field measurements. Additional physical tests in a wave flume completed the design.

The numerical modelling was done in three steps. First, a wave model computed important input parameters for the design. It was coupled with the hydrodynamic model, which was setup in a larger investigation area between Vung Tau and Ganh Hao and generated input parameters for the morphodynamic model. By the means of this third model, which was setup for the focus area at Vinh Tan, different options of erosion protection were investigated. Available data sets supplemented by specific field measurements were used to setup, calibrate and verify the numerical models.

In conclusion, recommendations for erosion protection measures are given based on the design process containing the model results, the field measurements and a cost analysis.

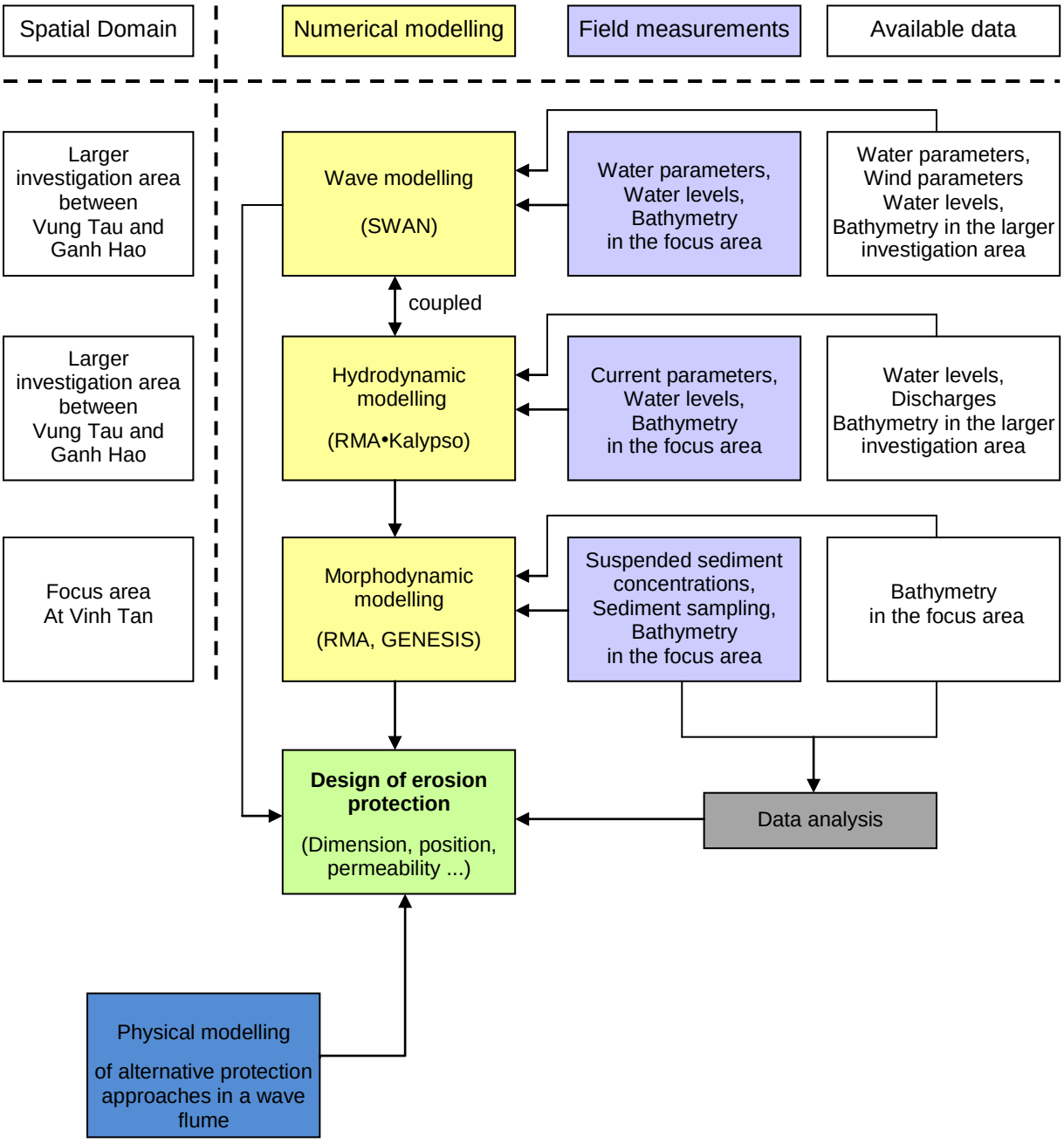

Figure 1: Flow chart of the design process the erosion protection.

2 Investigation area

Figure 2 shows an aerial view of the coast near Vinh Tan including the erosion site in December 2007 (Position: 9°16'46.7'' N; 105°54'55.6'' E). The red line indicates the shoreline in January 2011. Erosion of the flood plains in front of the dyke is clearly visible. At two hot spots the flood plains eroded up to the dyke.

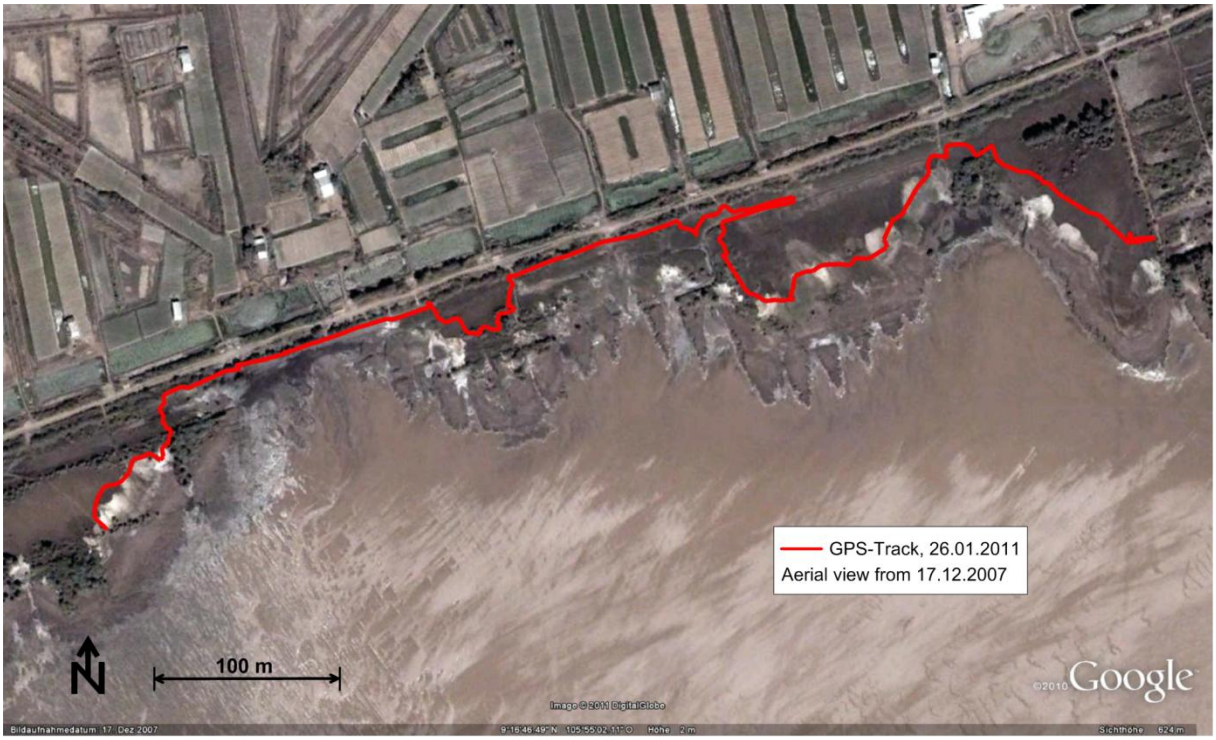

Figure 2: Aerial view of the coast near Vinh Tan including the erosion site in December, 2007.

Figure 3 shows the same area from the ground in January 2010 during low water and high water. This part of the coast is subject to proceeding erosion. The protecting flood plain in front of the dyke disappeared completely. Not only do extreme events lead to further erosion, but also smaller waves during normal tides erode the foreland (Figure 4).

Figure 3: Photo of the Vinh Tan erosion site in January 2010 during low water (left) and high water (right).

Figure 4: Proceeding erosion at the foreland of the dyke.

After failure, parts of the dyke at Vinh Tan were reinforced with a stone revetment. Wooden piles form the toe protection. In July 2010, for a length of approximately 10 - 12 meters, the outer slope of the dyke failed and 0.5 - 0.8 m of stones at the front broke away. On the complete length of this dyke section there was a gap of 0.10 - 0.15 m in the outer slope (Figure 5). Along that gap, the wooden piles that form the toe protection have an inclination towards the sea. The failure of larger parts of the outer slope was most likely to occur, and was finally observed in October 2010 (Annex). According to the information from locals, the damage occurred continuously and was not caused by a single extreme event. Along the outer slope there is a brim with a height of 1.00 - 1.20 m between the top edge of the stone cover (outer slope) and the top ground surface of the mud. Due to proceeding erosion, the anchoring depth of the wooden piles is reduced and the earth pressure of the outer slope exceeds the working load of the wooden piles.

Figure 5: Photo of the improved dyke at Vinh Tan with a gap in the revetment due to further erosion.

To assure the stability of the dyke, erosion protection measures become necessary. The priority of those measures is highest where the protecting floodplain is already completely eroded.

The flood approaches parallel to the southeast coast of Vietnam, from northeast to southwest. This leads to longshore currents, which are increased especially during the northeast monsoon season by strong wind-driven currents (Figure 6).

The sediments in the mouth of the Bassac River are sand dominated, whereas the coasts of Soc Trang and Bac Lieu are dominated by mud (NGUYEN, 2009).

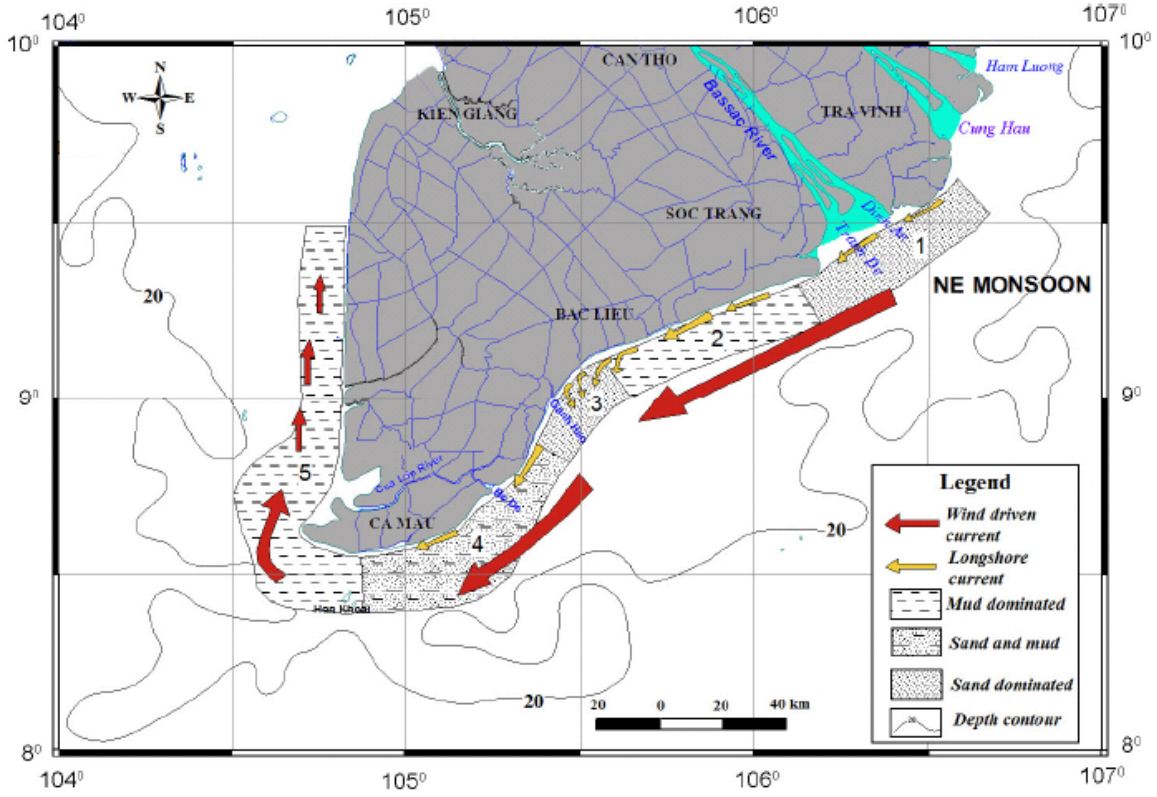

Figure 6: Sediment transport influenced by the northeast monsoon (NGUYEN, 2009).

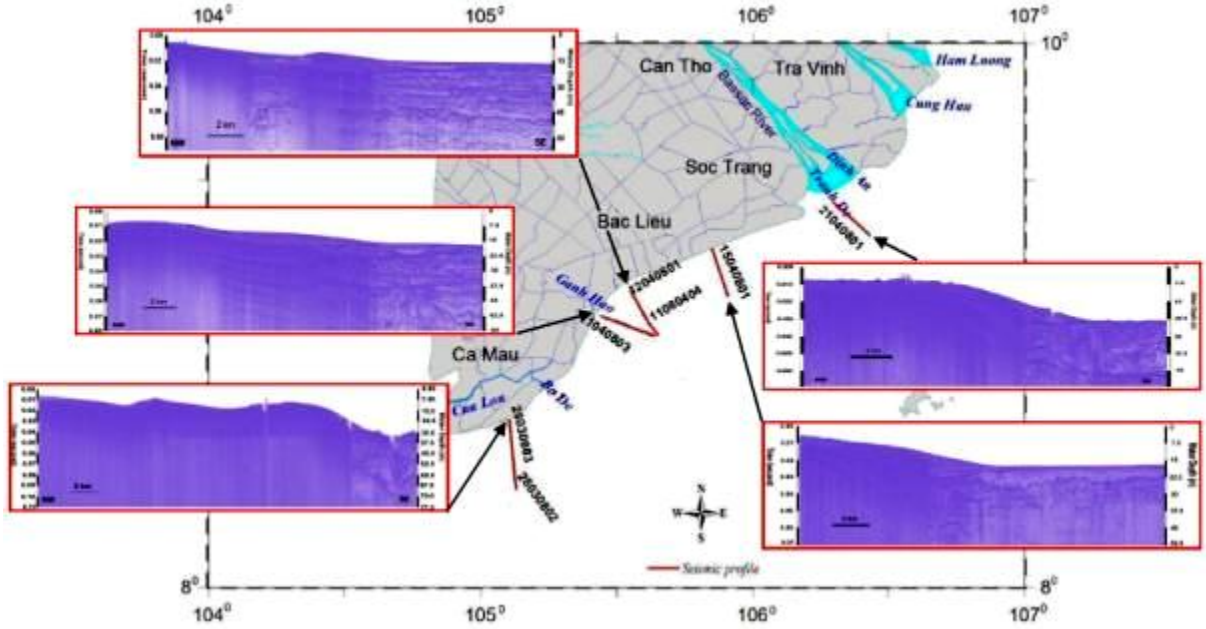

Figure 7: Bathymetric profiles along the southeast coast of Vietnam (NGUYEN, 2009).

Figure 7 shows bathymetric profiles along the southeast coast of Vietnam. In the river mouth of the Bassac, and at the coast of Bac Lieu, wide areas with relatively high bottom elevations form a natural protection for the coast. At the coast of Soc Trang, this basement, which decreases wave energy, is missing, and water depths increase faster with increasing distances to the shoreline.

In collaboration with the Southern Institute of Water Resources Research, available data with relevance for the coast of Soc Trang were researched and analysed. Figure 8 shows a map of South Vietnam with various gauges in the extended investigation area (in red). Data of those stations are used to control the numerical model. The erosion site at Vinh Tan is indicated in black, while the wave stations on the island Con Dao and the oilrig Bach Ho in yellow.

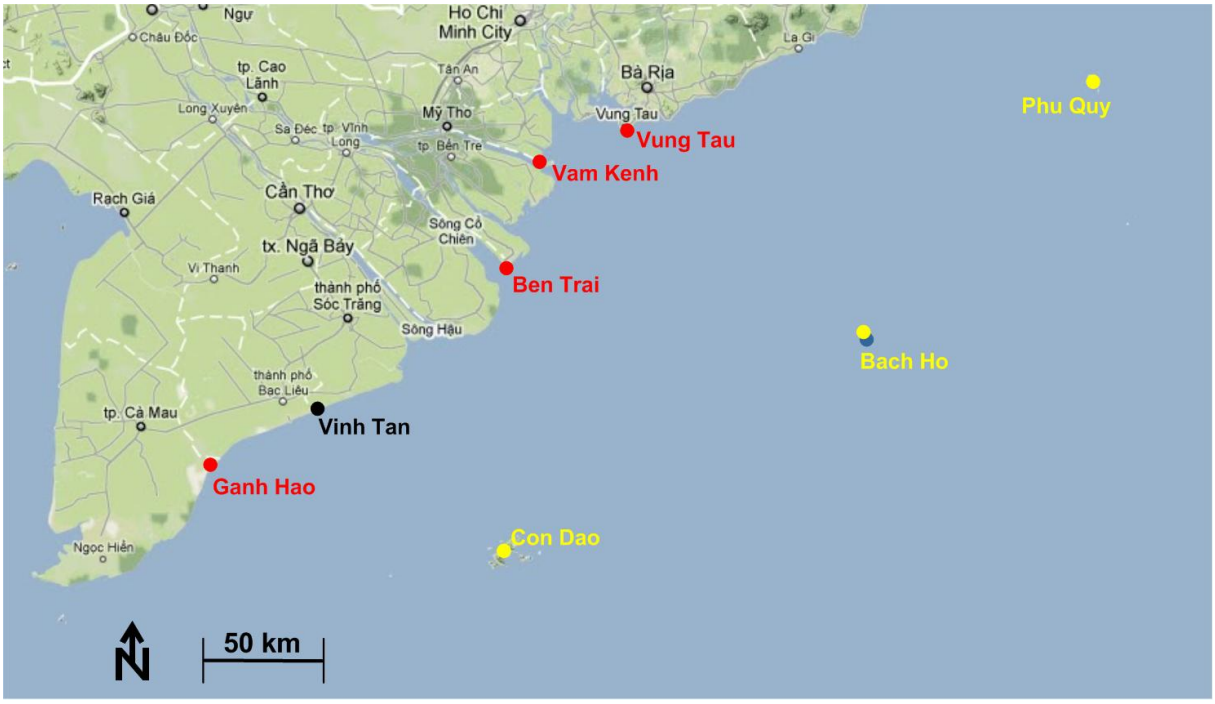

Figure 8: Map of southeast Vietnam including various gauges (red), wave stations (yellow) and the erosion site Vinh Tan (black).

In Figure 9 the seasonal, semi-monthly, diurnal and semi-diurnal variations of the water levels are due to the tidal regime of the South China Sea and the discharge regime of the rivers. These data and data from other stations are used as boundary conditions for the numerical modelling.

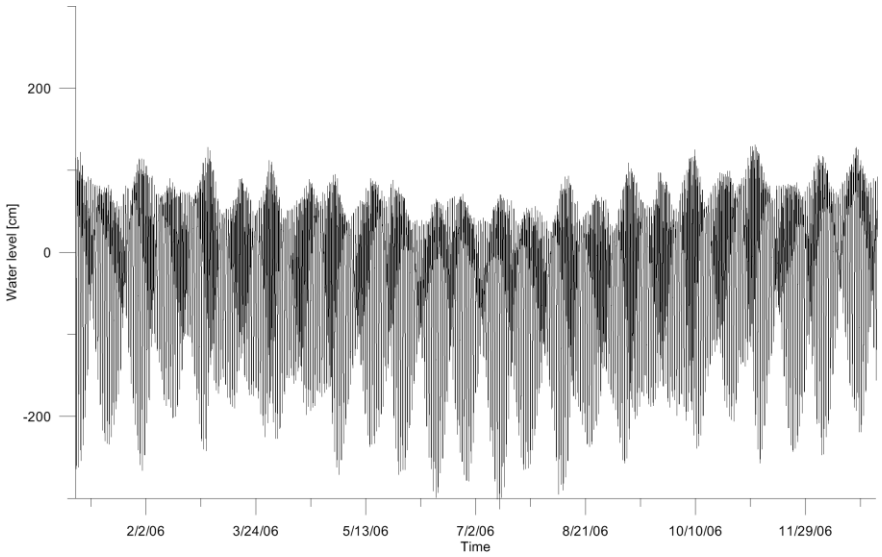

Figure 9: Water levels at Vung Tau in 2006.

Available bathymetric data were used for the geometrical setup of the numerical model. Near-shore high-resolution soundings in a 50 m grid were available. The resolution decreases further offshore (Figure 10). The chart datum is the Vietnamese National Datum.

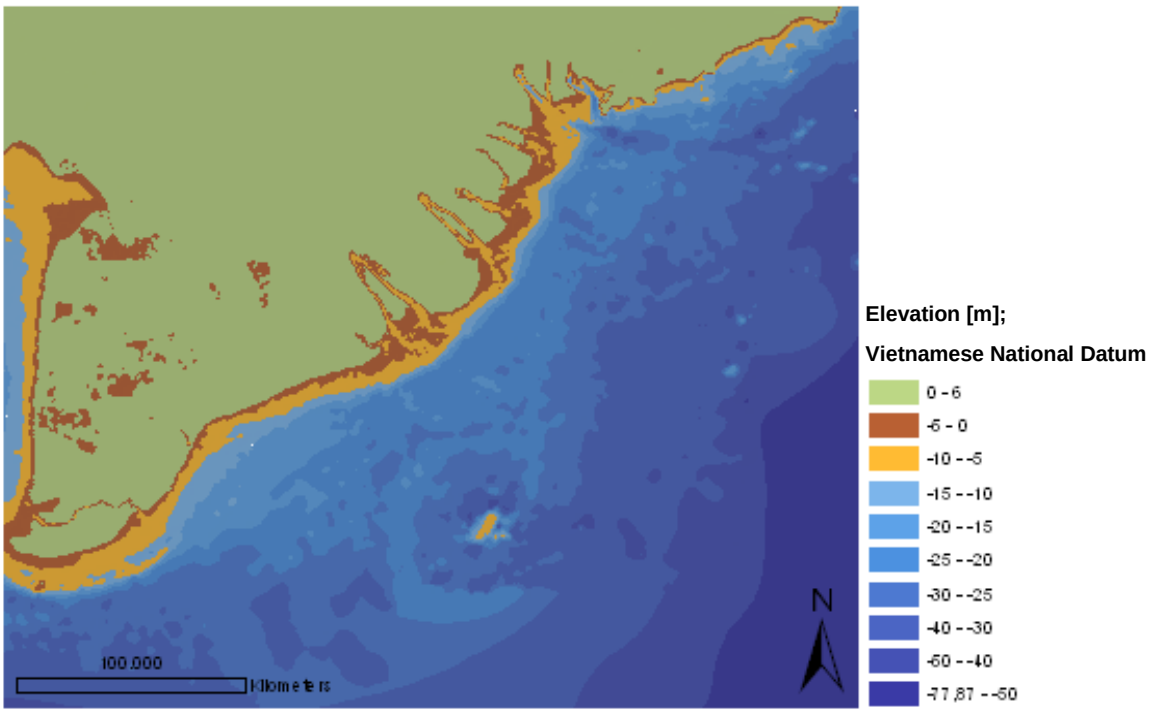

Figure 10: Bathymetry along the southeast coast of Vietnam.

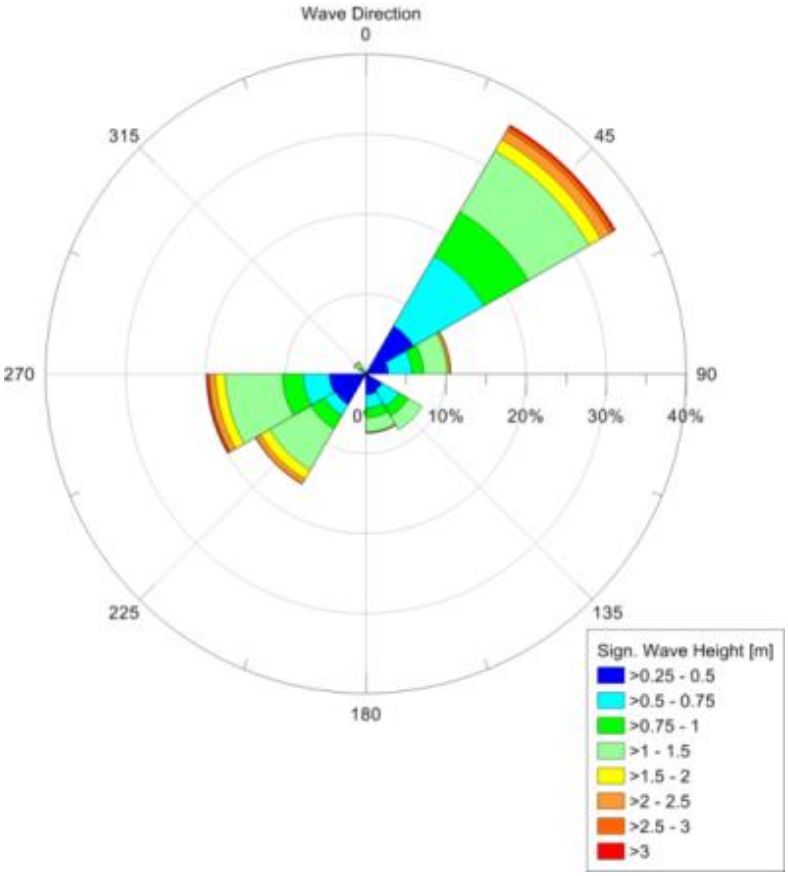

Figure 11: Wave rose of Con Dao.

Wave data from Con Dao highlights the two main wave directions, which are caused by the northeast and the southwest monsoons (Figure 11). In winter, a larger quantity of higher waves from the north-east dominates the wave climate, while the northeast monsoon winds cause an increased coastal long-shore drift. During summer the waves approach from the southwest and the appearance of larger waves is reduced.

Figure 12 shows two satellite images indicating the turbidity in the coastal waters of South Vietnam in February and October 2009. Orange and red colours indicate higher sediment concentrations in the water. The sediment plume of the Mekong at the end of the rainy season in October is clearly visible. A part of the sediment deposits at the mouth of the Mekong. The rest is transported along the coast and adds to the proceeding development of the spit at South Vietnam. In February, in times of the northeast monsoon, the sediment supply from the Mekong is limited. Higher wave energy and lower sediment concentrations increase the erosion during that season.

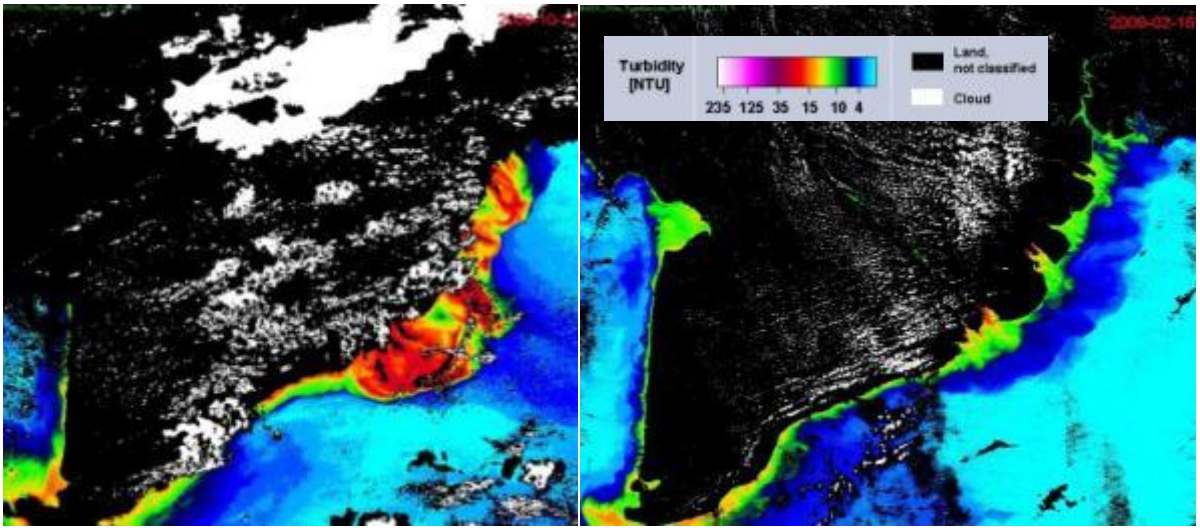

Figure 12: Satellite images of southeast Vietnam indicating the turbidity of the coastal waters in October 2009 (left) and February 2009 (right); Source: EOMAP.

Although data on the bathymetry, water levels, river discharges and sediment freights were available, essential data about the erosion site, especially about the wave climate, were missing. Therefore, a concept for selective field measurements in the focus area of Vinh Tan was worked out to close this gap.

The field measurements add to available data sets and allow assessment of hydrodynamic and morphodynamic processes, and to setup a detailed numerical model at the coast of Vinh Tan. After all, the final design of erosion protection measures is based on available data, in particular collected field data and the results of the numerical modelling.

3 Coastal processes and coastal protection

Coastal erosion and accretion are complex processes that depend on various influences. Key elements are the sediment transport under the influence of currents and waves, the overall dynamics of beaches in a coastal section and anthropogenic impacts (PRATESYA, 2007).

To identify the causes of erosion in certain coastal areas different parameters must be known (NRC, 1990):

- Coastal morphology
- Wind as the driving force for the development of waves
- Waves as the driving force for short-term profile changes
- Tidal currents as the driving force for long-term morphodynamics
- Cross-shore and longshore sediment transport induced by waves, tides and wind driven currents
- Vegetation as one factor for the stability of the profile

Anthropogenic influences also have to be considered:

- Measures of coastal protection, erosion protection and port engineering
- Removal of coastal vegetation
- Reduction of the sediment supply from the estuaries due to measures of river engineering
- Dredging and dumping of sediments

Some of these parameters were measured at certain positions and accordant data are available. If those positions are not in the area of interest, either of the numerical models can be used to compute the desired parameters or additional field measurements can be carried out. However, measurements in the area of interest are necessary to verify the results of the numerical modelling.

If waves approach shallow water areas, wave parameters change. The physical processes refraction, shoaling, wave breaking, bottom friction and percolation are called shallow water processes. Including effects induced by structures the so-called nearshore wave processes are illustrated in Figure 13.

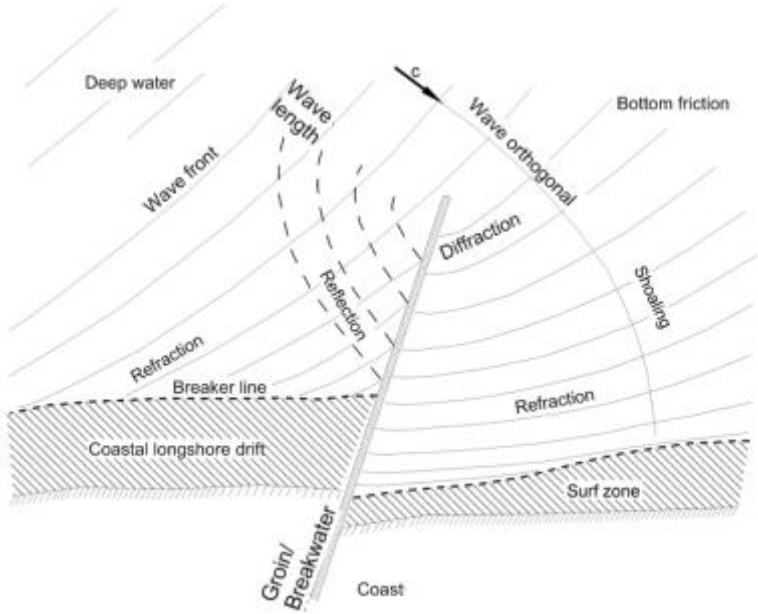

Figure 13**:** Schematic illustration of nearshore wave processes (EAK, 1993).

The largest fraction of the sediments (more than 90%) is transported in suspension; the rest is transported near the bottom in saltation.

Due to its vectorial character the sediment transport at the coast can be divided into:

- Cross-shore sediment transport (on-/offshore transport)
- Longshore sediment transport

Coastal cross-shore sediment transport induces short-term morphologic changes, e.g. during storm events. Coastal longshore transport causes long-term morphologic changes of a coastal section.

3.1 Cross-shore sediment transport

At a straight coastline, orthogonal approaching waves induce net transport of water in the direction of the waves. This leads to a backwater in the breaker zone, which is called wave setup and may be increased during storms by the wind setup. The gradient of the water level in the breaker zone leads to seaward-directed currents, which are in equilibrium with the approaching currents. The landward-directed currents run at the surface, the seaward-directed currents run at the bottom. The currents depend on the length, period and height of the waves, on tidal currents and the bottom friction. If the water-level gradient and the wave parameters are constant, a beach profile is formed, which is in equilibrium with the waves and stable as long as the wave conditions do not change.

At natural coasts, tides and daily, as well as seasonal, changing wave conditions avoid the formation of an equilibrium profile. The beach profile reacts on every change of the wave parameters with the attempt to form a new equilibrium profile. The result is an oscillating cross-shore sediment transport.

The landward-directed transport is induced by long and plane waves (e.g. swell). The seaward-directed transport occurs predominantly during short and steep waves and leads to erosion of the beach. Figure 14 shows the schematic changes of a beach profile due to a storm event. If the profile is not in equilibrium due to increasing wave activity, the upper part of the profile will first be eroded. The material deposits at lower parts of the profile and leads to a flattening of the profile. Consequently, the dissipation of the wave energy is distributed over a larger area, and the erosion rate is decreased. When the equilibrium profile is reached, the erosion rate becomes nearly zero.

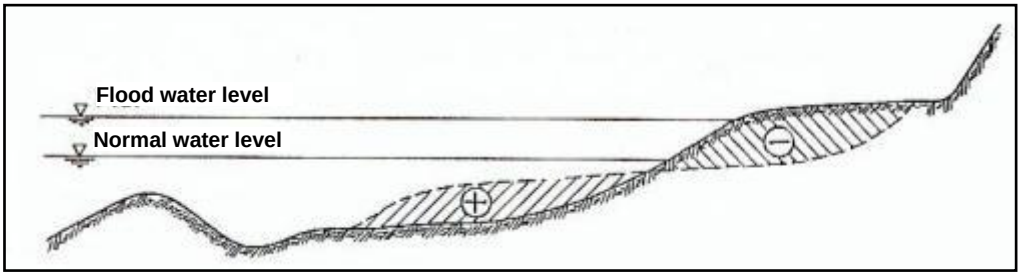

Figure 14: Schematic changes of a beach profile due to a storm event (US ARMY CORPS OF ENGINEERS, 2002).

3.2 Longshore sediment transport

As soon as the direction of the approaching waves is not orthogonal to the shoreline, a force component parallel to the coast is generated, leading to longshore currents. The sediment transported with these currents forms the longshore sediment transport. Longshore currents induced by waves can be superposed with tidal currents parallel to the coast. Even if the waves approach orthogonal to the shoreline, tidal currents may cause a longshore sediment transport.

The impacts of morphologic changes of a coast induced by longshore transport depend on the physiographic unit of the coastal section. Open and closed sand systems have to be differentiated (Figure

15). In open systems, sand leaves the coastal section due to longshore transport. The coast at Vinh Tan is such an open system.

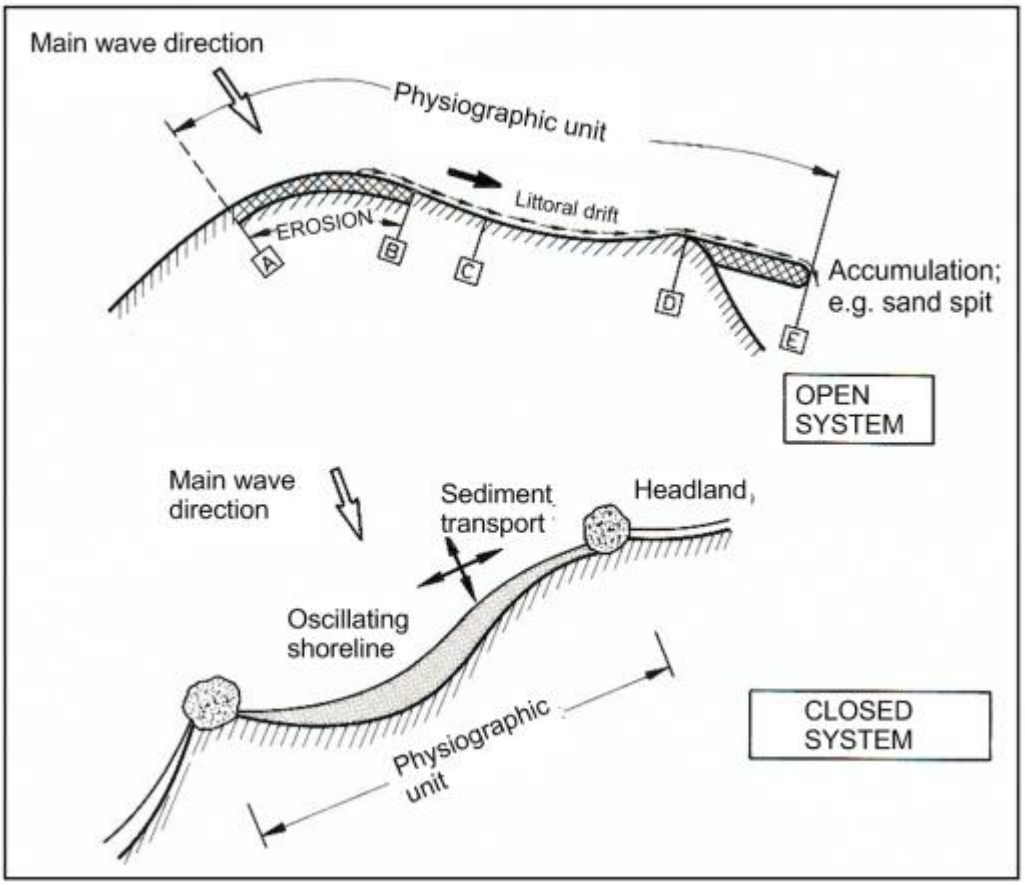

Figure 15: Open and closed sediment transport systems (US ARMY CORPS OF ENGINEERS, 2002)

In the course of a tidal cycle, sediments of tidal flat areas are subject to different transport processes. VAN RIJN (1993) differentiates:

- Settling
- Deposition
- Consolidation
- Erosion

PARKER (1986) developed a model that shows the processes and interrelations from mobile sediments to a consolidated bottom. During phases of increased currents and wave activity, sediments are in balance in the water column and are transported by the motion of the water (mobile suspension). If the intensity of the turbulence of the current decreases and the gravitation force overbalances, the sediments start to settle. Attractive forces of the cohesive particles cause the formation of flocs that consist of several sediment particles. With increasing floc sizes, the settling velocity increases in comparison to single particles. If a certain sediment concentration is exceeded, the flocs hinder themselves and the settling velocity decreases again (hindered settling). If no horizontal motion is possible anymore, but just a vertical settling with significantly decreased settling velocities, this phase of transport processes is called stationary suspension.

Currents and the impacts of waves may transport flocs from stationary suspension into mobile suspension again. The sediment particles' own weight at the bottom densifies the material. The pore water in the hollow spaces between the particles is pushed out during this process. The compaction of the deposited sediments by its own weight with parallel separation of the pore water is called consolidation.

Consolidation can progress as long as currents and waves are not strong enough to erode the deposited material. This contains the periods around slack water and around tidal low water, when the tidal flats fall dry. Consolidation of cohesive sediments leads to increasing stability against erosion, meaning that the sediments are not re-suspended even at increasing current velocities and turbulences. The bottom elevation increases to a certain degree. This phase of increased stability against erosion is called settled mud or settled bed.

3.3 Erosion protection measures

3.3.1 Breakwaters

To protect coasts with limited tidal range against erosion, nearshore breakwaters may be installed parallel to the shore.

After installation, the following mechanisms are effective (Figure 16 and Figure 17):

- Depending on the cross section of the breakwater, the water depth and the wave parameters of the approaching waves, only a small part of the wave energy is effective on the landward side of the construction. A wave shadow zone is formed.
- The waves passing the breakwater are subject to diffraction, which changes the propagation direction. The waves reaching the wave shadow have limited heights.
- The decreased wave motion in the shadow zone leads to deposition of the suspended sediments. The shoreline moves seaward. Depending upon the length of the breakwaters, the distance to the shoreline, and the damping of the waves, salients or tombolos are formed. The degree of the wave damping is influenced by the height of the breakwater and its porosity.
- The formation of the salients or tombolos is very stable because the new shoreline is nearly orthogonal to the approaching waves. The lateral sediment drift is heavily reduced.

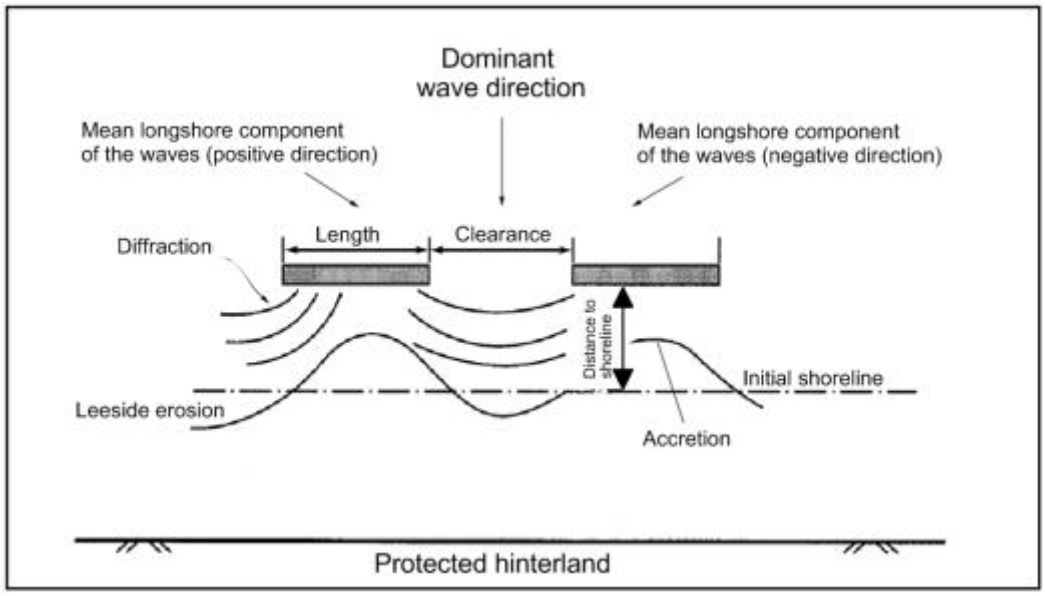

Figure 16: Installation of breakwaters (U.S. ARMY CORPS OF ENGINEERS, 2002).

Detached breakwaters allow longshore sediment transport to a certain extent, depending on the structure, position and the wave parameters. This reduces downdrift erosion. During storm events the partly eroded tombolos may provide a sediment supply for the downdrift area.

Detached breakwaters are used to protect individual, heavily loaded coastal sections. Nourishments may adjust the negative impacts of the disturbed longshore sediment transport.

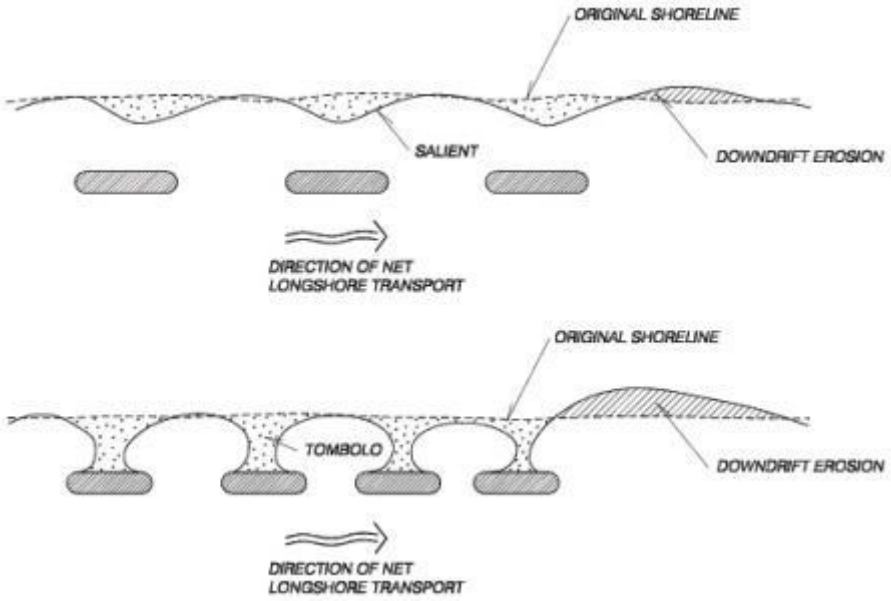

Figure 17: Typical beach structures with detached breakwaters (US ARMY CORPS OF ENGINEERS, 2002).

3.3.2 Groins

Groins are defined as dam-like, cross-wise arranged constructions to protect beaches, flood plains, longitudinal constructions and other constructions. They interrupt the natural longshore transport and lead to accretion at the windward side. There sediments are deposited and the sediment transport to the lee side is reduced.

Impermeable groins form a complete barrier against the longshore transport. After completed deposition at the windward side, material is transported over and around the groin.

Permeable groins are constructed if a certain transport through the groin is desired. This leads to a sufficient sediment supply to avoid downdrift erosion.

Groins are constructed cross-wise to the shoreline and form a barrier for the longshore sediment transport. In the same amount as sediments deposit at the windward side, the sediment transport to the lee side is reduced. If the impact of the groin is too strong, downdrift erosion occurs. Directly behind the groin the sediment transport component directed to the shore is smallest. It increases with increasing distance to the groin. If the distances between the groins are too small, the sediment supply of the shoreline is insufficient.

The slope of the beach at the windward side is steeper than at the lee side. If a certain slope is exceeded, no more sediment is deposited and natural longshore transport passes the groin.

As a general rule groins are constructed in groups with the intention to protect larger coastal sections. In a group of groins, the distance has to be defined so that the protecting effect is large enough to avoid erosion caused by currents and waves. The distance between impermeable cross-shore groins of the same length is defined by $s_n = 2 \cdot e \cdot \cot \beta$ (Figure 18).

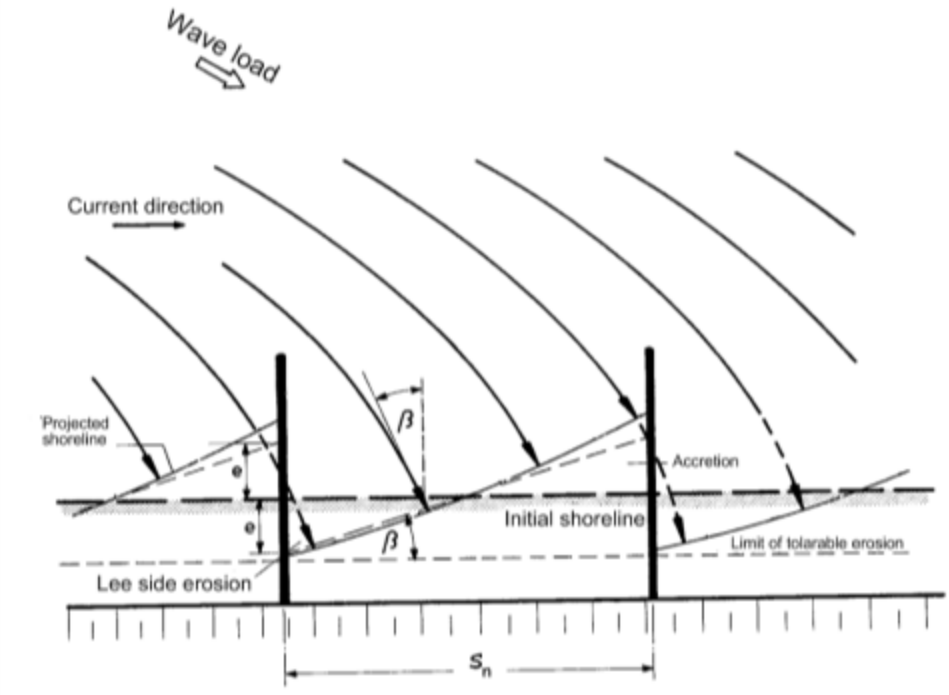

Figure 18: Procedure to calculate the distances between groins (EAK, 1993).

If groups of groins are constructed with different lengths, such as in the transition area to an unprotected section of the beach, the Handbook of Coastal Engineering (HERBICH, 1999) defines the calculation of the length l_n and the distance s_n of the groins as follows (Figure 19):

$s_n = (R_{SL} \cdot l_{n-1}) / (1 + (R_{SL} / 2) \cdot \tan \theta)$

$l_n = ((1 – (R_{SL} / 2) \cdot \tan \theta) / (1 + (R_{SL} / 2) \cdot \tan \theta)) \cdot l_{n-1}$

$R_{SL} = s_n / l_n$

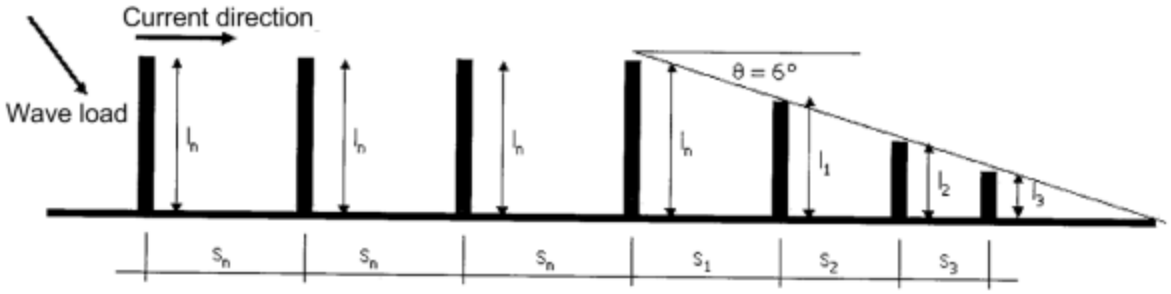

Figure 19**:** Scheme for the calculation of the groin distance and the groin length in the transition zone (HERBICH, 1999).

Figure 20 shows different profiles of groins. The design influences the impacts of the construction. Groins with a wide crest avoid wave overtopping, which might lead to further erosion in the lee side groin field.

Groins are a very common coastal protection system. In many cases the intended effects were achieved. In other cases though, the effectiveness was limited and some examples are known where groins caused severe damage due to downdrift erosion. Due to that reason, the construction of groins needs to be planned carefully.

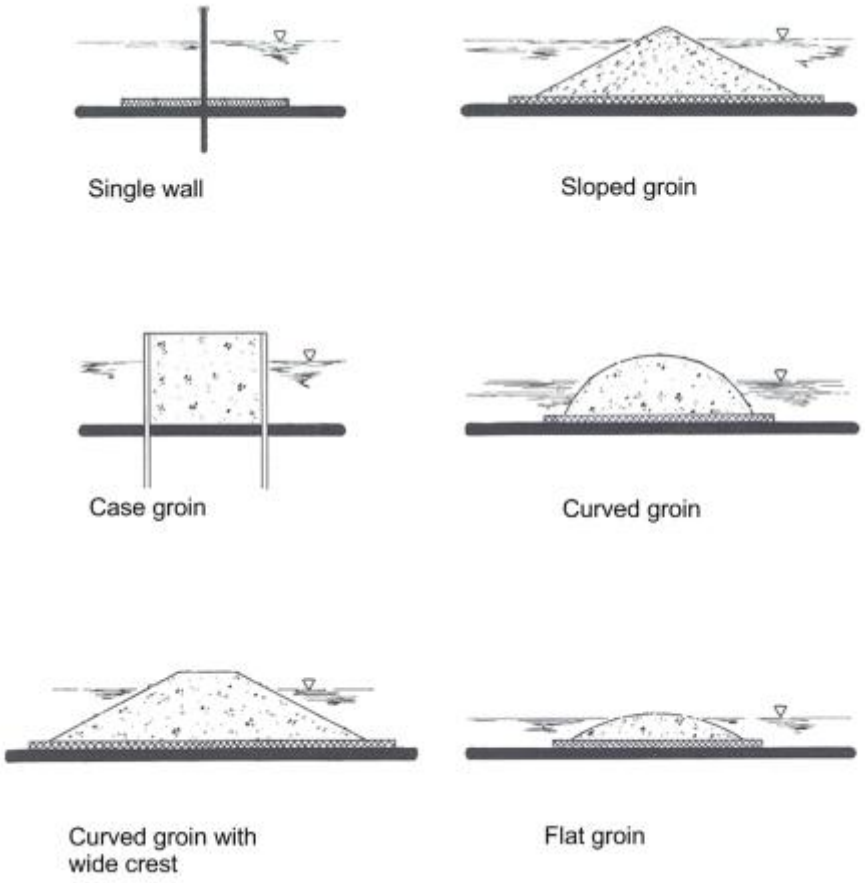

Figure 20: Examples of groin profiles (EAK, 1993).

3.3.3 Land reclamation

Suspended sediments are transported to nearshore areas by tidal currents and waves. Due to decreasing turbulence, the transport capacity of the current decreases and sediment particles start to settle. This process, for example, takes place in basins and at the lee side of islands. By means of methodical measures, the deposition of sediments can be increased in an artificial way. At the North Sea coast a large mesh of chequered fields of calmed water areas was formed. Fence-like permeable constructions form a barrier against the turbulent currents and waves, and assist in the deposition of sediments.

Land reclamation started around the year 1362 after several severe storm surges, which caused large erosion at the coasts. In 1847, the Danish government established methodical land reclamation (PROBST, 1996).

Cross-shore and longshore constructions form fields of 100 m x 100 m and up to 400 m x 400 m, in which currents and waves are damped and deposition is forced (Figure 21). The fences parallel to the shoreline have openings to secure the drainage of the field. The cross-shore constructions decrease the longshore currents and the longshore constructions damp the incoming wave energy.

Until the middle of the 20th century, the aim of land reclamation was to create new fructuous areas for agricultural cultivation. For 30 years now, the wave-breaking and wave-damping effects of the developed flood plains in front of the dykes has been used for coastal and erosion protection. Land reclamation is an active measure of coastal protection (KRAMER, 1989).

Nowadays, the fences are constructed by two rows of wooden piles with faggots (fascines) in between (Figure 22). The faggots are fixed with stainless wire. Erosion around the wooden piles can be

avoided by roughcast at the toe of the fences. Normally, the top of the construction is equal to the mean high water (MHW). The elevation of the tidal flats should not be lower than MHW -0.70 m to -0.80 m. Initially one row of fields is constructed in front of the dyke. With proceeding siltation of the first fields, a second row of sedimentation fields may be constructed further offshore.

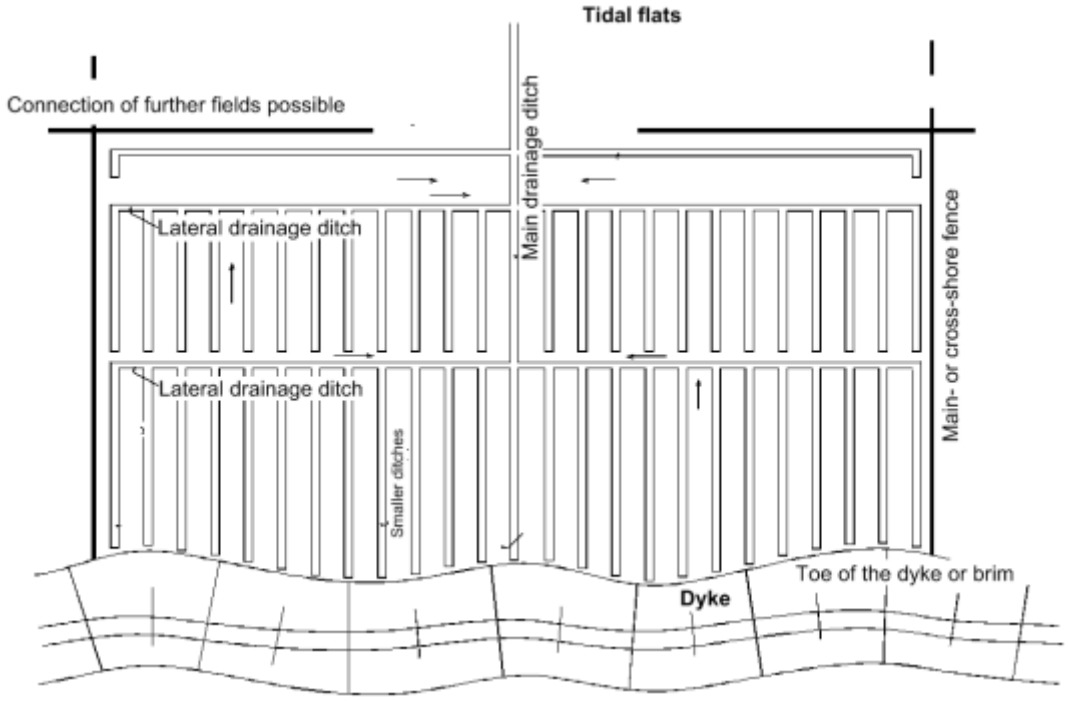

Figure 21: Land reclamation using cross-shore and longshore fences (VON LIEBERMAN, 1998).

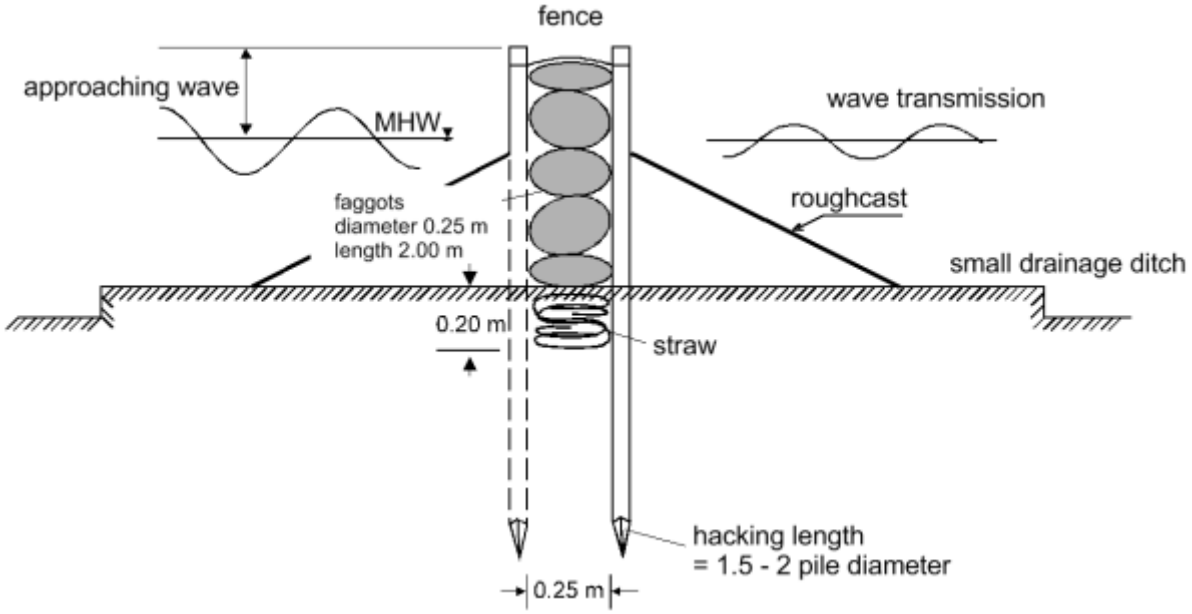

Figure 22: Construction of a fence in a sedimentation field.

When the flood plain reaches an elevation of MHW -0.50 m to MHW -0.30 m, an artificial drainage system is created that consists of cross-shore main ditches and lateral drainage ditches (Figure 21). Smaller ditches lead the drainage water to the lateral ditches. To secure the discharge capacity of the small ditches, they are dredged if necessary, whereupon the excavated material is dumped in the middle between the small ditches in order to accelerate the siltation process.

The shallow water depths on the developed flood plains create a large surf zone in which the wave energy is dissipated. The wave load on the dyke decreases significantly (Figure 23). The physical safeguarding measures at the dyke and the resulting costs can be reduced.

With increasing width and elevation of the flood plain, the wave run-up at the dyke is reduced significantly. Consequently, the design height of the dyke may be reduced, which becomes very important in times of a rising sea level.

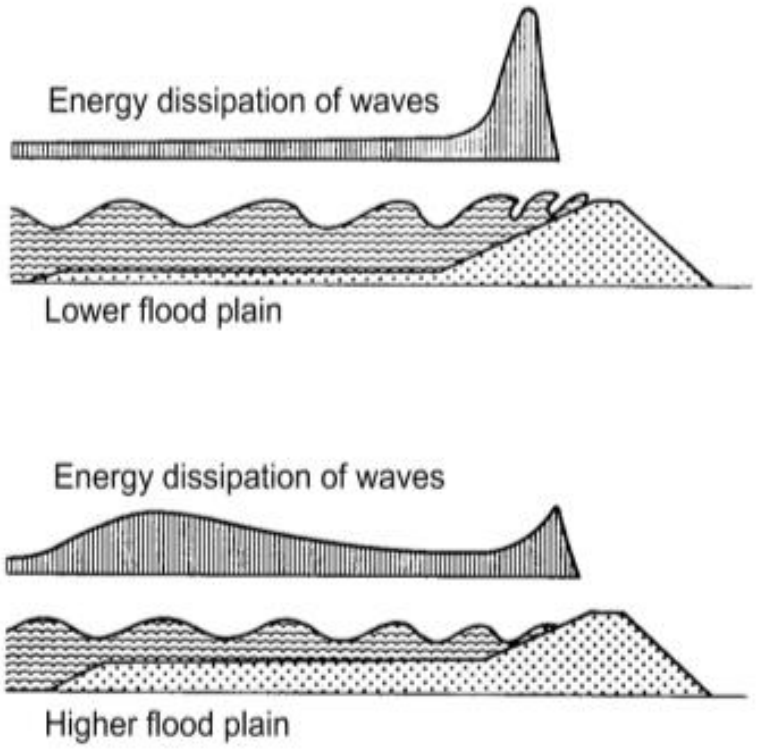

Figure 23: Impact of the flood plain on the wave energy dissipation **(**STADELMANN, 1981).

4 Field measurements

Some data with relevance for the hydrodynamics and morphodynamics of the investigation area were available. The position of those measured data is generally further away from the focus area at the endangered dyke at Vinh Tan. Available data were used to setup, control and calibrate the numerical models. Additional field measurements are carried out

- To verify the results of the numerical modelling; and
- To understand the hydrodynamic and morphodynamic processes in the focus area.

Within three measurement campaigns in October 2009, February 2010 and July 2010 information about currents, waves, sediment concentrations and the bathymetry were recorded. The field measurements covered different seasons including northeast and southwest monsoons.

At stationary measurement positions near the endangered dyke at Vinh Tan, wave parameters, suspended sediment concentrations and currents were measured. In an investigation area 20 km along the coast of the District Vinh Chau, mobile current measurements were carried out at profiles of 2 km length covering different tidal phases. Along those profiles in certain intervals sediment samples were taken.

4.1 Stationary measurements

To analyse processes of sediment transport, optical backscatter sensor (OBS) devices and pressure transducers were installed at 100m and 300m distances to the dyke at the erosion area.

In October 2009, a mild wave climate with significant wave heights of 0.20 - 0.25m, and maximum suspended sediment concentrations (SSC) between 2 and 4.5 g/l during flood tide, were recorded at 300 m distance to the dyke at Vinh Tan (Figure 24). The upper diagram shows the recorded water levels (black line). The red line indicates the suspended sediment concentration at the same location. The second diagram shows the significant wave heights, which is the average wave height (trough to crest) of the one-third largest waves. Tidal currents affect the course of the sediment concentration, while current velocities and wave heights influence the peaks of SSC.

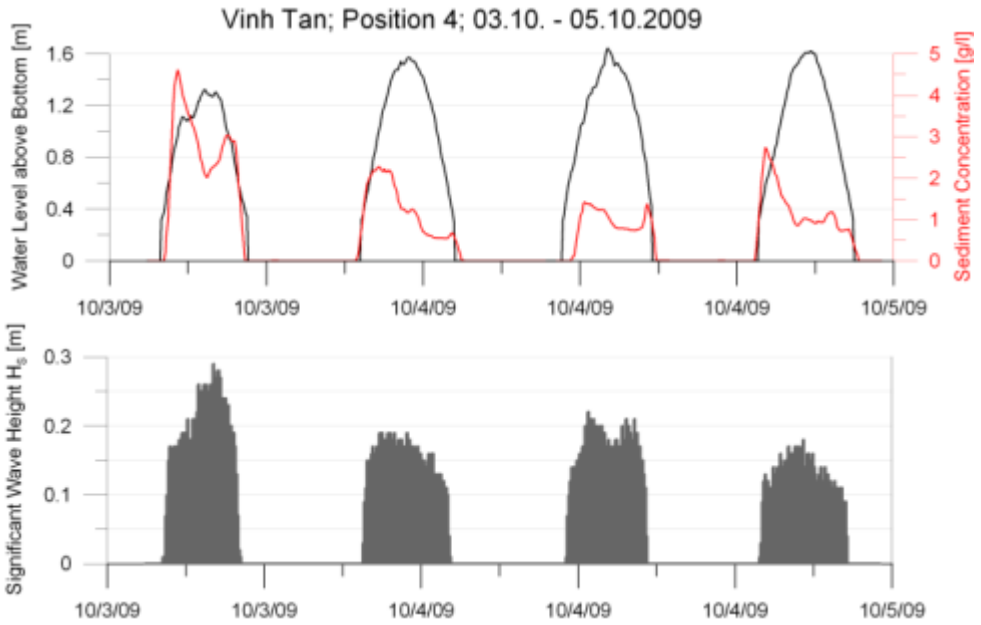

Figure 24: Water levels, waves and sediment concentrations at the coast of Vinh Tan in October 2009.

In January 2010, during the main period of the northeast monsoon, higher waves with significant wave heights of up to 0.55 m were recorded at a 300 m distance to the dyke (Figure 25). The upper diagram shows the recorded water levels. The second diagram shows the significant wave heights at the same location. Between January 21st and 28th the wind velocity increased, which resulted in larger waves at the coast. Furthermore, a dependency of the wave heights on the water depth is obvious.

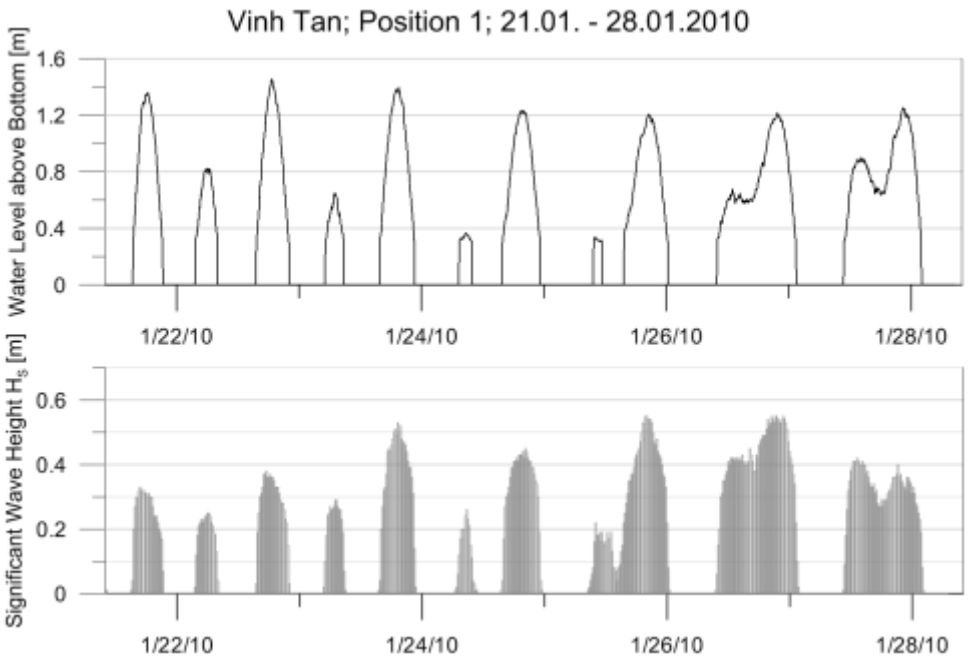

Figure 25: Water levels and wave heights at the coast of Vinh Tan in January 2010.

At 4 km distance from the erosion site, an Acoustic Wave and Current Sensor (Nortek AWAC) was installed at a water depth of 4 m during low tide (Figure 26). In a campaign during the northeast monsoon season, the sensor recorded wave and current data simultaneously. The analysis of the wave data assisted in investigating the development of the current velocities and directions over the course of the tides. The approach of waves from deeper water to the coast can also be described with the AWAC data and the measurements of the pressure devices at the dyke.

Figure 26: Installation of the AWAC at the coast of Vinh Tan.

During northeast monsoon season in January 2010, the installed AWAC recorded current velocities between 0.10 m/s and 0.60 m/s during flood tide (Figure 27). The diagrams show data of the AWAC survey between January 20th and 24th 2010. The upmost diagram shows recorded hourly averaged wind velocities from Bac Lieu Station (N 9.295°, E 105.720°). The second diagram shows recorded water levels at Vinh Tan, the third diagram indicates the velocities of the current, and the fourth one the directions of the current. The lowermost diagram shows the significant wave heights (black bars). The peaks in current velocity during ebb tide were less pronounced: between 0.10 m/s and 0.40 m/s.

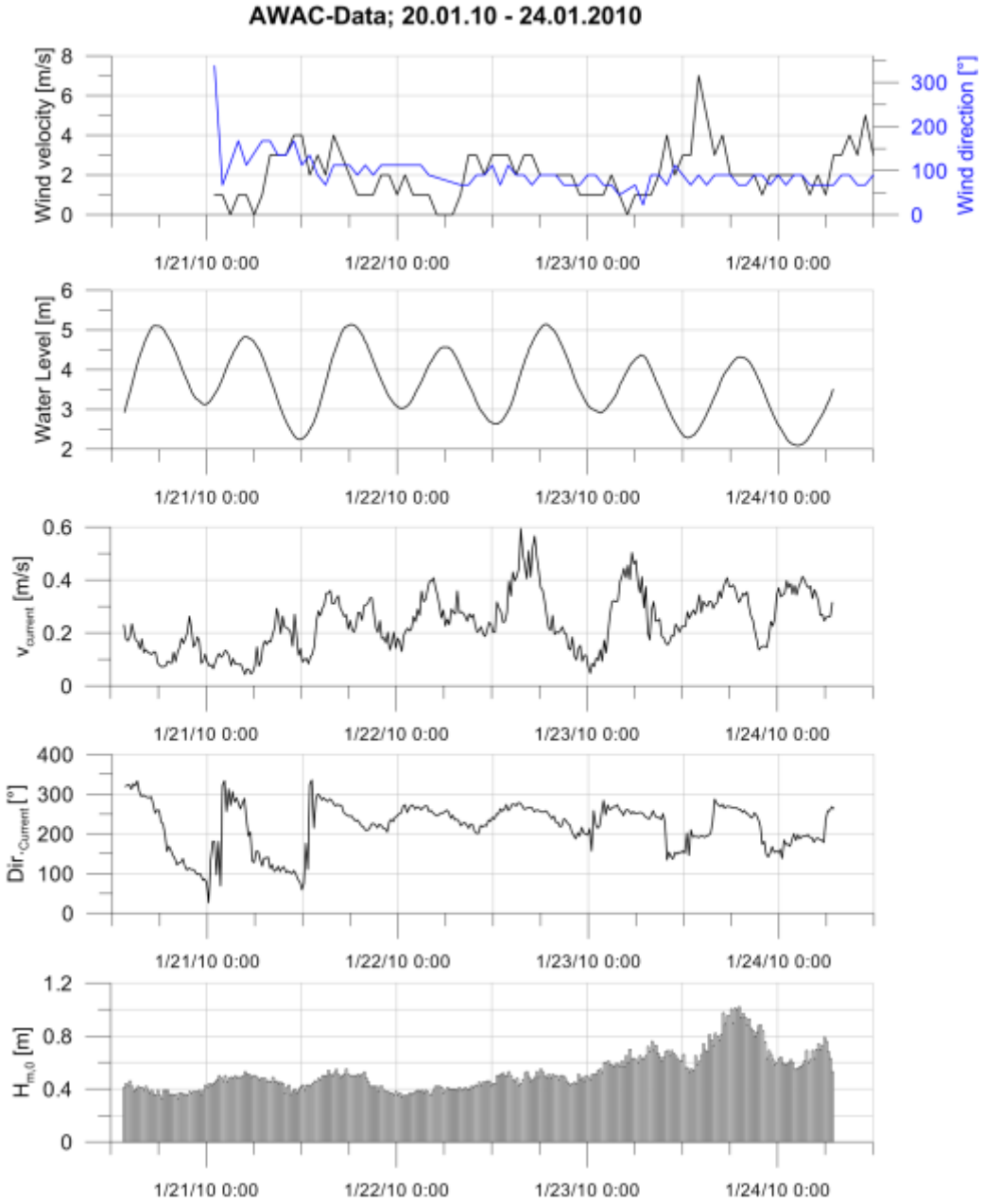

Figure 27: Results of the measurements with the AWAC in January 2010.

The current direction changed from 300° at the beginning of the flood tide to 250° at slack water. Between January 20th and 24th, the wind changed from a southern to a northeastern direction, with increasing wind velocities. During pronounced northeast wind conditions, the current velocities during flood tide increased and the directions were more or less constant between 270° and 250°, resulting in a strong long-shore component during flood tide. During ebb tide, the current direction changed from 250° to 100° in calm weather conditions and from 250° to 200° during northeast monsoon conditions.

The more pronounced the northeast monsoon conditions were, the larger the long-shore component of the ebb current was. Also, the maximum ebb velocities increased with increasing northeast winds. The significant wave heights increased from 0.40 m at the beginning of the measurements up to 1.00 m during northeast monsoon winds.

Due to the larger water depths, the influence of depth on wave height is decreased compared to measurement positions near the dyke. The natural coastal profile causes a reduction of height from the AWAC position to the dyke of up to 50%, whereas the damping effect is larger for higher waves.

4.2 Mobile measurements

In a 20 km long area along the coast of Soc Trang, seventeen 2 km long cross-shore profiles were surveyed during flood and ebb tide with a vessel mounted Acoustic Doppler Current Profiles (ADCP). The ADCP recorded current directions and velocities. The first ADCP campaign was carried out during October 2009, when seasonal discharge from the Mekong was at its greatest. Figure 28 shows the position of cross-shore profiles during flood and ebb tide. The red arrows indicate the average direction of the currents; the length of the arrows indicates the velocity. The green line in the diagram below shows the water levels during the survey. The survey direction is from left to right.

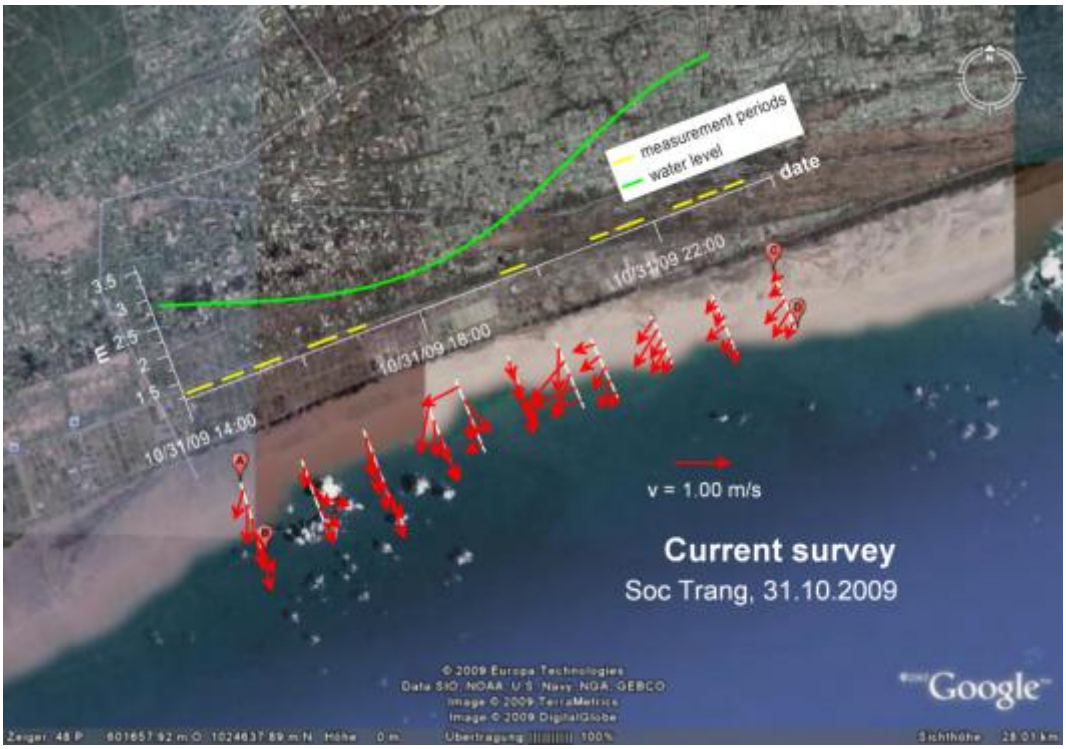

Figure 28: Results of the current survey in October 2009.

During ebb tide, seaward currents of around 0.40 m/s were recorded. Maximum long-shore currents of approximately 1.00 m/s were recorded temporarily during flood tide, and appear at the same time as the peaks of the suspended sediment concentration. This indicates increased long-shore sediment transport.

A second ADCP survey was carried out in January 2010 during the northeast monsoon season. Analogue to the description above, Figure 29 shows fourteen profiles. The red arrows indicate the average direction and velocity of the currents. The green line in the diagram shows the water levels during the survey on January 21st 2010. The yellow lines under the water level indicate the time of the ADCP profile measurements. The survey direction is from right to left. Even during low wind speeds the flood current had a strong long-shore component (similar to previous measurements). The ebb

current runs cross-shore in seaward directions. Due to low wind forces, the current velocities were not higher than during the campaign in October 2009.

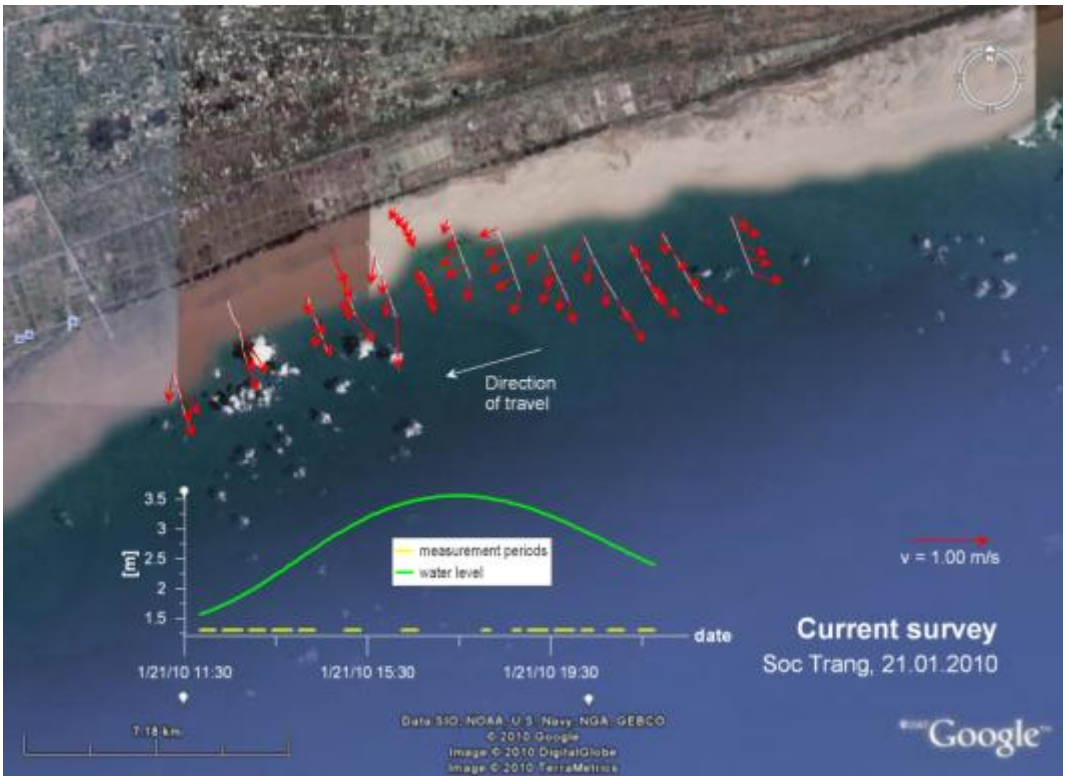

Figure 29: Results of the current survey in January 2010.

4.3 Sediment sampling

Samples of bed material were analysed in a geotechnical laboratory. Figure 30 shows the grain size distribution of two bed samples at the coast of Vinh Tan.

The median grain size is 0.0065 mm. The bed material is clayey silt. Further samples of the bed material in the focus area show silty and clayey material with a median grain diameter (D_{50}) between 0.003 and 0.007 mm.

Additionally, samples of suspended sediment concentrations were taken at 10 points of the five centre profiles (Figure 31). The concentrations were between 150 and 1000mg/l. In general, the concentrations are slightly higher near the coast than further offshore. Of overriding importance are the tidal influence and the influence of waves. Largest concentrations occur during flood tide, when currents and waves cause the largest shear stresses, due to high current velocities and a larger ration of wavelength and water depth L/d (Figure 24).

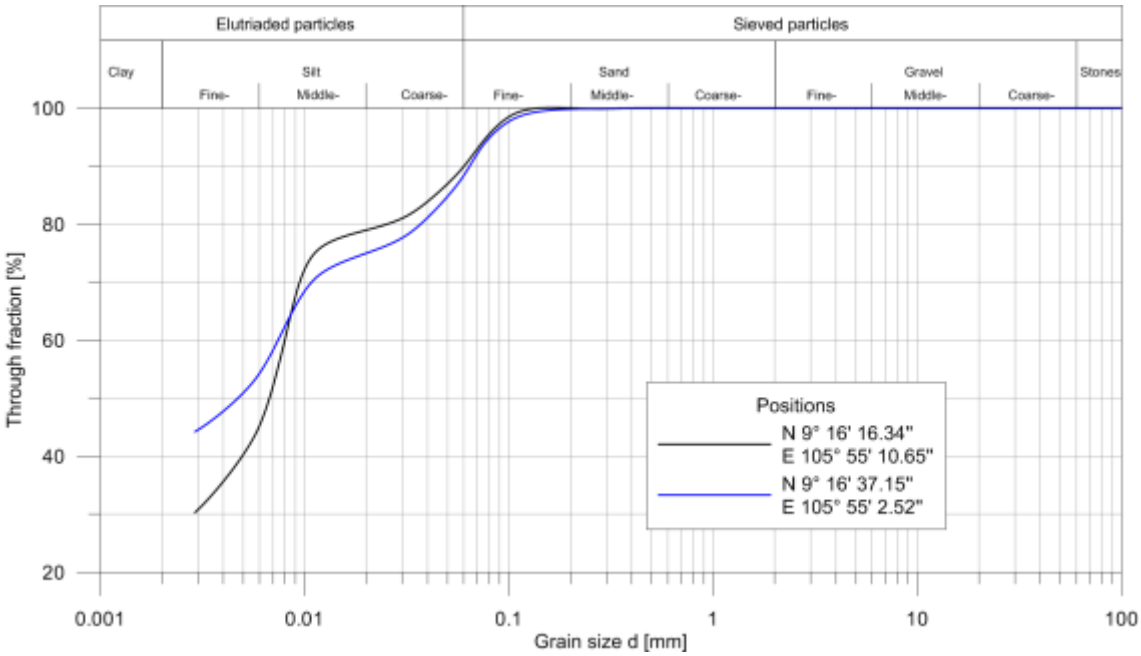

Figure 30: Grain size distribution at the coast of Vinh Tan.

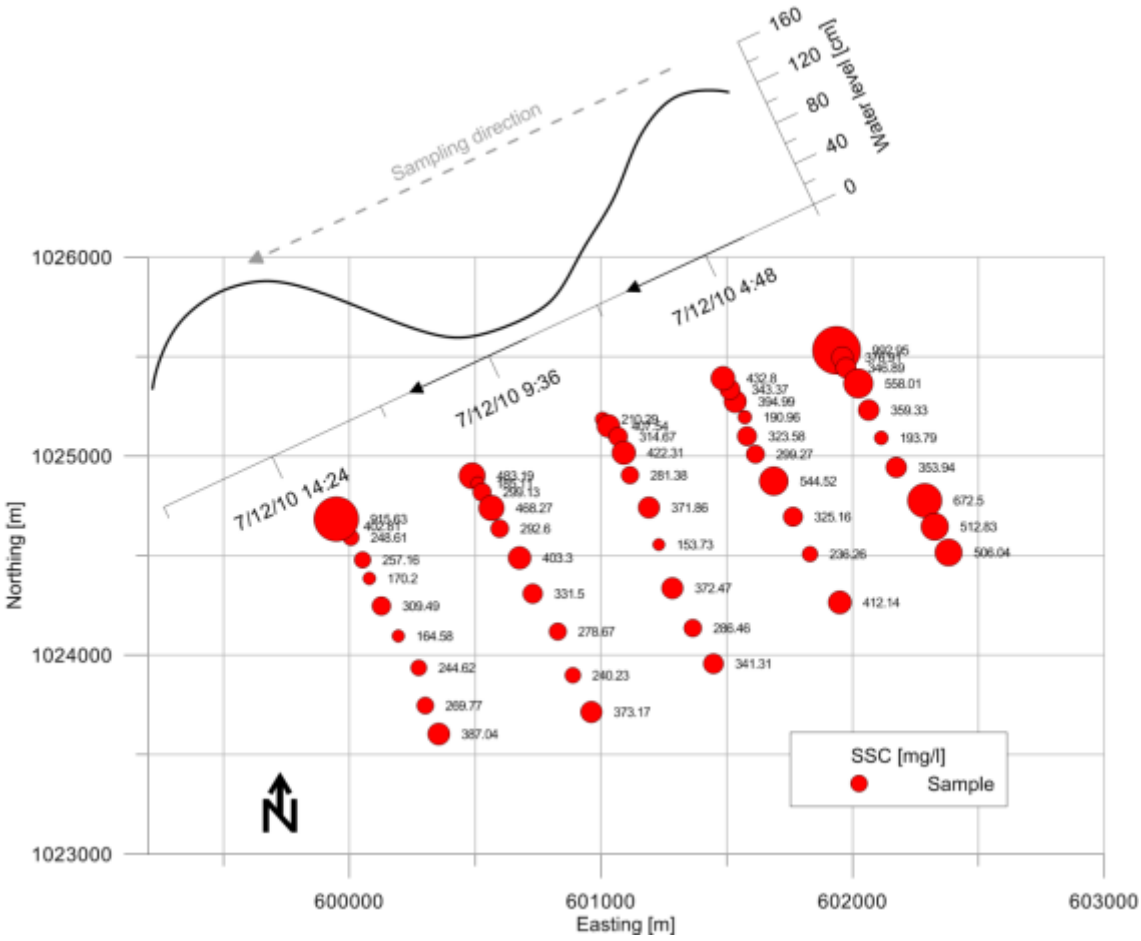

Figure 31: Measured suspended sediment concentrations along the survey profiles on July, 21st 2010.

5 Numerical modelling

The numerical modelling was done in three steps (see Figure 1). In a larger investigation area reaching from Vung Tau to Ganh Hao (app. 250 km) and 40 km from the coast into the South China Sea, a wave model was set up. The results were used as design parameters for the erosion protection measures at the coast. The wave model is coupled with the hydrodynamic model, which simulated currents and wave-induced currents. The results were then used as input parameters in the morphodynamic model simulating the shoreline changes. This third model covers the coast around the focus area at Vinh Tan. It simulates shoreline changes due to the occurring current and wave regime. Various structural measures are integrated in that model and the resulting effects are simulated.

5.1 Wave modelling

Information about the wave climate is essential when designing a breakwater. Field measurements of waves cannot cover all possible weather conditions. In order to obtain the missing information a numerical wave model was setup, calibrated and verified, using the SWAN model (Link: www.swan.tudelft.nl), available data and data of the field measurements from the focus area of Vinh Tan.

5.1.1 Boundary conditions and network

To control the numerical wave model, gridded information about water levels is necessary. Available gauges are located only at the coast. To provide the model with offshore water levels, a matrix was created based on gauges and information about the approaching semi-diurnal partial tide (M2-Tide). The locations of the gauges were crucial for the extension of the modelling area. Therefore, a mesh size of 100 km in x-direction and 80 km in y-direction resulted, covering an area of 96,000 km² (Figure 32).

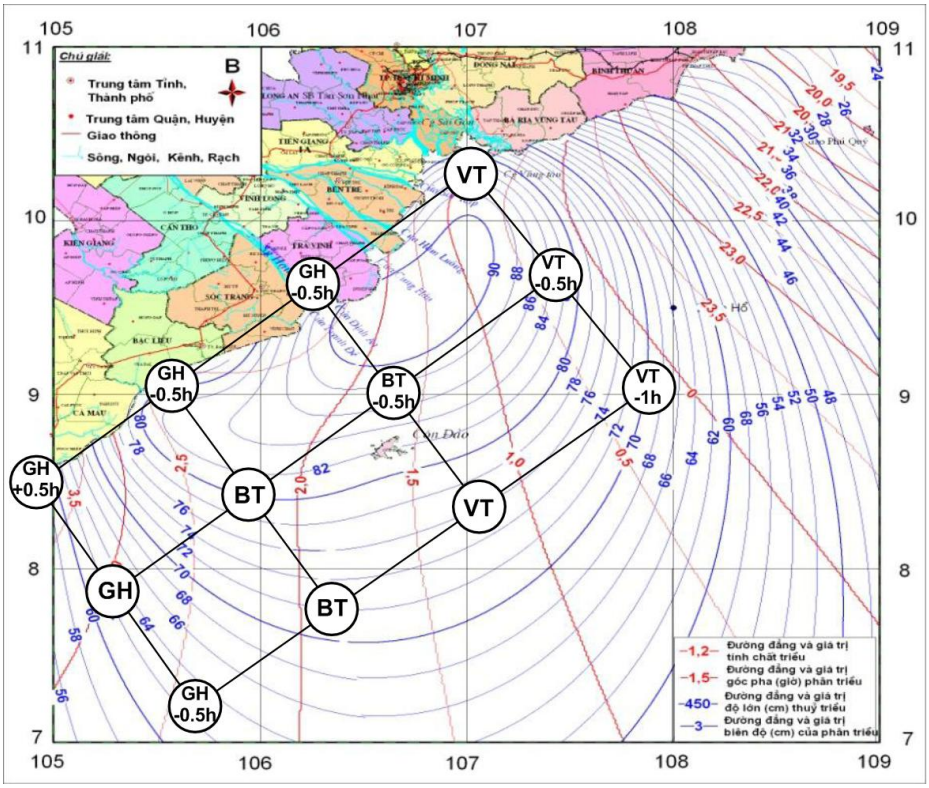

Figure 32: Mesh for water level boundary conditions for the wave model.

Figure 32 shows the created matrix, which provides the numerical model with water levels at every node of the mesh (marked with circles). The red lines describe the approach of the semi-diurnal partial tide. This information and the available gauges were used to design the matrix.

The geometric foundation of the wave model is a digital terrain model (DTM) based on bathymetric data. Therefore, a network of triangles was created to approximate the bathymetry. The DTM was developed for the east coast of the Mekong Delta from Vung Tau to Tan An using 80,000 triangles. The numerical model computes mathematical solutions for every node. At the focus area, where erosion protection measures will be investigated, the resolution of the model must be high enough to simulate the effects of that measure. To achieve the desired resolution of the model at the erosion site, the network was refined at the coast of Vinh Tan (Figure 33).

Figure 33 shows a part of the digital terrain model of the east coast of the Mekong Delta consisting of 80,000 triangles. The shaded area shows the refined network at the coast of Vinh Tan, where the triangles are significantly smaller than further offshore.

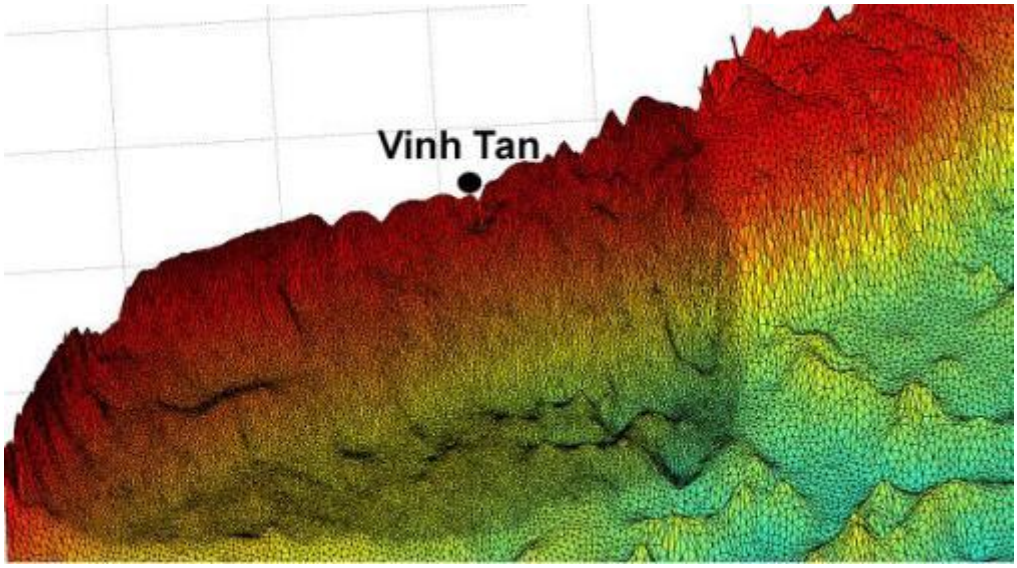

Figure 33: Parts of the digital terrain model at the coast of Vinh Tan with vertical exaggeration.

5.1.2 Results

The numerical model was then calibrated and verified using wind data, data from available gauges and data from field measurements. After that different scenarios were simulated. In one scenario, storm conditions during the southwest monsoon were simulated with peak wind velocities of 16 m/s. In that scenario waves with significant wave heights of 0.58 m were predicted at Vinh Tan. In Figure 34 (left), the light blue belt in front of the coast indicates the surf zone, where most of the wave energy is dissipated due to wave breaking. The location of the surf zone basically depends on the bathymetry and the water level. Therefore, it moves depending on the tides. Some spots are visible along the coast, where the surf zone is located close to the coastline. At the mouths of the Mekong branches, deposition of transported sediments occurs due to decreasing current velocities. Those sandbanks force the waves to break further offshore. Therefore, the river mouths are comparatively sheltered areas. The average wave direction at Vinh Tan is from south-southwest during that event. Due to wave refraction and the course of the coastline, the waves approaching the coast of Soc Trang and Bac Lieu induce a small longshore sediment transport component (Figure 34, right).

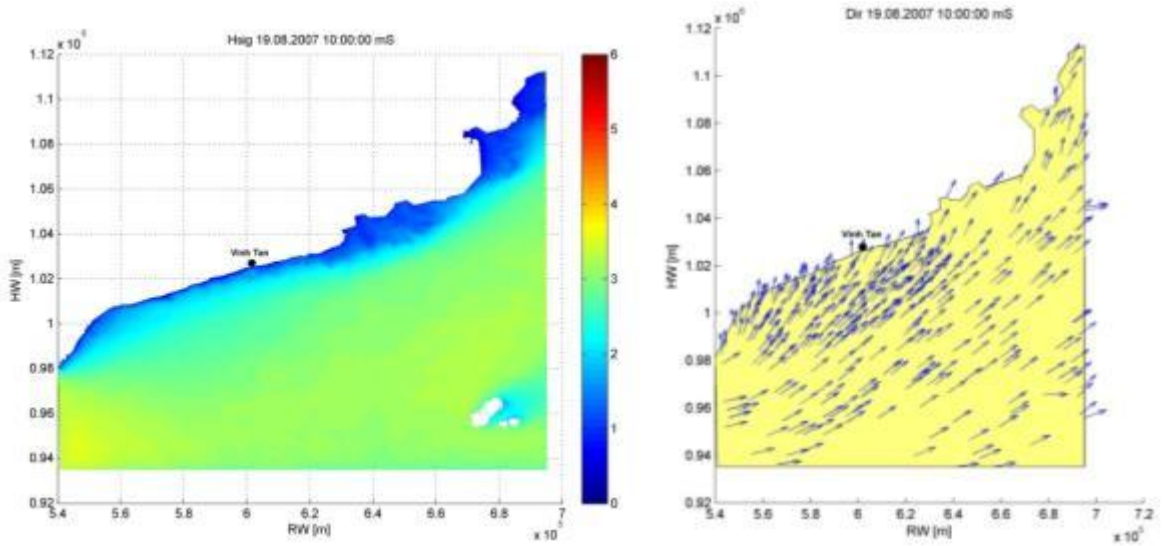

Figure 34: Significant wave heights (left) and wave directions (right) in the modelling area during the southwest monsoon.

Another model run simulated waves during northeast monsoon season with peak wind velocities of 25 m/s (Figure 35, left). For the coast at Vinh Tan, significant wave heights of 0.63 m were computed. Although the wind velocity is higher than in the southwest monsoon scenario, the waves are not significantly higher because Vinh Tan is located in the wave shadow of the Mekong Delta with its sandbanks. Due to refraction, the wave direction changes from northeast offshore to east near Vinh Tan (Figure 35, right). This causes a larger longshore sediment transport component.

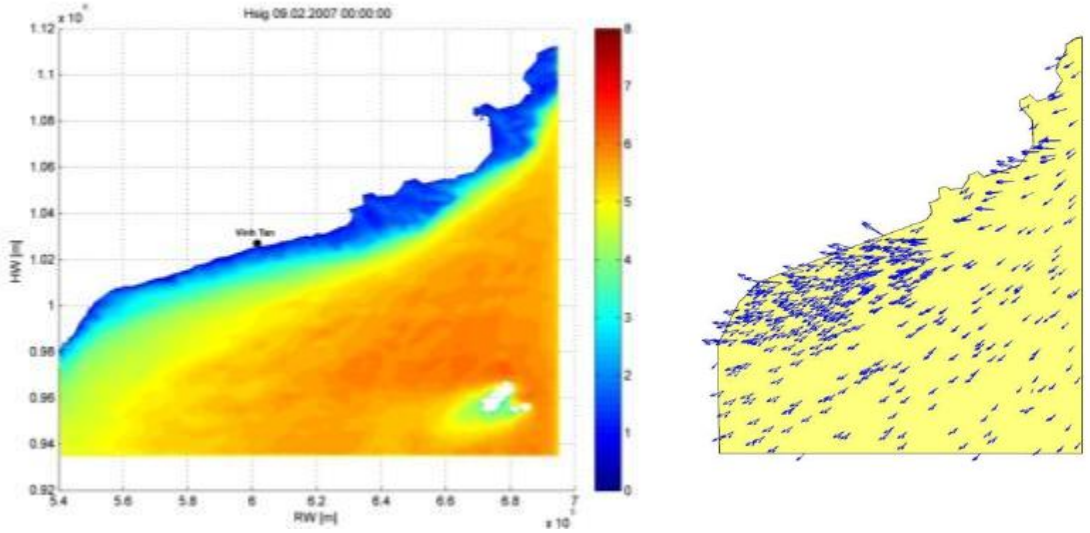

Figure 35: Significant wave heights (left) and wave directions (right) in the modelling area during northeast monsoon.

Table 1 shows a comparison of measured and simulated waves at Bach Ho during various scenarios. A good accordance of the model with field data could be found.

Table 1: Simulated and measured waves at Bach Ho during southwest and northeast monsoon.

			Simulated			Measured	
Scenario	Wind direction [°]	Wind speed [m/s]	Peak period T_P [s]	Sign. wave height H_S [m]	Wave direction [°]	Sign. wave height H_S [m]	Wave direction [°]
1a	SW	16.28	7.3	3.07	227	3.50	270
1b	WSW	18.90	7.3	3.64	240	3.50	270
1c	W	15.75	6.04	2.62	320	3.00	270
2a	NNE	20.53	12.89	6.82	50	6.75	45
2b	NE	25.24	9.70	5.61	50	5.00	45

Table 2 shows the results of the different model runs for the coast of Vinh Tan. The 2b scenario simulating northeast monsoon conditions delivers the wave height relevant to design a coastal protection measure at Vinh Tan.

Table 2: Simulated waves at Vinh Tan during southwest and northeast monsoon.

Scenario	Peak period T_P [s]	Sign. wave height H_S [m]
1a	6.04	0.58
1b	6.04	0.58
1c	9.70	0.54
2a	5.50	0.52
2b	5.50	0.63

5.1.3 Influence of morphologic changes

Possible influences of latest bathymetric changes at Cu Lao Dung and Island 15 (Figure 36) on the wave load at Vinh Tan were discussed. The accretion of sediments at the different mudflats possibly could limit the wave loads on the coast of Soc Trang, especially during northeast monsoon season. Based on new soundings the bathymetry of the model was adapted.

Figure 36 shows the mudflat southeast of Cu Lao Dung and Island 15. The impact of the growing mudflats on the wave load on the coast of Soc Trang was simulated.

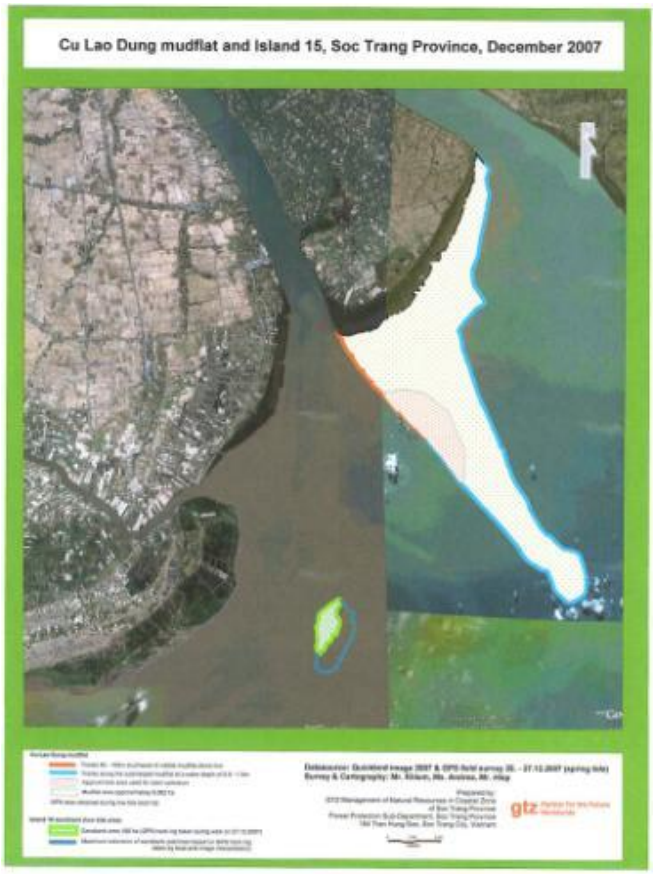

Figure 36: Dimensions of the Cu Lao Dung mudflat and Island 15 in December 2007 (Source GIZ).

For simulating the impacts of the growing mudflats on the wave load at the coast, the model was run with four different bathymetries:

- Model 00 is based on the initial bathymetry. The soundings were done in 2004 when the extension of the mudflats was less advanced
- Model 10 is based on the current (updated) bathymetry including the Cu Lao Dung mudflats and Island 15 (Figure 37)
- Model 11 is based on a scenario that shows a possible extension of the mudflats 25 years in the future. Therefore, in a simplified approach, the development of the last 5 years was extrapolated (. Figure 38)
- Model 12 shows a fictitious bathymetry that definitely has an effect on the wave parameters at the coast (Figure 39)

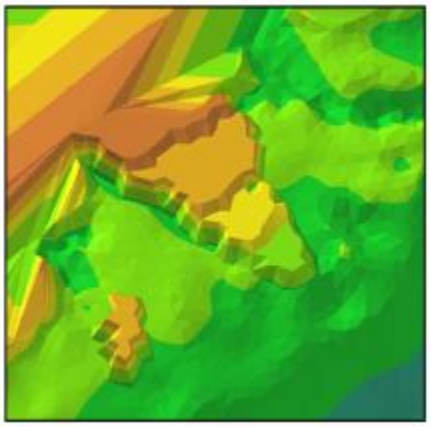

Figure 37: Bathymetry of Model 10.

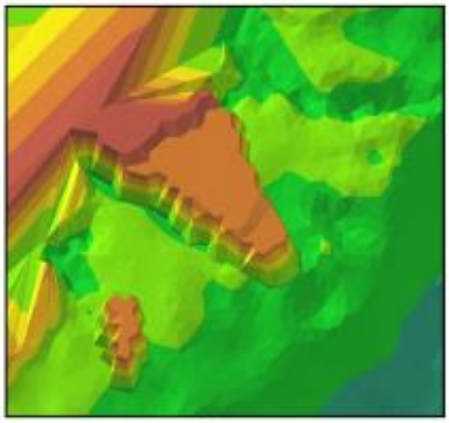

Figure 38: Bathymetry of Model 11.

To visualise the required dimensions of a mudflat at Cu Lao Dung, which has a significant effect on the wave parameters at the coast of Vinh Tan, a fourth model (Model 12) was developed including a fictitious bathymetry at Cu Lao Dung (Figure 39).

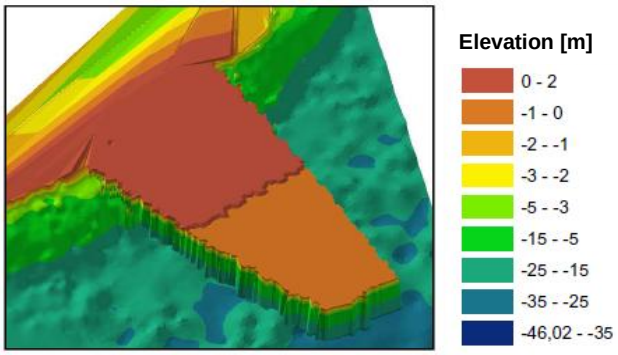

Figure 39: Bathymetry of Model 12.

Figure 40 shows the significant wave heights at the coast of Vinh Tan as a result of the simulation runs. The simulations were computed with a constant wind velocity of 25 m/s from the northeast. There are no significant changes in the wave parameters between Model 00, Model 10 and Model 11. Therefore, the development of the Cu Lao Dung mudflats and Island 15 will not have an influence on the wave load at the coast of Vinh Tan. Nevertheless, the wave climate in the nearer surroundings of these mudflats will be influenced by the changing bathymetry.

The simulation of Model 12 computed a reduction of the wave height of 40% compared to the other simulation runs. A morphodynamic development leading to a mudflat of this dimension is not realistic, but pure fiction.

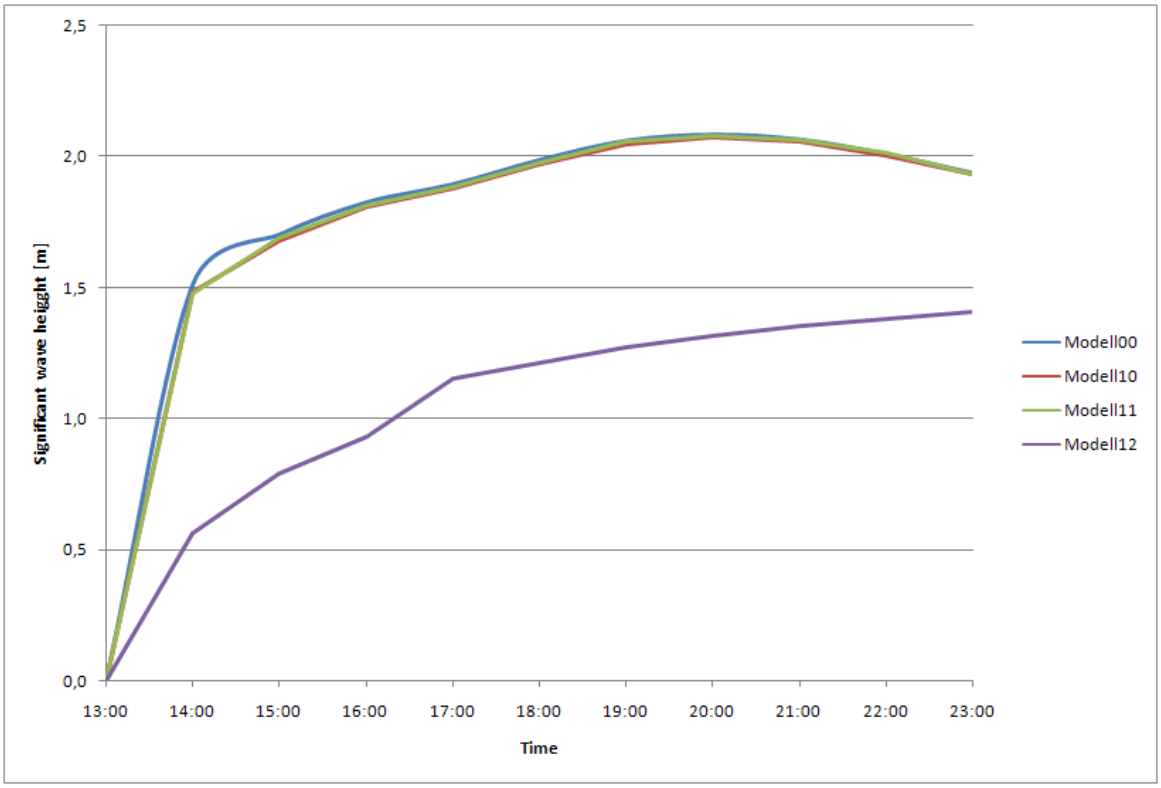

Figure 40: Significant wave heights at the coast of Vinh Tan due to various model runs.

5.2 Hydrodynamic modelling

5.2.1 Boundary conditions and network

Bathymetric data were available in a 500 m grid offshore and a 50 m grid nearshore. Water levels were recorded at different stations at the coast, and river discharges were recorded at the station Can Tho. Figure 41 shows the positions of the various stations and the lines of the same occurrence time of the flood. These data form the boundary conditions for the hydrodynamic modelling.

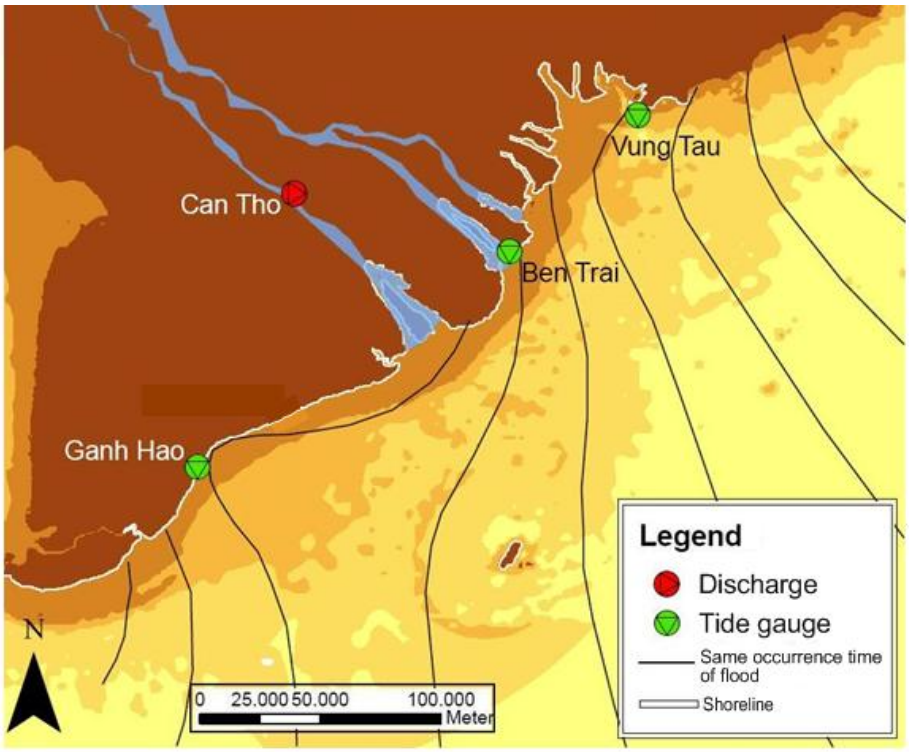

Figure 41: Gauges and discharge stations in the investigation area.

On the basis of the bathymetric data, a two-dimensional depth-averaged numerical model was set-up. Therefore, the Open Source Software system RMA•KALYPSO was used (http://ibpm.bjoernsen.de/kalypso), which consists of various sophisticated hydrological, hydraulic and damage modelling tools, and modern decision support tools for spatial planners in flood risk management. The source code of the numerical model is based on the software RMA 10S (KING, 2006), which is based on RMA2 (DONNELL ET AL., 2006). The further development of the model has been done by the Institute of River and Coastal Engineering of the Hamburg University of Technology (SCHRAGE ET AL., 2009). The drying and rewetting of finite elements of the tidal flat areas is modelled with the marsh porosity method, which is a form of the thin slot algorithms (NIELSEN & APELT, 2003). RMA•KALYPSO has been applied in comparable studies several times (e.g. FALKE & VON LIEBERMAN, 2010, ALBERS ET AL., 2009).

Due to the availability of data and the size of the investigation area, some simplifications were necessary. In the northwest of the modelling area, the boundary of the model is given by the coastline of the provinces Bac Lieu, Soc Trang, Tra Vinh and Ben Tre, including the five most southern branches of the Mekong (Figure 42). These branches discharge approximately 93% of the water (AKIRA, 2005). The modelling area extends over a length of 100 river kilometres into the inland. Smaller branches are neglected. Near the station Vung Tau the boundary runs laterally to the coast in a south-southeastern direction over a length of 80 km, following a line of the same occurrence time of the flood. Then the model boundary continues to the south-southwest parallel to the shoreline. The modelling area is

closed by the southwestern boundary, which runs orthogonal to the coastline. Therefore, the model borders an area of approximately 25,000 km². The maximum distance from west to east as well as from north to south is about 230 km.

The Coriolis force causes problems with angled model boundaries. Due to the nearness of the equator in this case, the problem might be manageable. However, the corners of the model were made round.

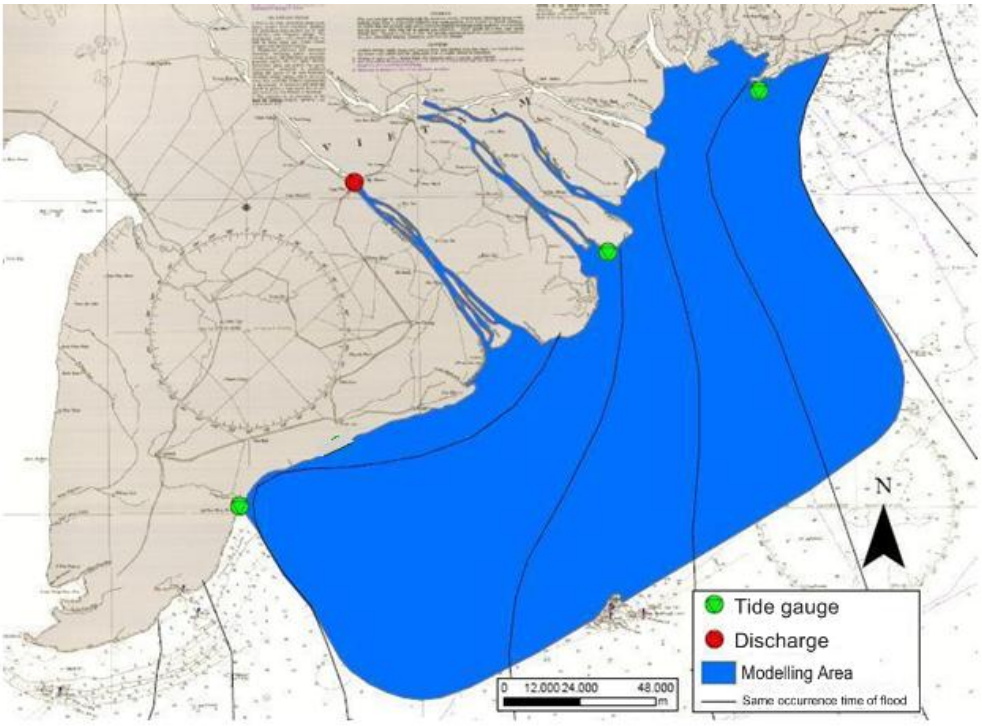

Figure 42: Modelling area including gauges, discharge stations and lines of same occurrence times of the tide.

Due to the size of the modelling area, the boundary conditions do not have an influence on the area of interest. Water levels and discharges are used as boundary conditions. Therefore, the recorded discharges at Can Tho were applied. Figure 43 shows the averaged daily values of discharge in Can Tho. Long-time empirical values show a ratio between the discharge at Can Tho and the other branches of the Mekong (AKIRA, 2005). This simplification is used to create further discharge boundary conditions. It is necessary due to a lack of discharge data at the other branches of the Mekong.

For the northeast and southwest boundary water levels of the stations Ganh Hao and Vung Tau were used as boundary conditions, whereas an offset of 30 minutes was necessary to fit the lines of the same occurrence time of the flood. For the boundary parallel to the coast, a linearly changing water level boundary condition was applied. To create a good approximation to natural conditions, the water level data of Ben Trai was additionally used. Figure 44 shows the generation of the water level boundary conditions.

The northeast and southwest boundaries of the model follow the line of the same occurrence time of the tide. The water levels at the boundary running parallel to the coast are created by a linearised intersection between those lines.

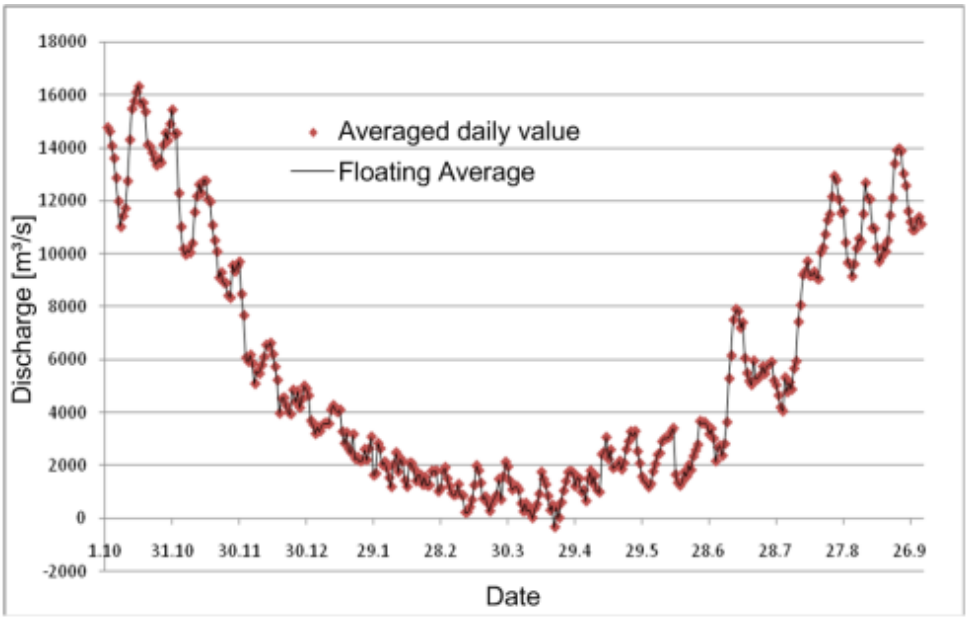

Figure 43: Averaged daily values of discharge in Can Tho (Data: SIWRR).

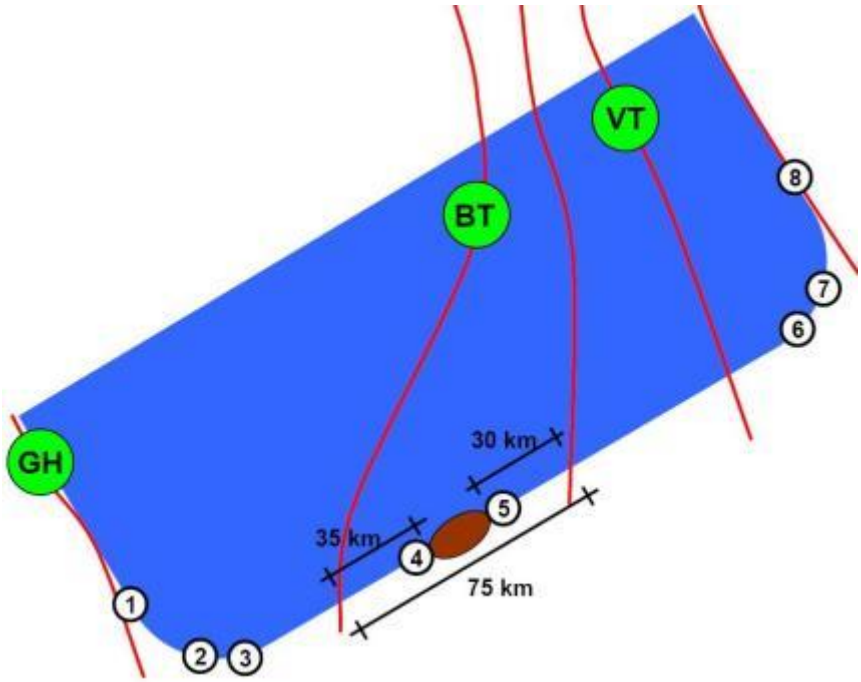

Figure 44: Positions of the computed time series.

The time series were generated as follows:

- (1) equates the time series of the station GH
- (8) equates the time series of the station VT with an offset of -30 minutes
- (3) equates the mean value of the time series GH and BT
- (6) equates the mean value of the time series VT and (8)
- (2) equates the mean value of the time series (1) and (3)
- (7) equates the mean value of the time series (6) and (8)
- (4) and (5) were computed by weighting the time series of BT and the generated time series between BT and VT.

Two simulation scenarios, identical to the wave modelling, covering the northeast and southwest monsoons were chosen. A transient oscillation of five tidal cycles was chosen to eliminate the influences of the initial conditions of the model.

Data from 2006 and 2007 are available as hourly values. To improve the stability of the simulation the time steps are reduced to 20 minutes, whereas a linear interpolation of the data was done.

At the boundary of the fluid and the sediments the current induces shear stresses. If a critical shear-stress is exceeded, bed material starts to move. The bottom friction decelerates the current. To quantify this loss of energy the bottom friction is assessed using empirical parameters. Following the approach of VAN RIJN considering the grain size $d_{90}$and the presence of dunes, a bottom friction k_s* = 1.5 mm is used near the coast. For the areas covered with mangroves, the bed roughness class 3 implemented in RMA•KALYPSO was chosen. The included parameters are:

k_s = 0.25 m; $a_x = a_y$ = 3.00 m; d_p = 0.10 m.

The digital elevation model of the modelling area builds the foundation for the finite element network (Figure 45). It is integrated in the simulation in the form of a triangulated irregular network (TIN).

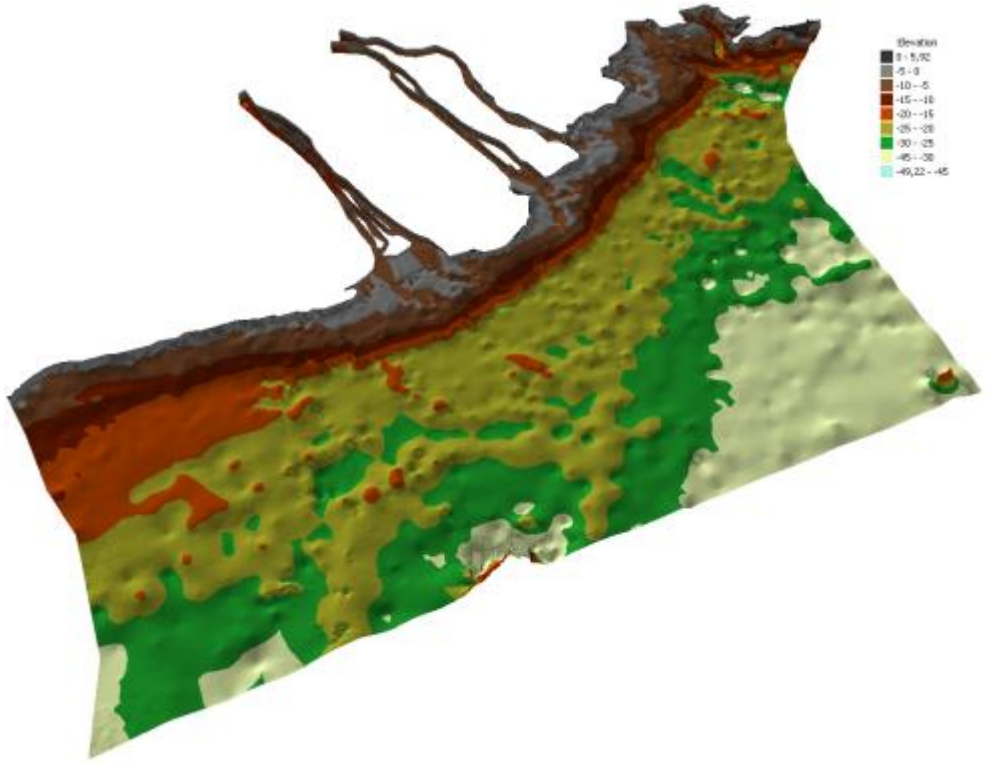

Figure 45: Digital elevation model.

The finite element network is created based on:

- The digital elevation model in the form of a TIN
- The model boundaries in the form of a polyline (*.shp-file)
- Break lines in the form of a polyline (*.shp-file)

The break lines are used to refine the network in certain areas. For example, along the embankments of the river branches a narrow row of elements is generated. The finite element network is created by means of the open source software Gaja3D, developed by the Institute of River and Coastal Engineering. Therefore, the desired maximum cell size and the minimum angle in triangular elements have to be defined. Small angles (< 15°) are not reasonable because they reduce the stability of the simulation.

Figure 46 shows the different roughness classes in the modelling area. Taking into consideration different roughness classes and zones of different eddy viscosities, it was differentiated between rivers, river mouths, shorelines and deeper and shallower ocean areas. Furthermore, at the model boundary, an additional class was introduced.

This last zone of high eddy viscosities supports the converging of the simulation. It has a damping effect on the velocity vectors and avoids a rotation of the computed currents. Figure 47 shows this rotation of the velocity vectors due to too small eddy viscosities causing divergence of the model.

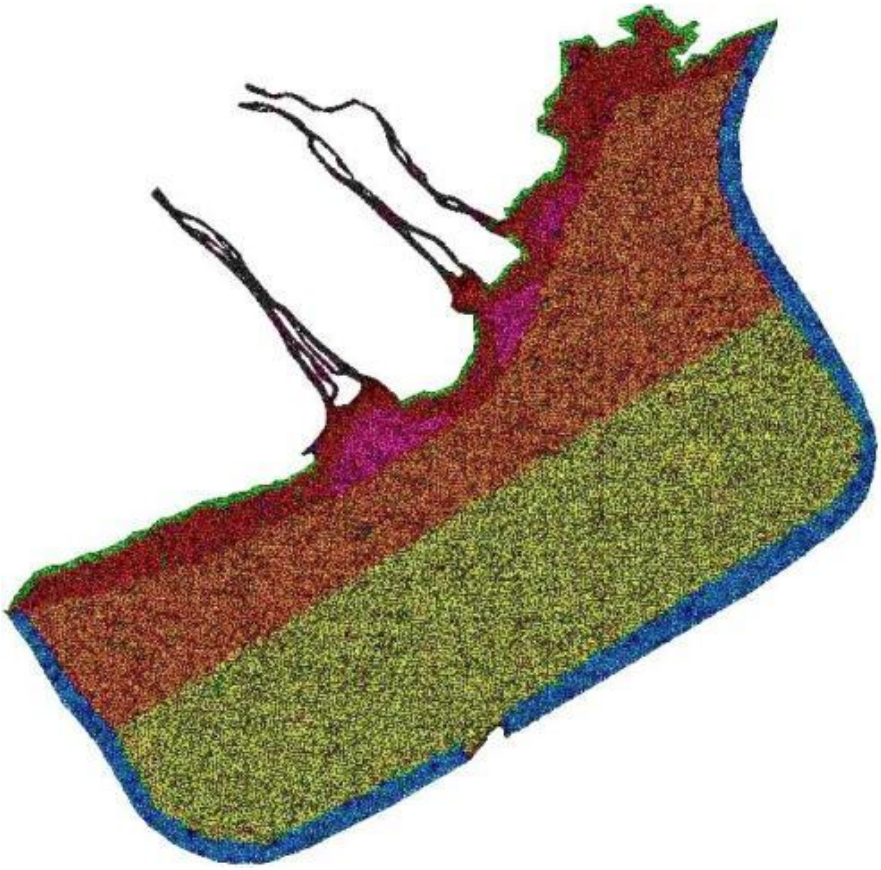

Figure 46: Different zones of roughness and eddy viscosities in the modelling area.

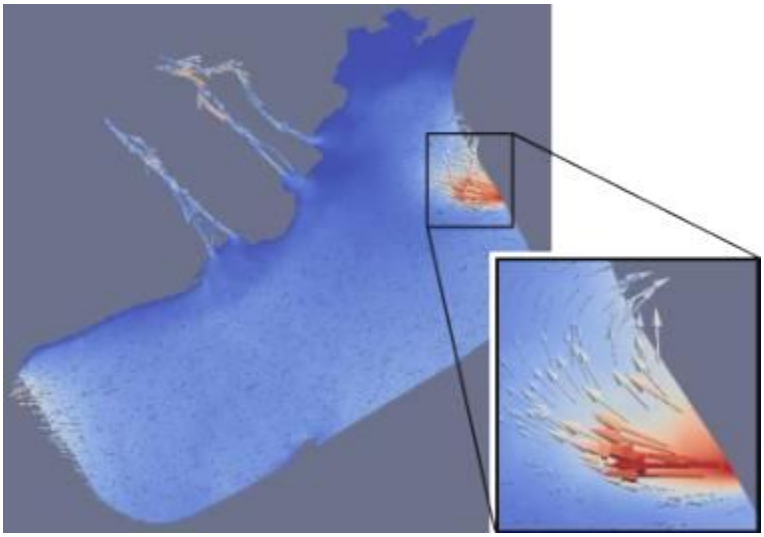

Figure 47: Formation of an eddy at the model boundary due to insufficient eddy viscosities.

5.2.2 Results

Figure 48 and Figure 49 show computed water levels and current parameters during flood tide. The approach of the tide from the northeast to the southwest and the resulting currents are clearly visible. The flood current is running parallel to the coastline, whereas lower water depths and an increasing influence of the bottom friction decelerate the current velocity with decreasing distance to the shore. In the nearshore area, the current velocities are between 0.20 and 0.50 m/s. The current measurements in the focus area were used to verify the results of the simulation. Measured and computed currents show a good correlation.

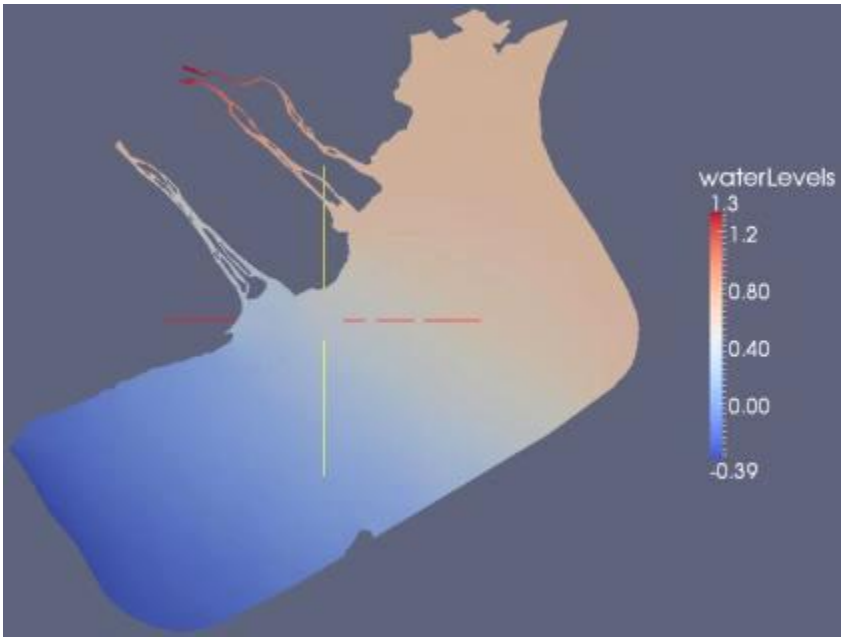

Figure 48: Computed water levels in the modelling area.

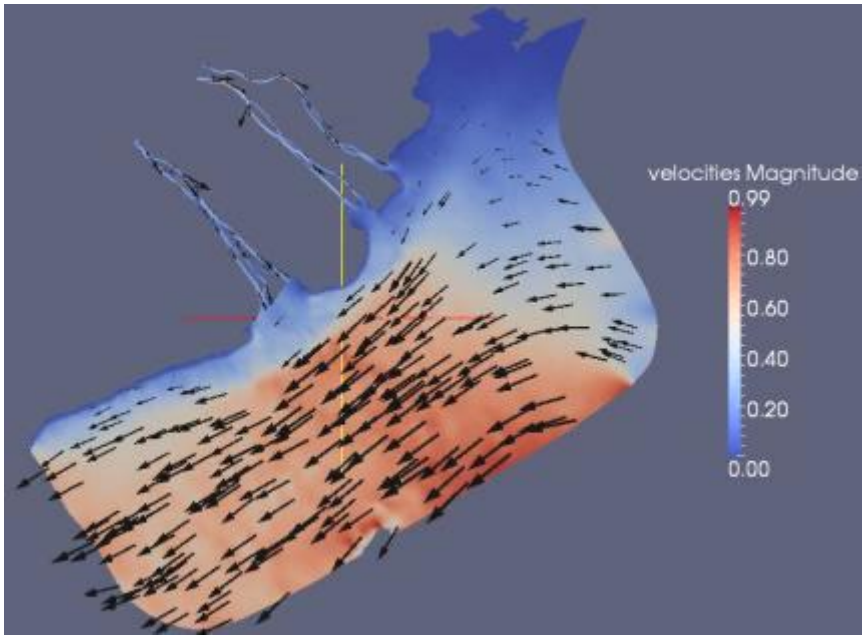

Figure 49: Computed current velocities in the modelling area.

5.3 Modelling of shoreline changes

The results of the hydrodynamic modelling were handed over to the morphodynamic model, which simulates the shoreline changes in the focus area. Therefore, the numerical model GENESIS (HANSON & KRAUS, 1989) was used. It has been applied in numerous comparable surveys (e.g. FRÖHLE ET AL., 2008).

Again, the bathymetric data built the geometric basis for the model setup. Wave conditions, current parameters, sediment characteristics and water levels form the boundary conditions of the model.

The soundings carried out in 2010 were used to calibrate the model. Afterwards, various measures of erosion protection were integrated and the changes of the shoreline were analysed.

5.3.1 Boundary conditions

Available wave data of one year were analysed and summarised to 30 characteristic events. These events occur with a computed frequency and are the driving force for the shoreline changes. Figure 50 shows 4 exemplary events. The polar diagram of the wave spectra indicates the direction and the intensity of the wave conditions. During one characteristic year, wave events from northeastern directions dominate.

As further boundary conditions, the simulated water levels and current parameters were used. Characteristic sediment parameters were taken from the results of the sediment sampling.

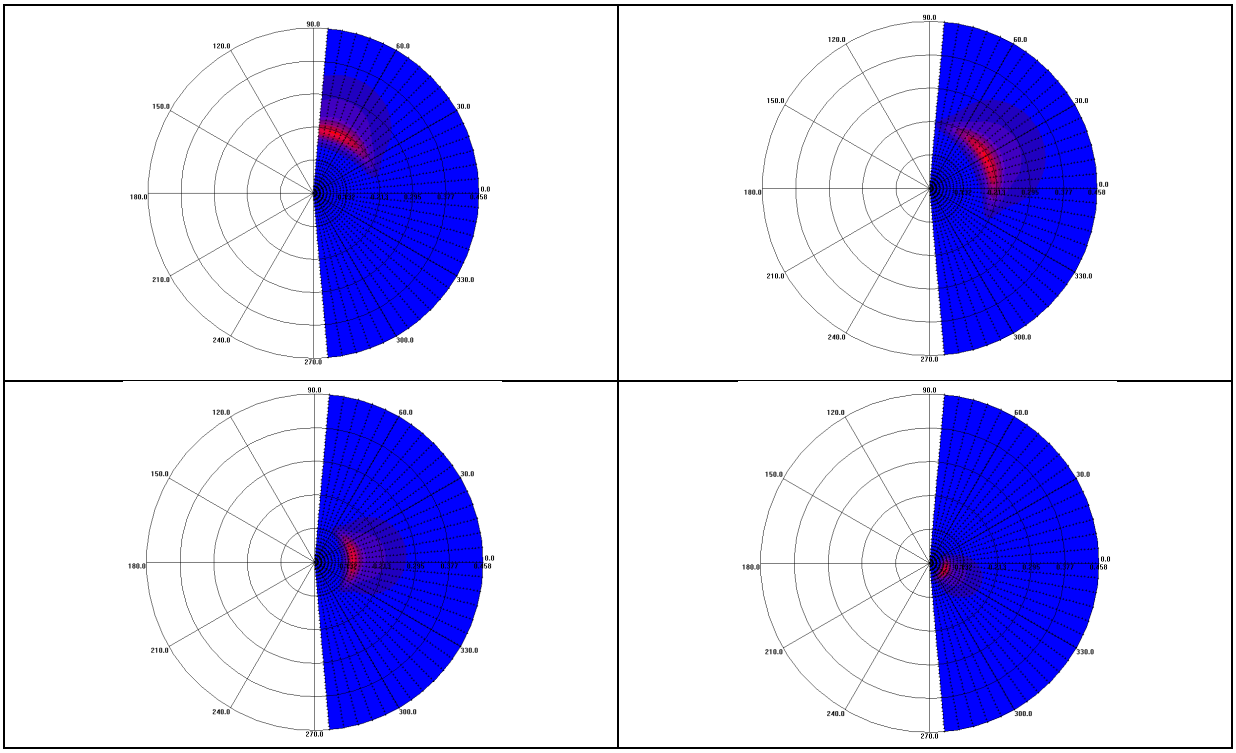

Figure 50: Different wave events considered in the morphodynamic modelling; red colour indicates high wave energy.

Figure 51 shows the domain of the morphodynamic model covering the focus area. The isolines indicate the bathymetry, the colours connote the wave heights and the arrows show the wave directions. Due to the bathymetry, a corridor of higher waves approaches the coast pointing to the coast at Vinh Tan.

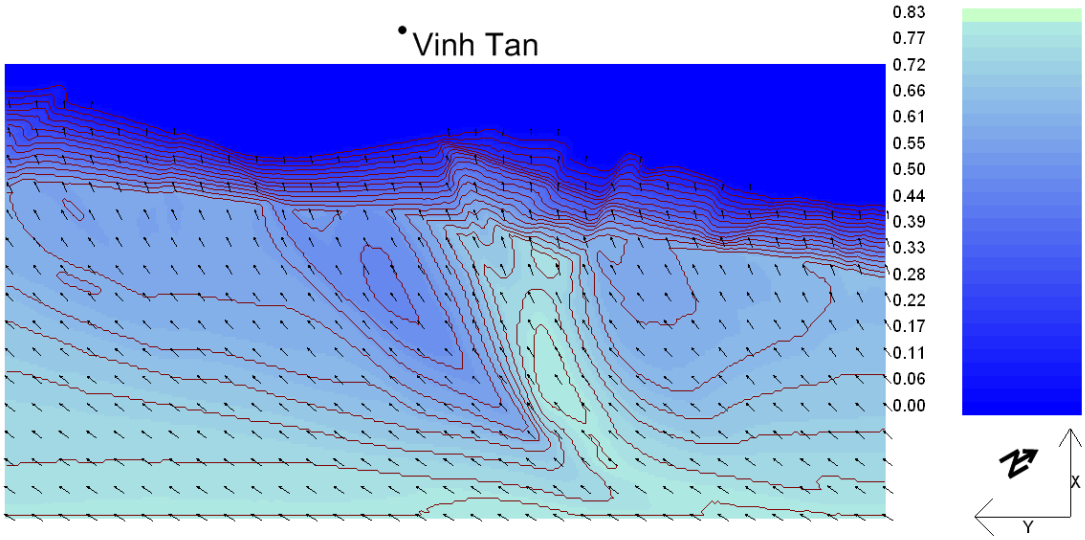

Figure 51: Bathymetry, wave heights and wave directions in the modelling area at the coast of Vinh Tan.

For the initial shoreline, a simplified approach is used: the bathymetry is available in a 50 m grid. Due to this resolution and the acquisition date of the data, the latest and detailed dimensions of the flood plains cannot be integrated into the simulation. The shoreline is defined as the -0.20 m isoline and approximately matches the erosion edge of the floodplain and the adequate connection between adjacent floodplains in case of eroded areas such as the focus area. At the endangered dyke, the initial shoreline of the model does not match the toe of the dyke, but rather the connecting line between the floodplains east and west of the focus area (Annex).

5.3.2 Morphologic changes without countermeasures

Figure 52 shows the natural shoreline changes in the modelling area without any countermeasures. Figure 53 shows the shoreline changes around Vinh Tan in detail. The diagrams at the top indicate the initial shoreline, the shorelines after 1 year, 2 years, 3 years and 5 years. Additionally, the shoreline after one year with increased wave activity was computed. The diagrams at the bottom show the differences between the initial shoreline and the computed shorelines. Negative values indicate erosion. The longer the simulation period is, the larger are the uncertainties of the results. A simulation time of 3 years and more just gives a rough estimate of the development.

Along the coast of Vinh Chau areas of accretion and erosion occur. East of Vinh Tan natural accretion occurs. The longer the simulation time is, the larger are the erosion and accretion rates. But also the wave activity has a large impact on the shoreline. If the wave energy increased by 50%, erosion or accretion may be twice or three times as large as during a normal year. It becomes clear that increased wave activity does not only lead to erosion. In some areas the eroded material deposits again. In the focus area around Vinh Tan in general the shoreline is eroded.

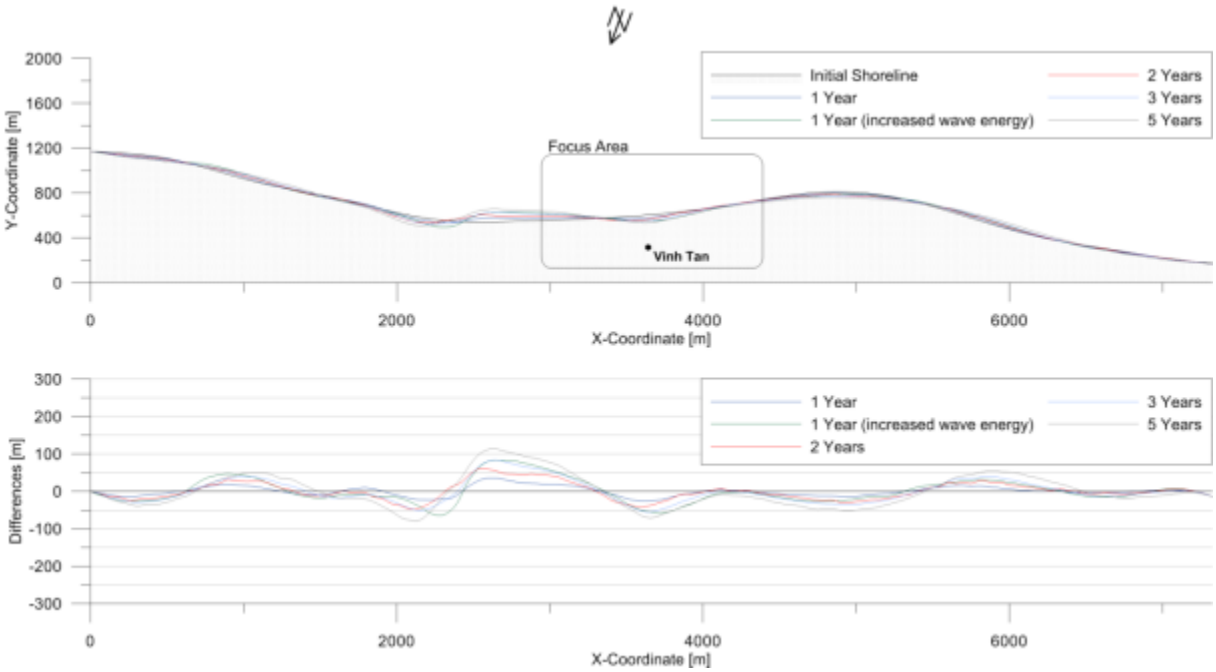

Figure 52: Shoreline changes in the modelling area without countermeasures.

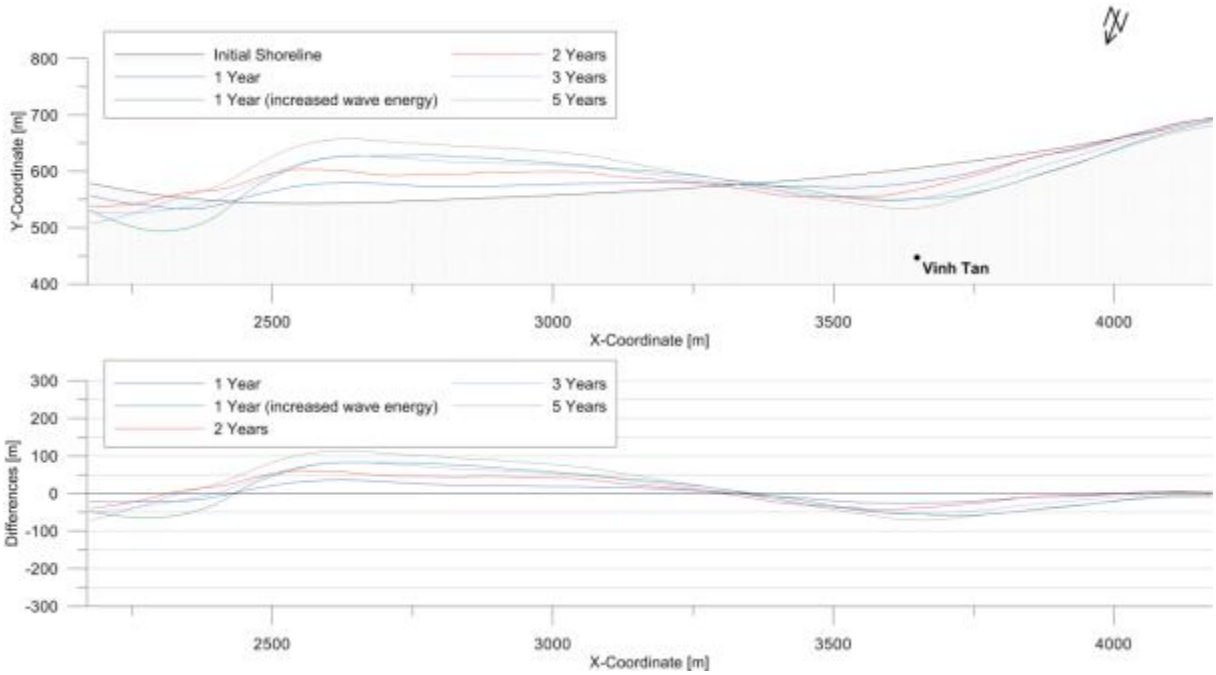

Figure 53: Shoreline changes in the focus area at Vinh Tan without countermeasures.

5.3.3 Installation of breakwaters

The shoreline changes after the installation of different erosion protection measures were simulated. The simulation time was one year. Figure 54 shows the effect of one breakwater with the length of 200 m at a distance of 300 m to the shoreline. A massive and impermeable structure is assumed. The transmission coefficient changes due to varying water levels and wave parameters. The average value is 0.3, which means that the wave heights landwards of the breakwater are less than one third of the wave height seaward of the breakwater. In the shaded area of the breakwater a salient is formed, which does not reach the breakwater. The salient affects the longshore sediment transport significantly and erosion occurs especially west of the salient.

The erosion rate is between 50 and 80 m per year. The dyke is an artificial boundary and will decelerate the erosion. However, if the simulated shoreline intersects the current course of the dyke, the dyke stability is endangered.

Figure 55 shows the effects of one 100 m long breakwater, depending on the distance to the shoreline. The structure is less massive than in Figure 54, and the average transmission coefficient is 0.5. If the breakwater is constructed in a distance of 200 m to the shoreline, the effects on the shoreline are not significant. At the endangered dyke, accretion of less than 10 m occurs, but downdrift erosion does not occur at all. If the distance to the shoreline is reduced to 50 m, a complete tombolo is formed. East of the tombolo the shoreline does not change. West of the tombolo erosion of 10 to 20 m occurs. Larger wave activity increases the erosion up to 25 m to 30 m.

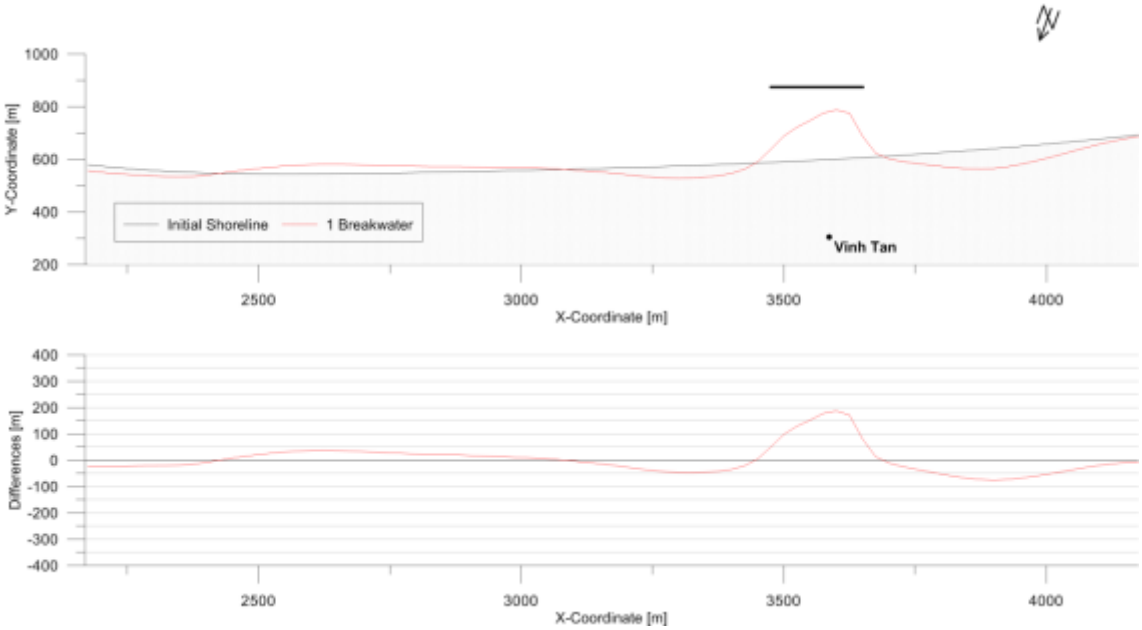

Figure 54: Shoreline changes in the focus area after the installation of one breakwater.

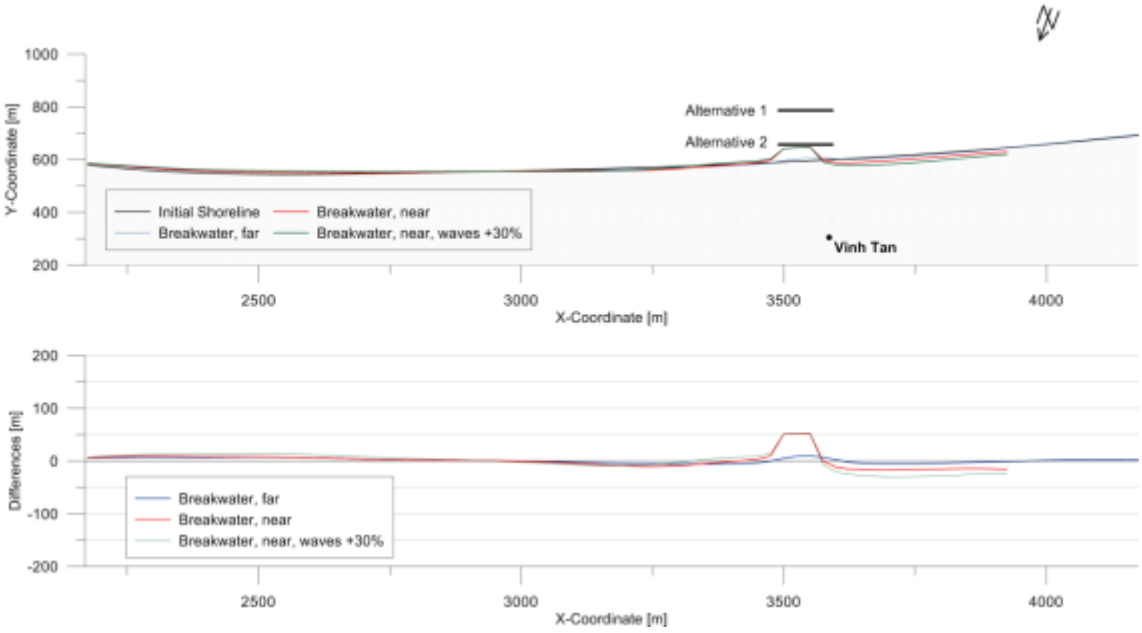

Figure 55: Shoreline changes in the focus area after the installation of a breakwater depending on the distance to the shore and the wave climate.

Figure 56 shows the effect of different types of breakwaters. Depending on the construction, the average transmission coefficient varies. If the construction is nearly impermeable, the transmission coefficient is low and a complete tombolo is formed. With increasing permeability, the transmission coefficient increases and the tombolo shrinks. If the transmission coefficient is 0.8 the downdrift erosion is least, but the dimensions of the salient are not significant.

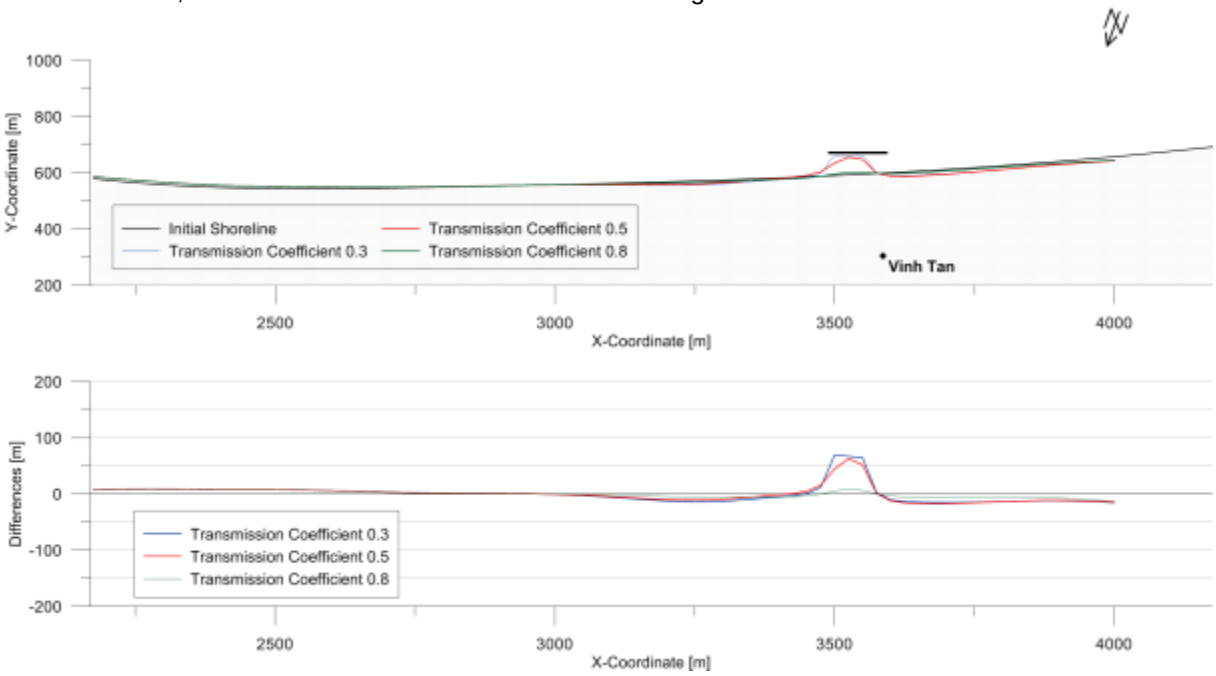

Figure 56: Shoreline changes in the focus area after installation of a breakwater depending on the transmission coefficient; distance to the shoreline: 50 m.

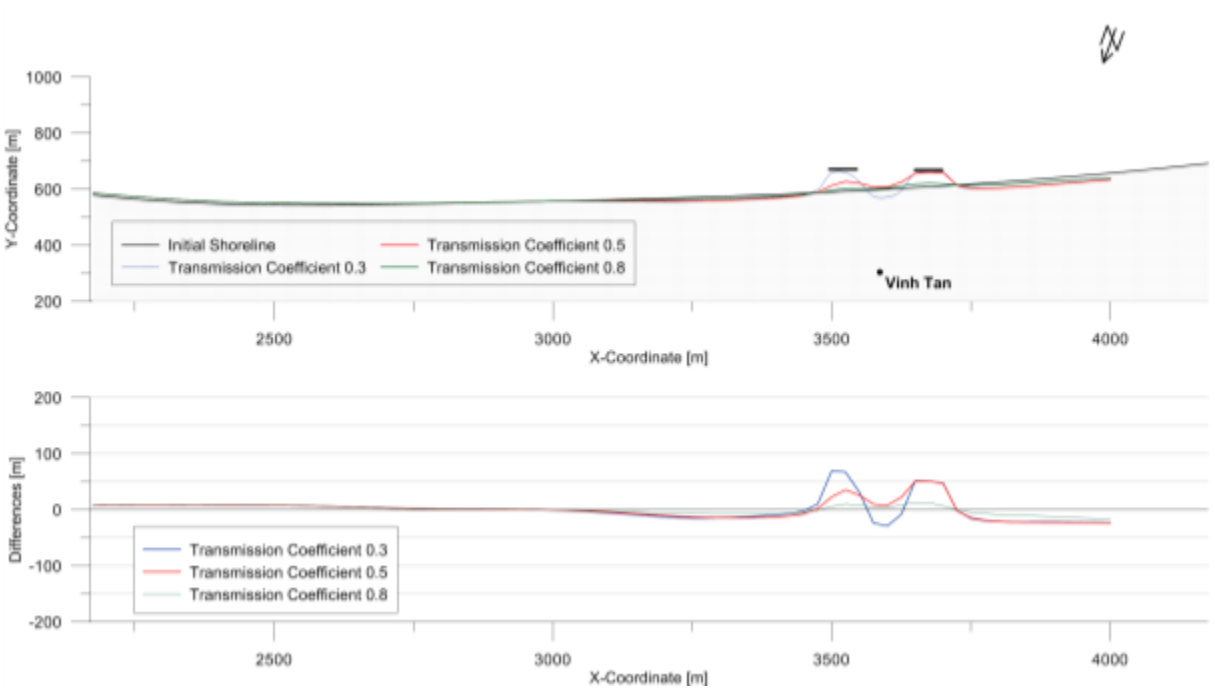

Figure 57: Shoreline changes in the focus area after installation of two breakwaters depending on the transmission coefficient.

Figure 57 shows the installation of two shorter breakwaters (50 m) at a distance of 50 m to the shoreline. With a transmission coefficient of 0.5 one complete tombolo and one salient are formed. The gap between the breakwaters does not create erosion at the shoreline. The downdrift erosion west of the tombolo is around 20 m. The downdrift erosion east of the tombolo is not significant.

Based on the simulation runs described before, Figure 58 shows a possible configuration of breakwaters in the focus area to protect the endangered dyke. The length of the section, which has to be protected, is 200 m. The studies above showed that the best distance to the shoreline is about 50 m and the mean transmission coefficient should be 0.50. The gap between the breakwaters is 25 m. A length of the breakwaters of 100 m offers a wider protection area. There are no significant differences concerning the downdrift erosion compared to a length of the breakwater of 75 m. In both cases, the downdrift erosion west of the structure is approximately 25 to 30 m.

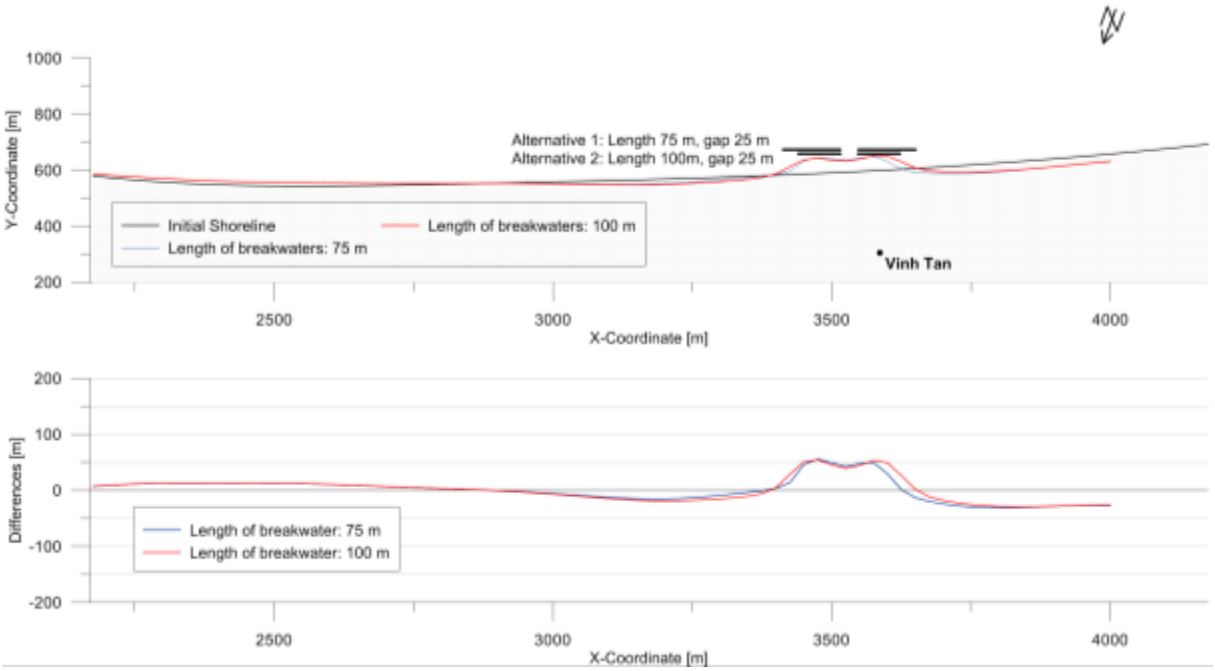

Figure 58: Shoreline changes in the focus area after installation of two breakwaters depending on the length of the breakwaters.

5.3.4 Installation of groins

In addition to the installation of breakwaters, the effects of groins were investigated. Figure 59 shows shoreline changes after the installation of three groins with a length of 250 m each and at a distance of 200 m. In the nearer surroundings of the groins accretion occurs. Due to the main wave direction from the northeast in the west part of the groin field erosion dominates. The positive effects of the groins on the shoreline are negligible, because accretion only occurs in limited areas.

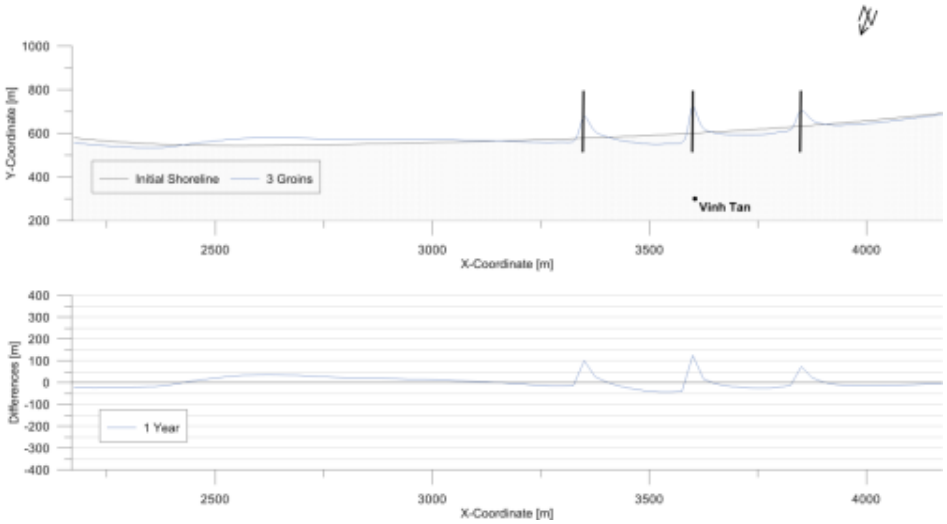

Figure 59: Shoreline changes in the focus area after the installation of three groins.

6 Design of erosion protection

The aim of the structural measures is to reduce erosion and to increase accretion. Negative effects, such as downdrift erosion, must be avoided as far as possible. In Chapter 5, the effects of different erosion protection measures on the shoreline were simulated. The sufficiency of the measures, the positions and the best transmission values were identified. Figure 60 shows the recommended arrangement of breakwaters in the focus area as the result of the modelling. The distance to the idealised shoreline is 50 m. The distance to the dyke is approximately 100 m. Two breakwaters with a length of 100 m each and a gap of 25 m between them lead to the formation of a nearly complete tombolo. Only at the gap is the salient relocated backward. The computed shoreline shows downdrift erosion, which means that the existing floodplains will be further eroded.

In this chapter the design of the breakwaters itself is carried out. Different application examples are discussed.

Important boundary conditions for the design are:

- Soft soil with silty and clayey material
- Significant wave heights of 0.65 m
- Wave periods between 5 s and 6 s
- Tidal range of 3.50 m
- Water depths at the dyke of up to 2 m at high water.

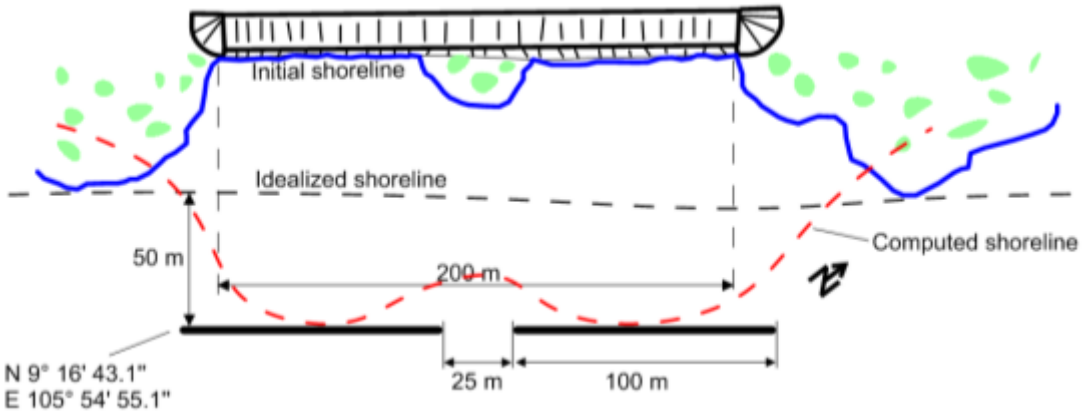

Figure 60: Recommended arrangement of breakwaters in the focus area.

Due to the boundary conditions in the focus area some structures are not sufficient. Because of the soft soil, heavy structures should be avoided. An adequate foundation would be too expensive and the risk of base failure due to wave action and liquefaction is too high. Floating breakwaters are also not applicable. Their effectiveness is limited to areas with wave periods less than 4 s (SORENSEN, 2001).

In the medium term mangroves should be replanted in the developing accretion area. When the mangroves reach a certain size they should be able to form a natural erosion protection system (CHONG, 2005). So, temporary structural measures are possible as well.

6.1 Conventional breakwaters

Breakwaters differ in position (deep/shallow water), construction type (dumped, vertical, floating) and effectiveness (development of salients or tombolos). Combinations are possible.

Furthermore, differences in the construction height of the breakwater exist. Some breakwaters are emerged, while some are submerged. The most commonly used type of breakwaters is the dumped breakwater with a crest height above mean high water (U.S. ARMY CORPSOF ENGINEERS, 2002).

Dumped breakwaters consist of several layers of graded stones (Figure 61). In general, they are constructed as detached breakwaters. The layered arrangement is used to reduce construction costs and to decrease permeability.

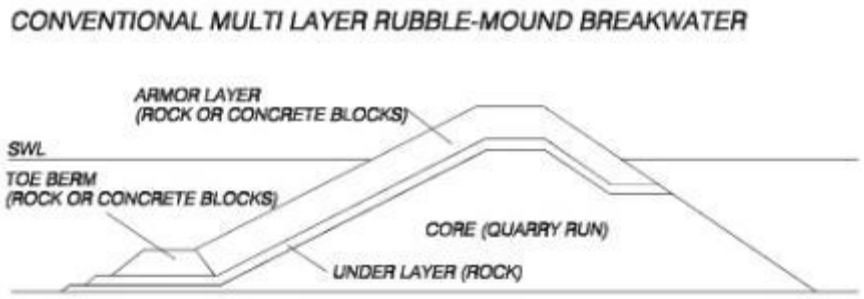

Figure 61: Rubble mound breakwater (U.S. ARMY CORPS OF ENGINEERS, 2002).

The most important parameter for the design of a rubble mound breakwater is the required stone size of the armour layer. This size is influenced by:

- The design wave height, normally H_s
- The characteristics of the armour layer (thickness, arrangement)
- The slope of the armour layer
- A possible overflow

Following the approach of Hudson (U.S. ARMY CORPS OF ENGINEERS, 2002), the required specific weight can be assessed by:

$$W_{50} = \frac{\gamma_S H^3}{K_D (\frac{\gamma_S}{\gamma_W} - 1)^3 \cot\theta}$$

W_{50} = Weight of a single armour stone
γ_s = Specific weight of the stone material
H = Design wave height
K_D = Stability coefficient
γ_w = Specific weight of water
θ = Slope

After the length of the breakwater, the distance to the shoreline and the number of breakwaters are set by means of numerical modelling, and then the construction of the breakwater itself has to be designed. Design parameters are crest height, crest width, permeability and slope.

According to the Hudson Formula, the weight of a single armour stone can be calculated:

$$W_{50} = \frac{\gamma_S H_S^3}{K_D \left(\frac{\gamma_S}{\gamma_W} - 1\right)^3 \cot\theta} = \frac{25 \cdot 0.60^3}{1.2 \cdot (\frac{25}{10} - 1)^3 \cdot 3} = \underline{0.44\ kN}$$

Additionally, the mean diameter of the armour stones can be calculated:

$$\frac{H_S}{D_{N50}} = \left(\frac{\gamma_S}{\gamma_W} - 1\right)(K_D \cdot \cot\theta)^{1/3}$$

$$D_{N50} = \frac{H_S}{\left(\frac{\gamma_S}{\gamma_W} - 1\right)(K_D \cdot \cot\theta)^{1/3}} = \frac{0.60}{\left(\frac{25}{10} - 1\right)(1.2 \cdot 3)^{1/3}} = \underline{0.26\ m}$$

The Hudson Formula contains some simplifications. For example, regular waves are assumed, while wave periods and the duration of a storm are not taken into consideration. For comparison, the formula of van der Meer is applied. The formula is a modification of the Hudson Formula, and additionally considers the breaker type, porosity, damages to the armour layer and the number of waves occurring during a storm event:

$$\frac{H_S}{\left(\frac{\gamma_S}{\gamma_W}-1\right)\cdot D_{N50}} = P^{-0.13}\cdot\left(\frac{S}{\sqrt{N}}\right)^{0.2}\cdot\sqrt{\cot\alpha}\cdot\xi_m^P$$

D_{N50} = mean diameter of an armour stone
P = Porosity of the armour layer (0.1…0.6)
S = Degree of damage to the armour layer
N = Number of waves during the designed storm event (<7500)
ξ = Irribaren number (ξ_m = 2.9, ξ_{crit} = 2.5)

$$D_{N50} = \frac{0.60}{\left(\frac{25}{10}-1\right)\cdot 0.5^{-0.13}\cdot\left(\frac{8}{\sqrt{3600}}\right)^{0,2}\cdot\sqrt{3}\cdot 2.9^{0.5}} = \underline{0.19\ [m]}$$

The results of the two approaches are comparable. Due to the larger number of considered parameters, the formula of van der Meer should be applied.

Figure 62 shows the arrangement of a rubble mound breakwater in the investigation area. The upper diagram (1) shows the coastal profile from July 2010 with the mean higher low-water (MHLW) and the

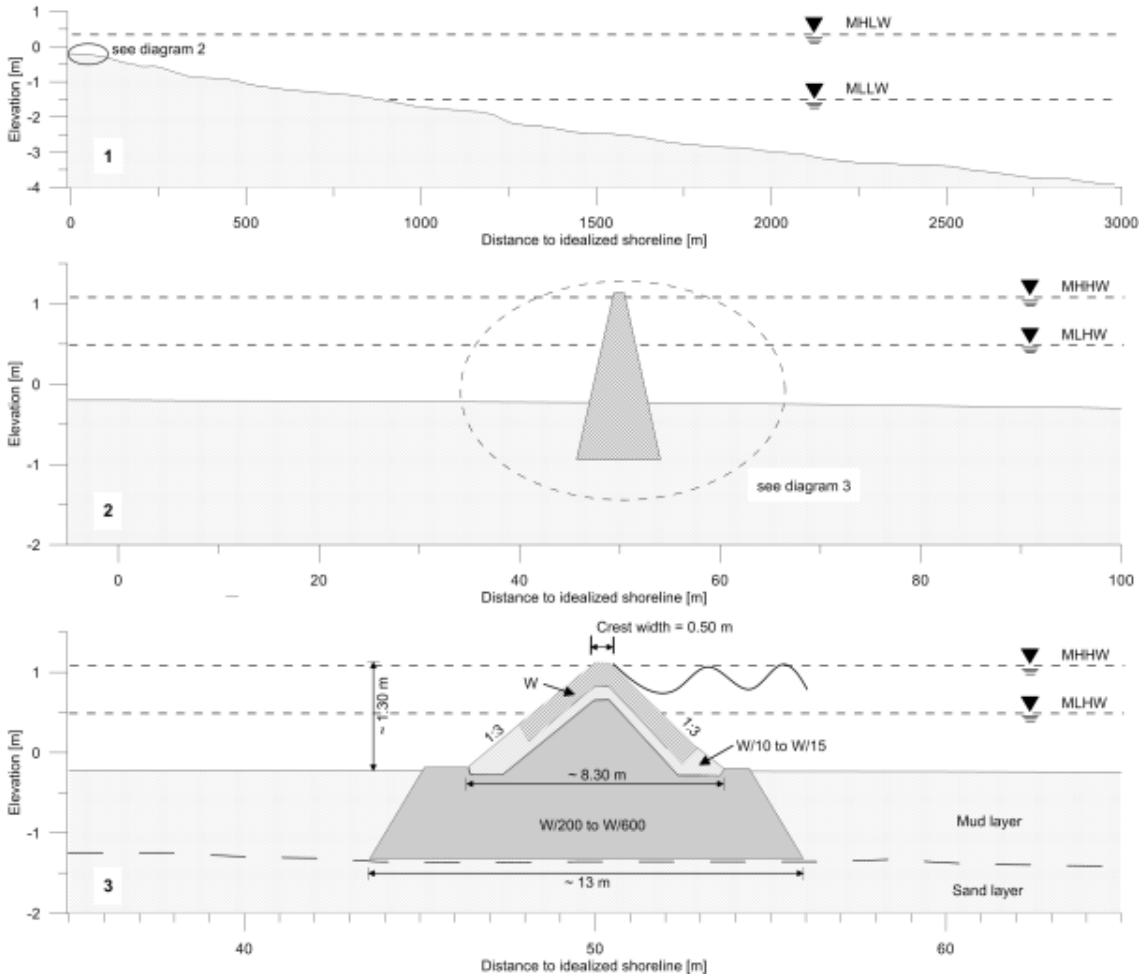

Figure 62: Arrangement of a rubble mound breakwater in the investigation area.

mean lower low-water (MLLW). The diagram in the middle shows a section closer to the coast and the diagram below shows details of the construction of the breakwater including the mean higher high-water (MHHW) and the mean lower high-water (MLHW). The breakwater is completed as a standard unit (U.S. ARMY CORPS OF ENGINEERS, 2002). The foundation of the construction has to be on the sand layer.

The construction of a nearshore breakwater is complex. Large amounts of quarry stones and armour stones are required. Therefore, the costs of a rubble mound breakwater are high. A detailed calculation has to be done by means of local quotations. International prices for rubble mound breakwaters are between 60,000 USD and 160,000 USD for 100 m, depending on the construction site, required foundation, availability of stones, labour costs, etc.

6.2 Groins

The design of groins is similar to the design of breakwaters; just their arrangement differs. They have to be designed based on the same loads as the breakwater. The diameter of stones of the armour layer is the same as in Chapter 6.1.

6.3 Geotubes

Within the last decade geotextiles were used to construct breakwaters and groins. Geotextiles are a synthetic, very tough texture filled with sand or a sand-fluid-mixture. Bags, mattresses and tubes are differentiated (PILARCZYK, 2003). For these systems, only few design approaches exist. Experiences from successful and non-successful projects are integrated into new applications. A large advantage is the short transportation of the filling material.

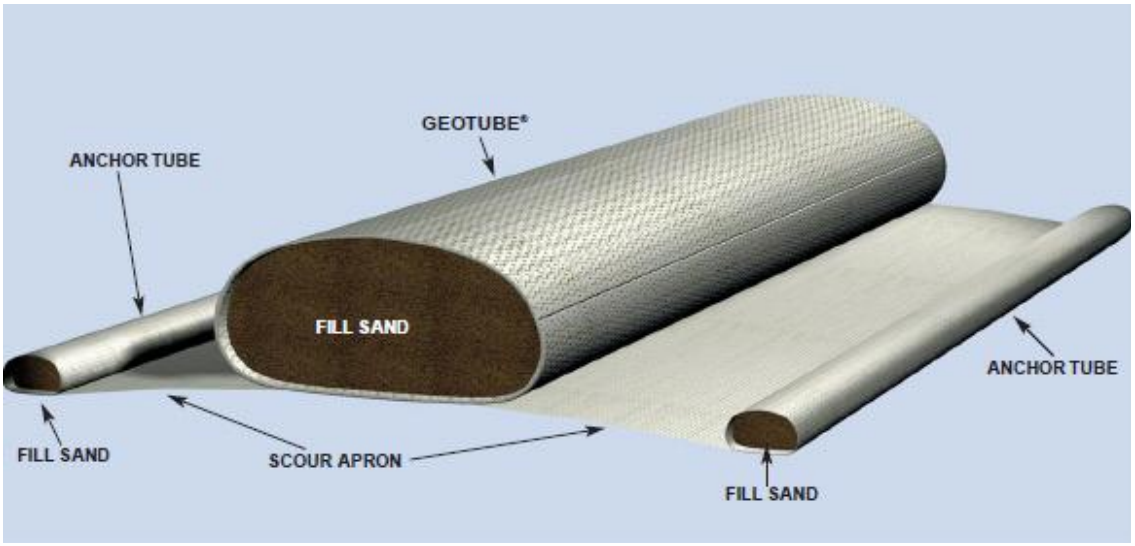

Figure 63: Example of a Geotube® (Source: INGENIERIA AyS.; http://www.geotubosvenezuela.com).

Geotubes® (Figure 63) were applied as coastal protection system, such as breakwaters, several times (PILARCZYK, 1999). Geotubes are supplied as ready-for-use tubes with intakes in regular distances. The tubes are filled by pumping a sand-fluid-mixture into them.

The design is carried out based on the approach by PILARCZYK (1999). The stability of a geotextile tube is secured, if the following condition is followed:

$$\frac{H_S}{\Delta \cdot b} < 1$$

$$\frac{H_S}{\Delta \cdot d} < 1$$

$\Delta = \frac{\rho_s - \rho_w}{\rho_w}$ = Ratio of the densities of water and filling [-]

b = Width of the tube [m]

d = Mean height of the tube [m]

Due to the internal instabilities of the sand, the maximum wave height for Geotubes used as breakwaters is between 1.50 m and 2.00 m.

The design formulas result from experiments with a Geotube filled with mortar. The application of the approach for a Geotube filled with sand is not completely clear.

For the existing loads, the dimensions of the Geotube can be assessed by the following approach:

$$\Delta = \frac{\rho_s - \rho_w}{\rho_w} = \frac{1.6 - 1.025}{1.025} = 0.56$$

$$\rightarrow d > \frac{H_s}{\Delta} = \frac{0.60}{0.56} = \underline{1.07\ m}$$

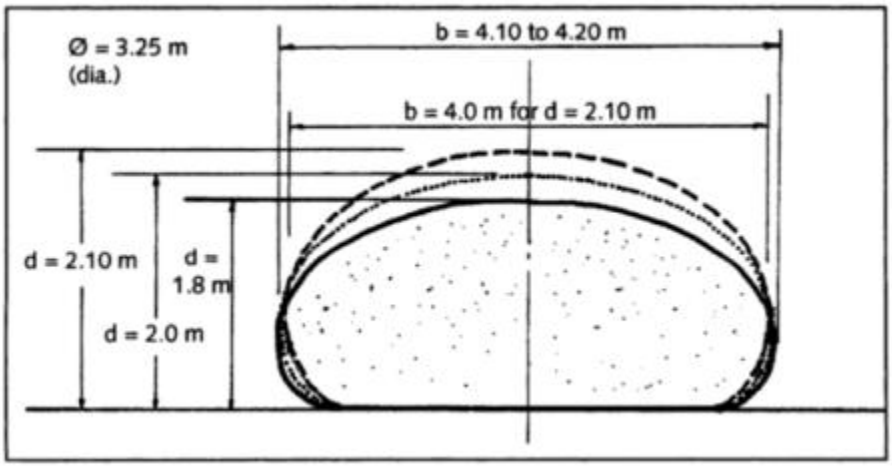

Figure 64: Examples of various Geotextile-Tube sizes (PILARCZYK, 1999).

Figure 64 shows examples of various sizes of Geotubes (PILARCZYK, 1999). Due to deformations, large widths are necessary to achieve the desired heights. Consequently, Geotubes are massive constructions.

Figure 65 shows the arrangement of a breakwater constructed from Geotubes. The pre-design and the water depths in the focus area result in the height of the Geotube. Producers offer adequate products and secure the stability. For a height of 2.00 m, a perimeter of 15 m is required, which results in a width of approximately 6.00 m. The construction has to be founded on sand, whereas the foundation may be constructed from two further Geotubes.

The costs for a breakwater constructed from Geotubes vary very much depending on the foundation, the dimensions, the personnel costs and the costs for construction equipment. The price for a Geotube in Vietnam (incl. customs and import tax) should be around 300 USD per running meter, plus construction costs, costs for the sand and personnel costs[1].

A comparable construction of a groin was realised in Malaysia. According to the Ministry of Natural Resources and Environment (2010), the costs amounted to approximately USD 53,000 per 100 m[2].

The costs for a construction of a Geotube breakwater on Shamrock Island, Texas in the year 1999 were quoted as 80,000 USD per 100 m (MOSELEY ET AL., 2000).

[1] Information of a German producer by telephone.

[2] http://www.water.gov.my/index.php?option=com_content&task=view&id=128&Itemid=279

These amounts show the possible range of costs. It is reasonable to use the sums of realised projects because the information of producers of geotextile systems contain several uncertainties. For example, the price for a running meter depends on the delivery quantity.

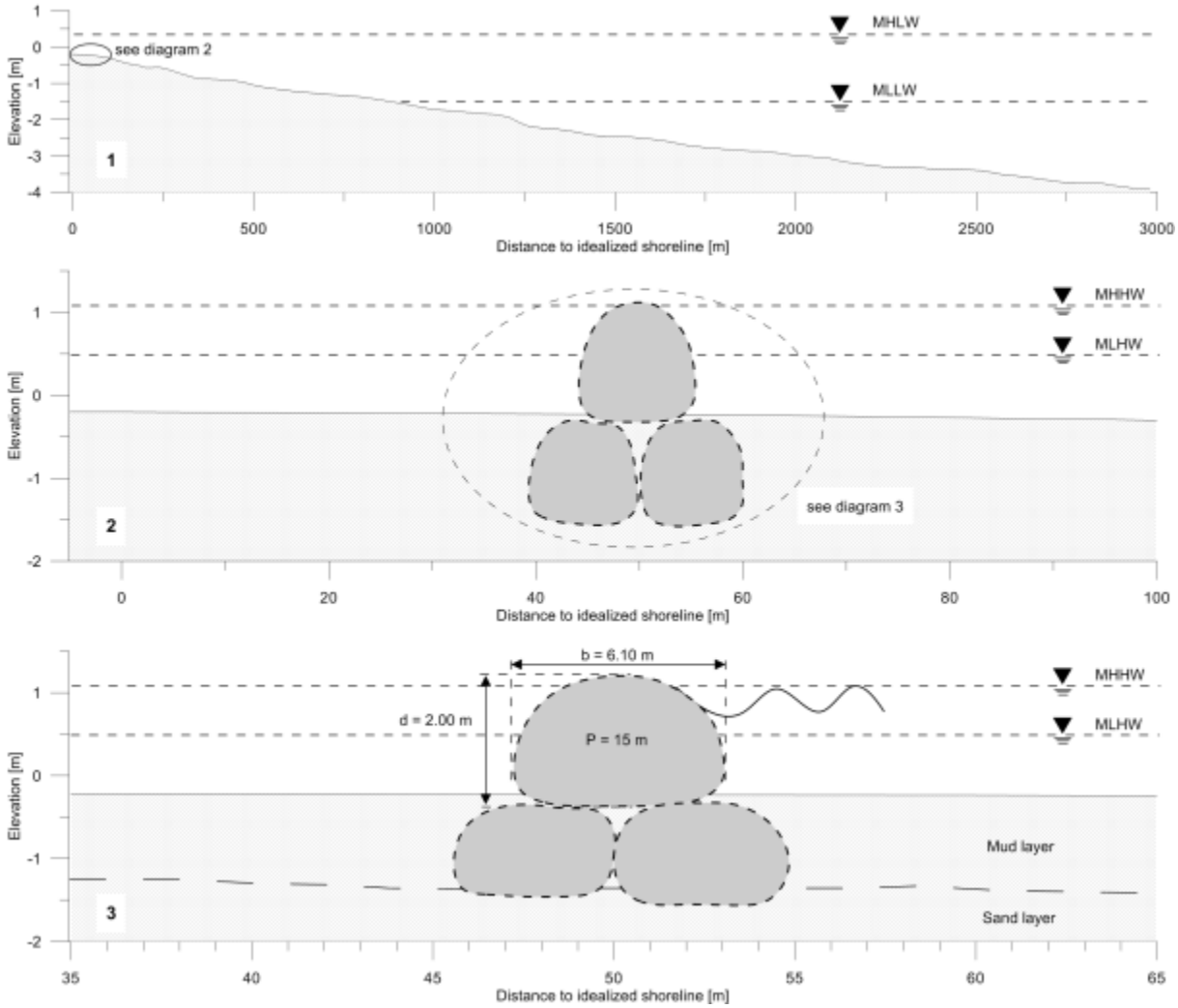

Figure 65: Arrangement of a breakwater constructed from Geotubes.

6.4 Submerged structures

Due to the demand of cost-effective, flexible and environmentally sound coastal protection measures, new systems are developed. Besides systems based on geotextiles, artificial reefs or other submerged structures are applied (PILARCZYK, 2008).

Reef Balls (Figure 66) are a relatively new and innovative coastal protection measure (PILARCZYK, 2003). They are temporally submerged structures that dissipate wave energy and provide a habitat for animals and plants. In some applications, they were used to replant mangroves in sheltered areas (Figure 67).

The installation of submerged structures like Reef Balls is very time-consuming and costly. Therefore, it is only applicable at small erosion sites. The success of such a measure depends on experience and cannot be predicted for the focus area. A further design is not done in this study.

Figure 66: *Reef Ball* (REEF BALL FOUNDATION, http://www.reefball.org/index.html).

Figure 67: Mangrove planting with *Reef Balls* (REEF BALL FOUNDATION, http://www.reefball.org/index.html).

6.5 Constructions using local materials

In addition to the application of conventional breakwaters (e.g. rubble mound breakwaters) and innovative methods (e.g. geotextile tubes), adapted approaches using local materials were investigated.

In many developing countries, people living near the coast use bamboo for housing, furniture, bridges and rafts. Bamboo has also found application in aquaculture ponds for construction and for caging mangrove seedlings in nursery areas. The extensive usage of bamboo in developing countries is mainly based on its strength and availability at all times at a minimum cost (HALIDE ET AL., 2004).

Breakwaters and groins respectively made of bamboo are considered to have good attributes as wave attenuators. Physical model tests were carried out in a flume to quantify the wave transmission coefficient of bamboo groins.

Figure 68 to Figure 72 show models of different bamboo breakwaters in the scale 1:20. In Figure 68, the model with the highest permeability is shown. 26% of the transverse section is obstructed. The lower parts of the bamboo piles are embedded in the soil. The barrier consists of two rows of piles. In the upper part two horizontal bars are connected to the vertical piles.

The model in Figure 69 consists of four rows of bamboo. All piles are connected with each other (Figure 70). 84% of the transverse section is obstructed.

Figure 68: Model of bamboo breakwater; lowest density.

Figure 69: Model of bamboo breakwater; highest density; front view.

Figure 71 and Figure 72 show a fence constructed by two rows of bamboo piles with filling material in between. This leads to 96% obstruction with less bamboo piles. The filling material, which can be any kind of brushwood, is wired to the vertical piles.

Figure 70: Model of bamboo breakwater; highest density; top view.

Figure 71: Model of bamboo fence breakwater; filling material between two bamboo rows; top view.

Figure 72: Model of bamboo fence breakwater; fill material between two bamboo rows; side view.

To assess the attributes of the bamboo breakwater, physical modelling was done in a wave flume. Figure 73 shows a sketch of the experimental setup. Regular waves were generated at the left end of the flume with a wave paddle, and wave parameters were measured in front of and behind the bamboo fence.

A transmission coefficient is the ratio between the transmitted wave height (H_T) and the initial wave height (H). The freeboard R_C is the distance from the top of the structure to the water surface. Negative freeboard indicates a submerged crest.

Figure 74 shows a photograph of the tests with the approaching wave from the left side. On the right side of the structure, the area of attenuated waves is visible. In this case, the bamboo breakwater with four rows of bamboo piles was tested.

Figure 75 shows a photograph of the tests with the structure consisting of two rows of bamboo sticks. In between these, parts of vegetation were packed. Although less bamboo is used, an attenuating effect is clearly visible; the layer between the two rows of bamboo especially has a wave damping effect.

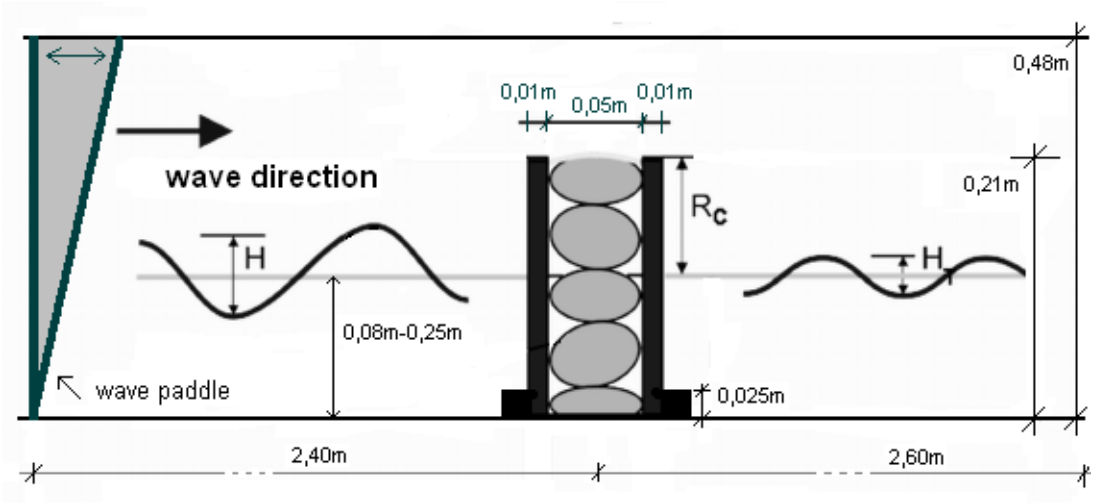

Figure 73: Experimental set-up in the wave flume.

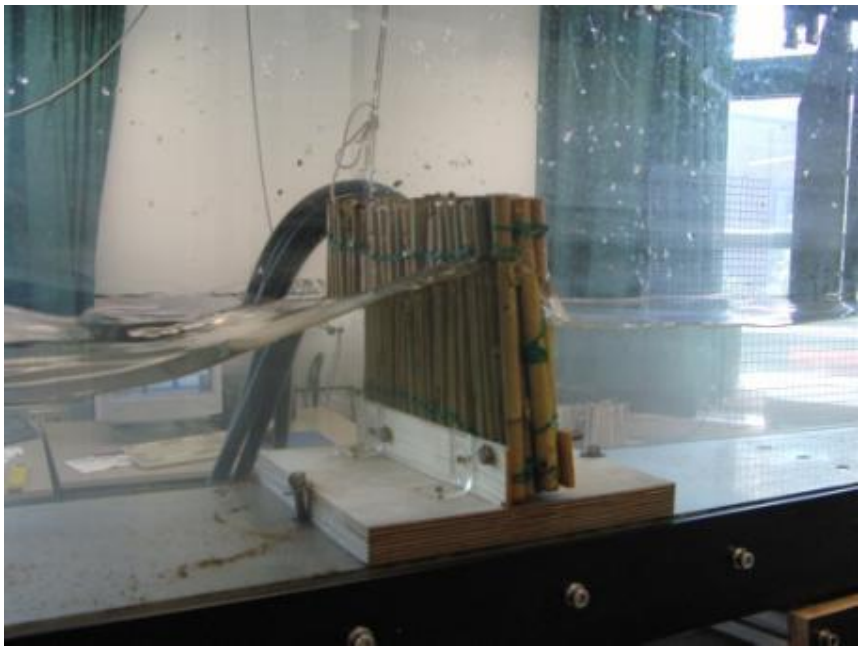

Figure 74: Physical modelling of wave transmission with the bamboo breakwater with highest density.

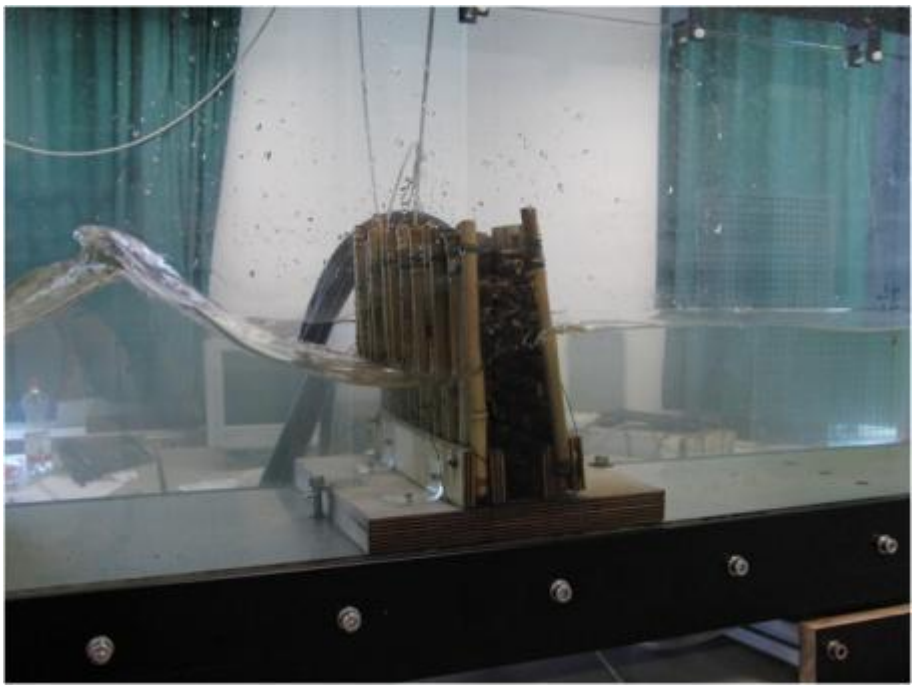

Figure 75: Physical modelling of wave transmission with the bamboo fence.

Figure 76 shows the results of the physical modelling. On the horizontal axis, the ration of the free-board and the initial wave height is plotted. On the vertical axis, the transmission coefficient is plotted. The black triangles indicate the results of the breakwater with four rows of bamboo; the red crosses indicate the results of the fence with two rows of bamboo and a filling; and the grey crosses show the results for the rubble mound breakwater. At a ratio R_C/H_S of approximately 1.6 (0.6 respectively for the breakwater with four rows of bamboo) the transmitted wave height is only 10% (15%) of the initial wave height. For higher submergences or larger wave heights, the transmission coefficient becomes 0.8 (1.0 respectively).

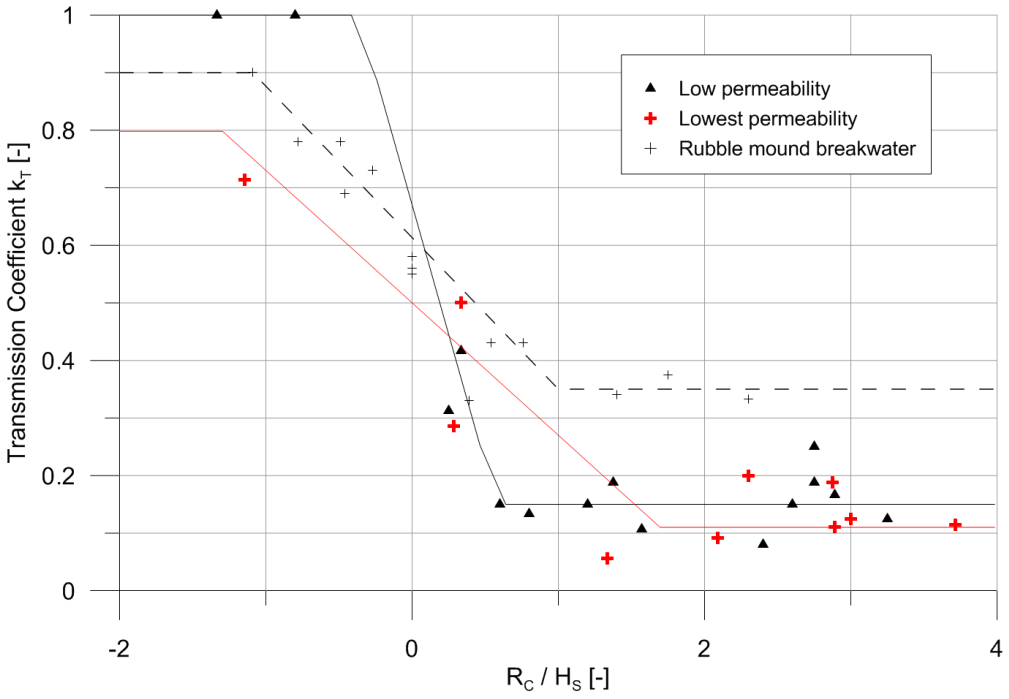

Figure 76: Results of the physical modelling.

Especially for normal water levels and normal wave heights, both bamboo breakwaters reduce the initial wave heights significantly.

The physical tests were also carried out for conventional rubble-mound breakwaters, which showed slightly lower wave attenuating effects.

The larger the diameter of the bamboo and the higher the density of the structure, the greater the wave attenuation is. This is to be expected since energy dissipates more with increased obstructions to the flow, and hence increased drag. The same effect can be achieved by using the construction of the fence. Results also show that, as expected, wave attenuation increased with the increasing width of a bamboo band.

The anchoring depth should be between half and two-thirds of the length of the pole. It is important that the pole is not only anchored in soft soil (mud). In Vinh Tan, the mud layer ended after 1m or less. HALIDE ET AL. (2004) investigated the breaking forces of embedded bamboo piles and carried out a series of physical tests. With a depth of embedment of 0.70 m and a location of the applied force of 0.50 m above the bed, a breaking force of an 8 cm bamboo pile of 30.50 N resulted. With an increasing depth of embedment, the breaking force increases. Based on the results and the assumption that the embedment depth is 1.50 m (0.80 m in mud, 0.70 m in sand), an extrapolation leads to a breaking force of 42.5 N.

The design of pile constructions is done based on the superposition method of Morison, O'Brian, Johnson and Schaaf (MOJS). The current forces and acceleration forces of the tidal current and the waves result in the following formula (EAK, 2002):

$$f_{total} = f_D + f_M = C_D \cdot \frac{1}{2} \cdot \rho_W \cdot D \cdot u \cdot |u| + C_M \cdot \rho_W \cdot \frac{\pi \cdot D^2}{4} \cdot \frac{du}{dt}$$

f_{total} = Sum of current force and acceleration force [kN/m]
f_D = Current force on the pile [kN/m]
f_M = Acceleration force on the pile [kN/m]
C_D =Current resistance coefficient [-]
C_M = Inertia resistant coefficient [-]
ρ_W =Density of water [t/m³]
D = Diameter of the pile [m]
u = Horizontal component of current/orbital velocity [m/s]
$\frac{du}{dt}$ = Horizontal component of current/orbital acceleration [m/s²]

The total load on the pile is determined by solving the integral of the calculated line forces. The different parts of the wave load are dephased. Different phases of the wave passage have to be considered.

Based on physical tests the coefficients C_D and C_M were determined by CERC (1984) for different Reynolds-Numbers:

$C_D = 0.75$
C_M =1.8

Tide:

$$f_{total} = 0.75 \cdot \frac{1}{2} \cdot 1.03 \cdot 0.08 \cdot 0.3^2 + 1.8 \cdot 1.03 \cdot \frac{\pi \cdot 0.08^2}{4} \cdot (1.04 \cdot 10^{-5})^2 = 0.0028\ [kN/m]$$

Waves:

1. Loading case: Maximum orbital velocity

$$f_{total} = 0.75 \cdot \frac{1}{2} \cdot 1.03 \cdot 0.08 \cdot 0.965^2 + 1.8 \cdot 1.03 \cdot \frac{\pi \cdot 0.08^2}{4} \cdot 0^2 = 0.029\ [kN/m]$$

2. Loading case: Maximum orbital acceleration

$$f_{total} = 0.75 \cdot \frac{1}{2} \cdot 1.03 \cdot 0.08 \cdot 0^2 + 1.8 \cdot 1.03 \cdot \frac{\pi \cdot 0.08^2}{4} \cdot 1.21^2 = 0.014\ [kN/m]$$

3. Loading case: Combination

$$f_{total} = 0.75 \cdot \frac{1}{2} \cdot 1.03 \cdot 0.08 \cdot 0.682^2 + 1.8 \cdot 1.03 \cdot \frac{\pi \cdot 0.08^2}{4} \cdot 0.857^2 = 0.021\ [kN/m]$$

The design load results from the tide and first loading case of the wave load, and adds up to 0.0318 kN/m. With a height above sea bottom of 1.30 m, the resulting force is 0.041 kN. The estimated breaking force of an 8 cm bamboo pile is 0.0425 kN. Due to this assessment the construction is stable. The connection of the bamboo piles increases the breaking force.

Figure 77 shows the construction of a breakwater made of bamboo.

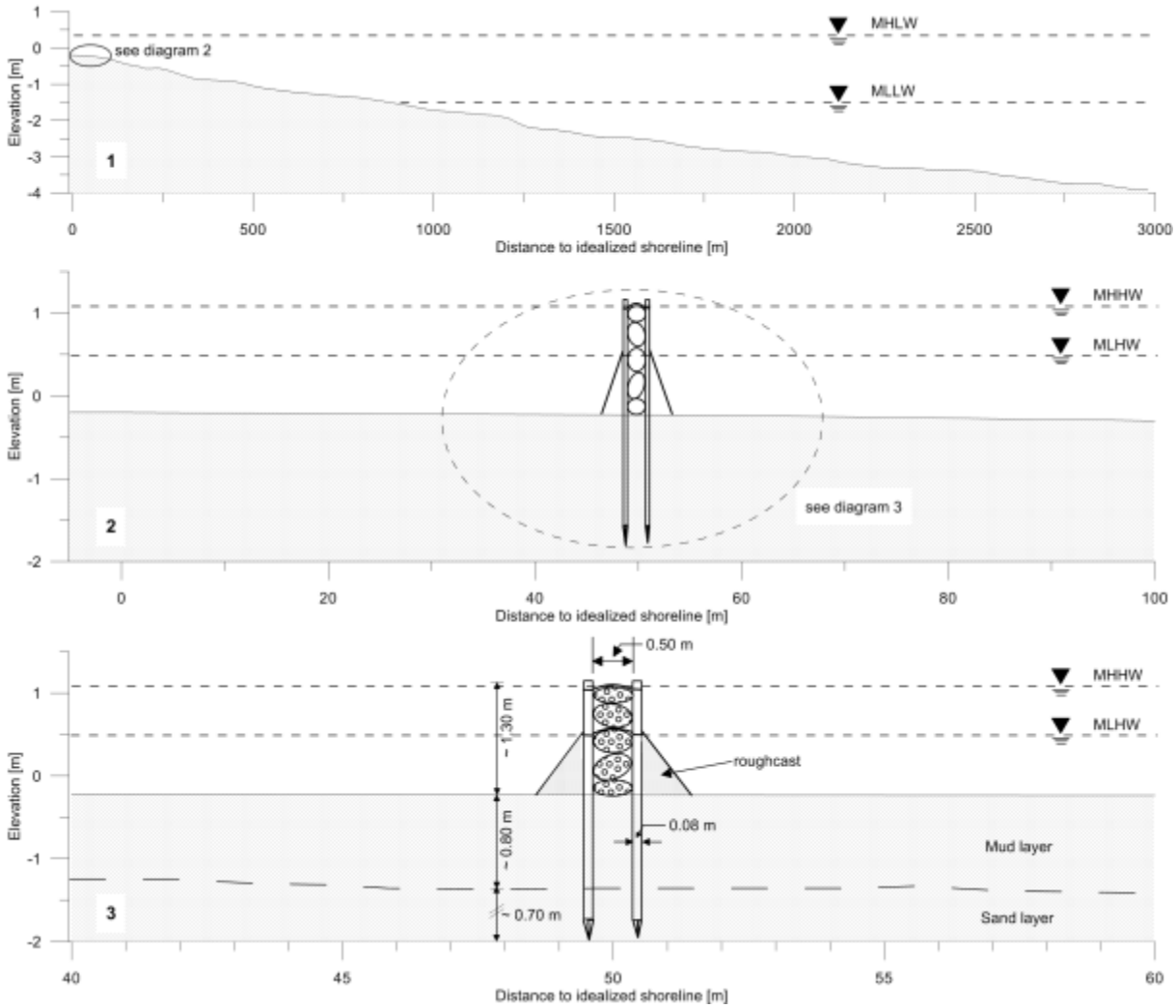

Figure 77: Arrangement of bamboo breakwater in the investigation area

An assessment of the costs is done based on appropriate literature. Resulting from the different percentages of bamboo in the different models, for the first model 1,811 piles are necessary per 100 m; 7,401 piles for model 2; and 4,596 piles for model 3. Assuming costs of USD 0.22 per meter bamboo and USD 0.30 per installation of a bamboo pile, the following costs are projected:

Type 1: 26% Bamboo	→ USD 5,903 per 100 m
Type 2: 84% Bamboo	→ USD 24,127 per 100 m
Type 3: 96% Bamboo & leafs	→ USD 14,984 per 100 m

The bamboo construction can be applied as a breakwater (detached, parallel to the coast, as indicated in Figure 60) or as a groin (transverse to the shoreline). Another option is to use the bamboo structures to develop land reclamation at the endangered positions at the dyke by means of a chequered arrangement of fences. It is the intention of this measure to close the gaps in the flood plains.

The physical modelling showed that the bamboo fences damp the waves significantly. During normal tidal conditions, the transmitted wave height is between 50% and 10% of the initial wave height. Due to the very high sediment concentration measurements near the dyke, the reduction of currents and wave heights will increase the sedimentation rate.

With the used numerical models and the available database, it is not possible to simulate the progress of the land reclamation under real boundary conditions. To assess the accretion rate. and therefore evaluate the success of the land reclamation, general numerical studies and simplified calculation approaches were applied.

In the frame of a numerical study, relevant parameters of the land reclamation fields were varied (number of fields, opening width, drainage). Figure 78 shows the sedimentation and erosion after one tide for two fields with the size of 200 m x 200 m and an opening width of 90 m. The suspended sediment concentration at the seaward boundary is 350 mg/l. All over the field accretion occurs, which is largest near the shoreline and the fences with values of around 100 g/m². These values decrease in areas of higher current velocities, e.g. at the ends of the longshore fences. Sedimentation is larger in the first field near the dyke. In all considered alternatives, the total volume of deposited material increased significantly with decreasing opening widths. The sedimentation rate increases with decreasing permeability of the construction. A sound drainage system increases sedimentation due to the prevention of rotating currents in the field.

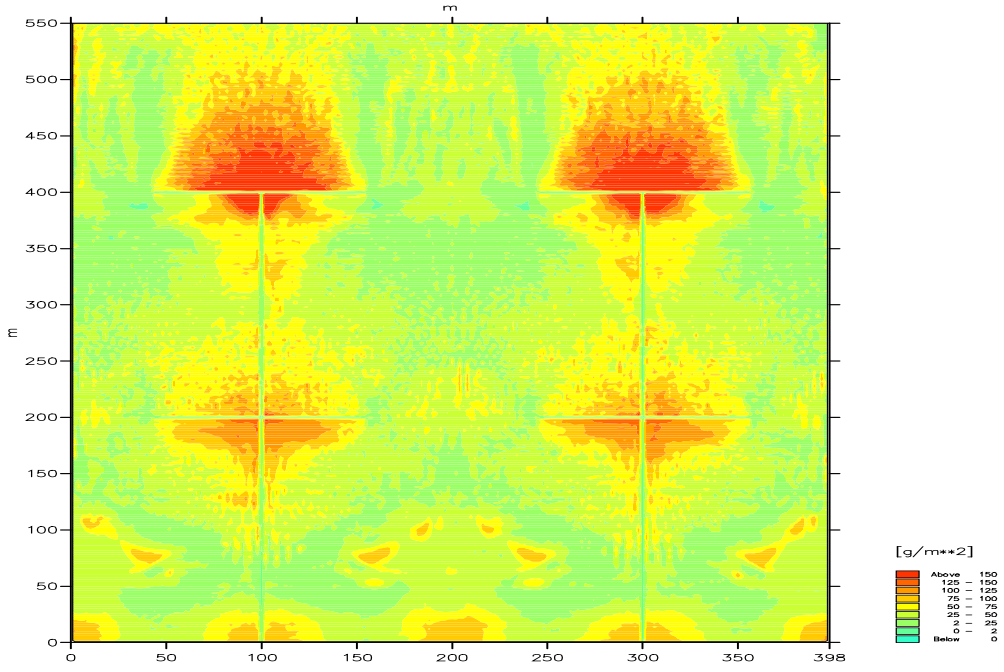

Figure 78: Sedimentation and erosion after one tide for two fields with the size of 200 m x 200 m and an opening width of 90 m.

In the numerical study, mean sedimentation rates between 0.044 and 0.067 kg/(m²·tide) occurred. A value of 0.050 kg/(m²·tide) leads to deposition of approximately 36 kg/(m²·year). Following the consolidation approach of MIGNIOT & BOULOC (1981) a suspension of 300 kg/m³ is necessary to establish plants. So, within one year approximately 0.12 m accretion occurs. This corresponds with on-site experiments at the Germany North Sea Coast (REIMERS ET AL., 1998), where the sedimentation year

within was between 0.15 and 0.20 m. The reclamation fields were smaller and increased the sedimentation rate.

At the coast of Vinh Tan the suspended sediment concentrations along the ADCP profiles were temporary up to 900 mg/l. Nearshore, at 300 m distance to the dyke, they were between 1000 mg/l and 5000 mg/l. These very high concentrations will lead to larger sedimentation rates, which also can be accelerated to the planting of mangroves.

Figure 79 shows an arrangement of bamboo fences at the endangered dyke at Vinh Tan. The first row of fields is constructed near the dyke. The distance between the dyke and the fences parallel to the dyke is approximately between 40 and 50 m and the width of a field is also between 40 and 50 m. The opening width of the fields should be around 10 m.

After sufficient siltation of the first row of fields, a second row may be installed to extend the floodplains. Mangroves should be replanted in the first row of fields to stabilise the soil. The installation and maintenance of a sufficient drainage system according to chapter 3.3.3 is essential. After consolidation of the soil and establishing mangroves, the fences lose their function. Therefore, rotting of the bamboo and the filling is not an issue. The developed floodplains protect the toe of the dyke. The first row of fields does not interrupt the longshore sediment transport. Therefore, downdrift erosion does not occur. If a second row of fields is installed, the measures have to be extended along the shoreline.

Figure 80 shows a lateral view of the bamboo fences. The height is reduced compared to the breakwaters. The goal is siltation up to the top edge of the revetment.

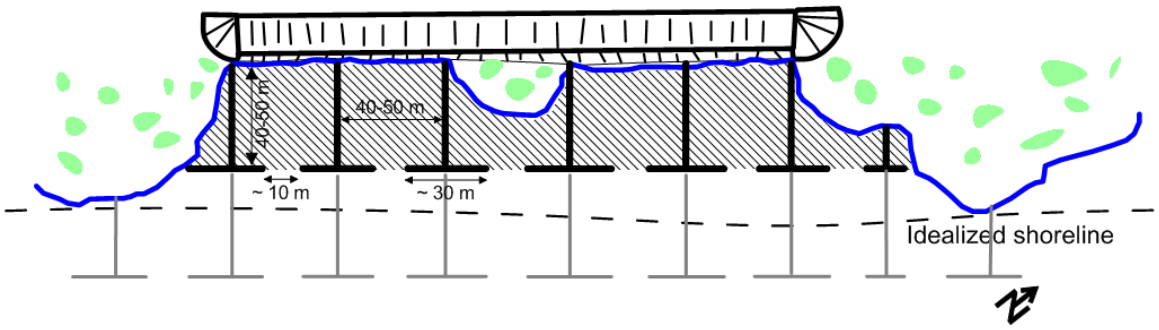

Figure 79: Possible installation of bamboo fences at the endangered dyke at Vinh Tan.

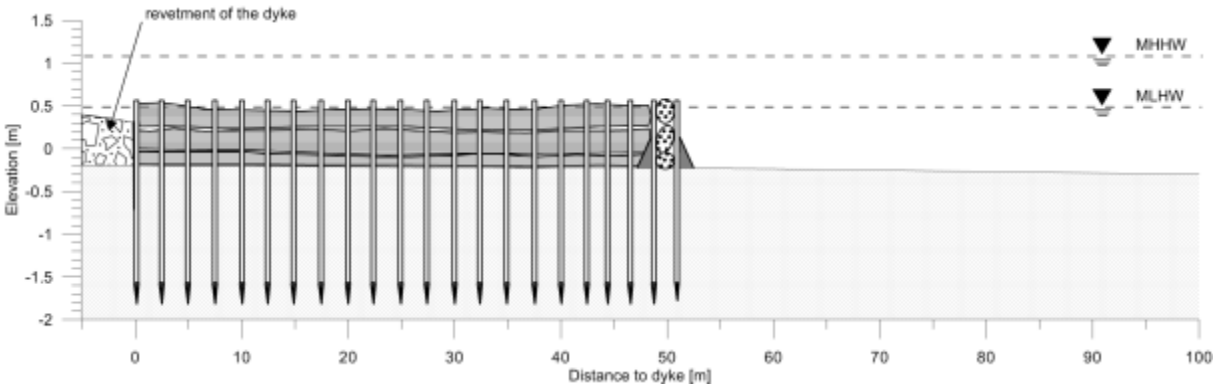

Figure 80: Lateral view of the bamboo fences (scheme); viewing direction: northeast.

7 Conclusions and recommendations

All coastal protection or erosion protection measures – except from beach nourishment – cause downdrift erosion. Hard coastal protection measures should only be applied if human lives or larger monetary values are endangered. In general, additional nourishment is necessary to reduce the negative effects of the installed structures. Coastal erosion protection has to be designed carefully to secure the desired effects and minimise downdrift erosion. A close to nature solution is worthwhile.

Morphodynamic modelling contains uncertainties due to the empirical character of the implemented sediment transport formulas. Medium and especially long-term simulations have to be evaluated carefully. Available data and monitoring programs advance both the knowledge about morphodynamic processes and the quality of numerical models.

Along the southeast coast of Vietnam, natural erosion and accretion alternate at different sections. Around the endangered dyke at Vinh Tan natural erosion occurs, which will proceed with time if no countermeasures are installed. Periods with increased wave activity will increase the erosion rate.

The construction of one massive and impermeable breakwater in a distance of 200 m to the coast will create a salient at the endangered section, and therefore protect that area. Severe downdrift erosion will occur, however. Furthermore, the construction costs of such a breakwater will be very high due to the difficult accessibility of the site, larger water depth and the massive structure. Therefore, this option is not a recommendable solution.

If the length of that breakwater is reduced and the permeability is increased, the downdrift erosion can be minimised. But at the same time the accretion in the focus area is reduced. Higher wave activity may even create erosion in the protected area. The desired function of this option is not secured.

A breakwater with the length of 100 m at a distance of 50 m to the shoreline will create a complete tombolo. Downdrift erosion is between 20 and 40 m depending on the wave activity. Varying the permeability can minimise the downdrift erosion. Permeability changes the transmission coefficient. A transmission coefficient of 0.30 leads to a complete tombolo and downdrift erosion of 15 to 20 m. The formation of a tombolo is not completed with a transmission coefficient of 0.50. Downdrift erosion is around 15 m then. A transmission coefficient of 0.80 is too low. The downdrift erosion is minimised, but the positive effect on the endangered area is not secured.

A construction of two breakwaters with a length of 50 m each leads to the development of one salient and one tombolo. Downdrift erosion is around 20 m. Increased wave activity or a decreased transmission coefficient may lead to erosion of the initial shoreline between the breakwaters.

At the endangered dyke in the focus area, a section of approximately 200 m has to be protected. The model runs showed a reasonable solution consisting of two breakwaters with a length of 100 m each and a gap of 25 m between them. This construction will protect the dyke. However, this measure is an intervention into the natural sediment transport system. Therefore, downdrift erosion between 25 and 30 m will occur. Protection of the existing flood plains, e.g. with mangrove plantings, will help to reduce downdrift erosion.

The construction of breakwaters will always lead to downdrift erosion. This effect has to be minimised, while at the same time the positive effect on the shoreline has to be adequate. Therefore, the recommended solution for endangered sections with lengths less than 100 m is one breakwater with a maximum length of 100 m at a distance of 50 m to the shoreline. The transmission coefficient should be around 0.50. If the section that has to be protected is larger, it is not possible to avoid downdrift erosion.

The transmission coefficient is important for the success of the erosion protection measure. Of course, the transmission coefficient varies with varying water levels and wave heights. In general, however, a higher permeability increases the transmission coefficient.

The construction of a multi-layer rubble mound breakwater, which is feasible for the focus area, leads to transmission coefficients around zero. The structure is impermeable and wave transmission only

occurs due to wave-overtopping in the case of high water levels and high waves. Therefore, the construction of an emerged rubble mound breakwater is not recommended. Furthermore, a conventional breakwater is a massive construction. Due to the soft soil the foundation of that structure is complex and increases the already high costs. Failure of the foundation during storm events is possible.

A further option is the installation of groins. The positive effect of this measure on the shoreline is negligible, and therefore the construction not recommendable.

Geotubes are also a massive structure and cause the same problems with the foundation as conventional breakwaters. This leads to high costs and a difficult construction. The design of Geotubes is based on experiences. The long-life cycle is not proved. Furthermore, Geotubes lead to transmission coefficients around zero, including the problems mentioned above.

The correct design of a submerged structure in an environment of oscillating water levels is very complex. Due to changing transmission coefficients, the simulation of effects on the morphology contains large uncertainties.

The installation of submerged structures like Reef Balls is only applicable and economically reasonable at small erosion sites. The success of such a measure depends on experiences and cannot be predicted for the focus area.

The application of local materials, like bamboo, has many advantages based on its strength, availability and costs. With a breakwater made of bamboo, the desired wave transmission can be achieved. Therefore, the construction of the bamboo breakwater is recommended. Furthermore, the costs of this solution are low, compared to the other options.

The design of the bamboo breakwater is done based on available design approaches. The breaking force is estimated based on appropriate literature. Beyond that and before the construction, the breaking force of bamboo piles with different diameters and embedment depths should be determined experimentally. A sound installation of the piles into the ground is essential.

If the gaps between the eroded floodplains at the endangered dyke are closed, the wave energy dissipates on the newly developed floodplain and the dyke is protected from erosion. Closing the gaps will create a close to natural situation, with no resulting downdrift erosion. Therefore, the chequered arrangement of bamboo fences at the dyke is recommended. Due to the strong reduction of wave energy and currents, and the high sediment concentration, siltation of the fields will occur fast. Replanting of mangroves should be done as soon as possible to protect the floodplain from erosion in case of storm events. A second row of fields should be constructed to protect the first fields. Also, existing but eroding flood plains can be protected by this kind of land reclamation. When mangroves, and therefore a natural erosion protection, are re-established, the bamboo fences lose their function. Therefore, a life cycle of the bamboo fences of two years is sufficient.

If possible, both measures – a bamboo breakwater parallel to the coast and chequered bamboo fences – should be used at the two hot spots. Figure 81 shows the suggested arrangement.

A comprehensive monitoring programme will lead to detailed information about the effectiveness of both measures and will enable an evaluation in terms of costs and benefits.

The total length of the bamboo fences shown in figure 81 add up to approximately 400 m. The length of the bamboo breakwater is 100 m. According to the calculation above the cost for both measures is approximately 75,000 USD.

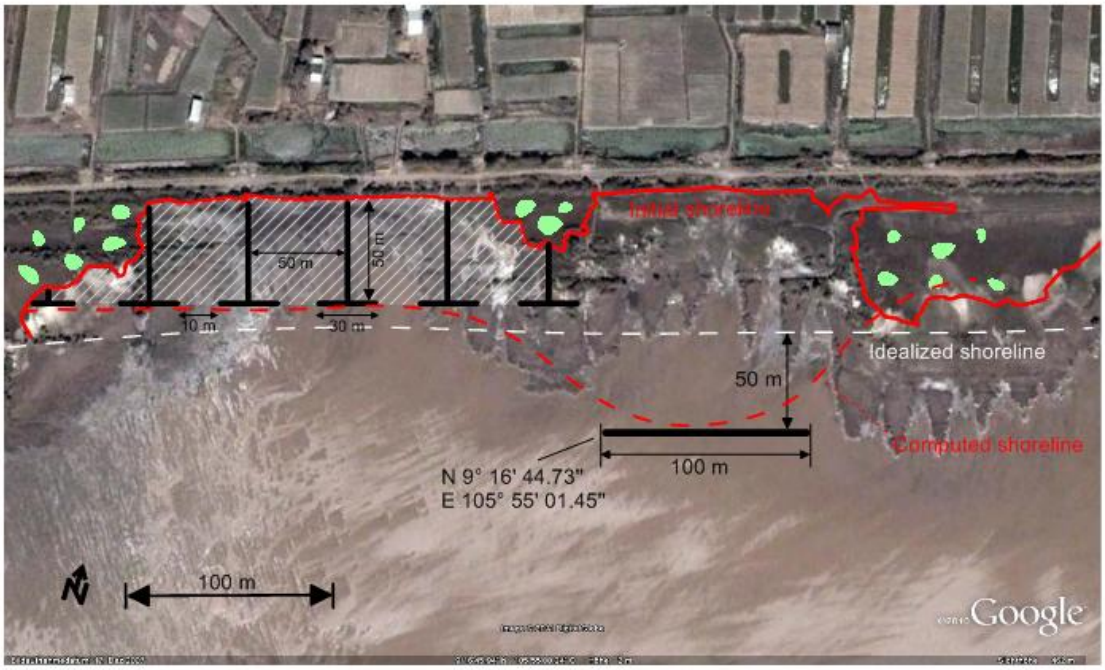

Figure 81: Recommended combination of bamboo breakwater and bamboo fences.

8 Summary and outlook

Along the coastline of Soc Trang Province, Vietnam, dynamic processes of accretion and erosion occur, as influenced by interaction between:

- The discharge regime of the Mekong Delta;
- The tidal regime of the South China Sea; and
- The monsoon weather patterns of Southeast Asia.

Coastal erosion and accretion are complex processes, depending on various influences. Key elements are the sediment transport under the influence of currents and waves, the overall dynamics of beaches in a coastal section and anthropogenic impacts.

Due to its vectorial character the sediment transport at the coast may be divided into:

- Cross-shore sediment transport (on-/offshore transport)
- Longshore sediment transport.

Coastal cross-shore sediment transport induces short-term morphologic changes of sediments, e.g. during storm events. Coastal longshore transport causes long-term morphologic changes of a coastal section.

In some areas, such as the focus area of Vinh Tan Commune, severe erosion endangers the dyke and consequently the people and farmland located behind the dyke. Based on available data, field measurements and numerical modelling, a sustainable erosion protection was designed.

Available data with relevance for the coast of Soc Trang were researched and analysed. Although data on the bathymetry, water levels, river discharges and sediment freights were available, essential data about the erosion site, especially about the wave climate, were missing. Therefore, a concept was developed to close this gap and build the foundation for sophisticated and effective erosion protection measures. Additional field measurements were carried out

- To verify the results of the numerical modelling; and
- To understand the hydrodynamic and morphodynamic processes in the focus area.

Within three measurement campaigns information about currents, waves, sediment concentrations and the bathymetry were recorded. The field measurements covered different seasons including the northeast and southwest monsoons.

The wave measurements showed a clear dependency on the monsoon season. Recorded currents show a long-shore component due to the approach of the tidal wave along the South Vietnamese coast. Those currents are increased by the northeast monsoon.

At the end of the rainy season in October 2009, a mild wave climate was recorded in the focus area. Tidal currents affect the course of the suspended sediment concentration, while current velocities and wave heights influence the peaks of SSC. During flood tide, long-shore currents occurred at the same time as the peaks of the suspended sediment concentration. This indicates long-shore sediment transport, which reaches its largest values at the end of the rainy season due to high sediment freights in the Mekong branches. In January 2010, during the main period of the northeast monsoon, higher waves were recorded in the investigation area. The waves approached the coast of Soc Trang and Bac Lieu with a strong long-shore component. In winter, while the sediment plume of the Mekong is less pronounced and less material is available, the northeast monsoon winds cause increased erosion.

Field measurements cannot cover all possible weather conditions. In order to obtain the missing information, available and generated data were used to setup, calibrate and verify different numerical models. Shoreline changes were computed considering various erosion protection measures. Besides conventional techniques, an alternative approach using local materials was investigated.

The numerical modelling was done in three steps. In a larger investigation area, a wave model was set up. The results were used as design parameters for the erosion protection measures at the coast and they were handed over to the hydrodynamic model, which was also covering the larger investigation area. This hydrodynamic model simulated currents and wave-induced currents, which were handed over to the morphodynamic model simulating the shoreline changes. This third model covered the coast around the focus area at Vinh Tan. It simulated shoreline changes due to the present current and wave regime. Various structural measures were integrated in that model and the resulting effects were simulated. The sufficiency of the measures, the positions and the best characteristic values were identified.

The aim of the structural measures is to reduce erosion and to increase accretion. Negative effects as downdrift erosion must be avoided as far as possible.

The results of both the field measurements and the numerical modelling were used to define important boundary conditions for the design of countermeasures:

- Soft soil with silty and clayey material
- Significant wave heights of 0.65 m
- Wave periods between 5 s and 6 s
- Tidal range of 3.50 m
- Water depths up to 2 m at high water.

In Chapter 6, the design of different application examples was carried out. In addition to the application of conventional breakwaters and innovative methods (e.g. geotextile tubes), adapted approaches using local materials were investigated. Therefore, physical tests in a wave flume were carried out.

Finally, recommendations for erosion protection measures are given based on the model results, the field measurements and a cost analysis.

The construction of breakwaters always leads to downdrift erosion. This effect is minimised if one breakwater is installed with a length of 100 m at a distance of 50 m to the shoreline. The transmission coefficient should be around 0.50. With a breakwater made of bamboo, the desired wave transmission can be achieved. The application of local materials like bamboo has many advantages based on its strength, availability and costs. Therefore, the construction of the bamboo fence is recommended. Furthermore, the costs of this solution are low, compared to the other options.

If the gaps between the eroded floodplains at the endangered dyke are closed, the wave energy dissipates on the newly developed floodplain and the dyke is protected from erosion. Closing the gaps will create a close to natural situation, with no resulting downdrift erosion. Therefore, the chequered arrangement of bamboo fences at the dyke is recommended.

If possible, both measures – a bamboo breakwater parallel to the coast and chequered bamboo fences – should be used at the two hot spots in Vinh Tan.

If the local authorities follow this recommendation, a detailed documentation and monitoring of the construction and the morphological development in the focus area are essential to gain information for future coastal protection measures at the southeast coast of Vietnam.

Before the construction, a practical plan has to be provided. The construction phase contains several measures of quality control, e.g. experimental identification of the breaking force of the bamboo and verification of sound installation of the bamboo poles.

For the chosen alternative, detailed plans must be created, which contain all accurate positions, dimensions and construction details in the form of cross sections and top views. The product specifications must be provided. Mass and cost calculations included in the submitted quotations must be verified based on local prices. During the construction supervision tensile tests of the bamboo piles must be carried out to quantify the breaking forces of single piles and pile groups. The depth of

embedment of the piles must be controlled. Based on the gained knowledge, the design can be optimised for future constructions.

In the frame of a monitoring program the development of the shoreline, floodplains and tidal flats between the dyke and the measures must be recorded. Due to the shallow water depths there, soundings by boat are not sufficient. The bottom elevation should be measured manually with a Differential GPS in a 10 m grid. Initially, monthly measurements should be carried out. After six months this interval should be reduced to quarterly measurements. The change of the grain size distribution and the consolidation grade in the surroundings of the measure should be analysed through quarterly sediment sampling in a 25 m grid. Measurements of suspended sediment concentrations, waves and currents should be carried out within campaigns covering different seasons, starting immediately after the construction and continued semi-annually. Georeferenced photos should be taken in the focus area monthly. The camera position on the dyke, and the height, angle and direction of every photo must be the same to observe the development of the floodplains. Aerial views or better ortho photos in an annual cycle are helpful to follow and quantify the morphologic development. Based on the monitoring, the adequate time for planting mangroves on the tidal flats can be identified.

All recorded data will be analysed to provide a detailed control of success of the measures.

References

ALBERS, T., VON LIEBERMAN, N., FALKE, E. (2009): Morphodynamic Processes on Tidal Flats in Estuaries. In: Journal of Coastal Research, Special Issue 56, ISSN 0749-0208, pp. 1325-1329.

AKIRA, Y. (2005): Zoning for risk assessment of water-related natural disasters in the Mekong-Delta. Can Tho University.

CERC (1984): Shore Protection Manual, Vol. I + II, Coastal Engineering Centre, Vicksburg, USA

CHONG, J. (2005): Protective values of mangroves and coral ecosystem: A review of methods and evidence. IUCN. G.V.

DAT, N.T., SON, N.M. (1998): Waves in the Marine Coastal Zone of the Mekong River System. In: Proceedings of the International Workshop on the Mekong Delta, pp. 72 - 81. Chiang Rai, Thailand.

DONNELL, B.P., LETTER, J.V., MCANALLY, W.H. (2006): Users Guide for RMA2 Version 4.5, U.S. Army Corps of Engineers, Engineer Research and Development Center, Waterways Experiment Station, Valhalla, USA.

EAK (1993): Empfehlungen des Ausschusses für Küstenschutzwerke – Empfehlungen für Küstenschutzwerke. In: Kuratorium für Forschung im Küsteningenieurwesen (Hrsg.): Die Küste, Heft 55. Heide in Holstein: Boyens, Germany.

EAK (2002): Empfehlungen des Ausschusses für Küstenschutzwerke – Empfehlungen für Küstenschutzwerke. In: Kuratorium für Forschung im Küsteningenieurwesen (Hrsg.): Die Küste, Heft 65. Heide in Holstein: Boyens, Germany.

FALKE, E., VON LIEBERMAN, N. (2010): Numerical Modeling of a Wadden Sea Area – Hydrodynamics and Morphodynamics. In: Congress Proceedings of the First European IAHR Congress (CD-ROM), Edinburgh, UK.

FRÖHLE, P., ZEMLYS, P., DAVULIENE, L., GULBINSKAS, S.(2008): Numerical Simulation of Sediment Transport as one Basis for the Assessment of Coastal Protection Measures in Palanga, Lithuania. In: Galappatti, R., van Schel, L., Al Maidoor, E., Al Zahed, K., Wens, F., Scheffer, H., Brühl, H. and Mocke, G. (eds.): Best Practices in the Coastal Environment - Proceedings of the 7th International Conference on Coastal and Port Engineering in Developing Countries (PIANC-COPEDEC VII), on CD-ROM, PIANC, Dubai, UAE, Paper No 164.

HALIDE, H., BRINKMANN, R., RIDD, P.(2004): Designing bamboo wave attenuators for mangrove plantations. In: Indian Journal of Marine Science, Vol. 33(3), pp. 220-225.

HANSON, H., KRAUS, N.C. (1989): "GENESIS: Generalized model for simulating shoreline change, Report 1: Technical Reference." Tech. Rep. CERC-89-19, U.S. Army Engineer Waterways Experiment Station, Coastal Engineering Research Center, Vicksburg, MS.

HEIN, H., 2007: Vietnam Upwelling - Analysis of the Upwelling and Related Processes in the Coastal Area off South Vietnam. Hamburg: Universität Hamburg, Germany.

HERBICH, J.B. (1999): Handbook of Coastal Engineering. McGRAW-HILL, USA.

HU, J., KAWAMURA, H., HONG, H., QI, Y. (2000): A Review on the Currents in the South China Sea: Seasonal Circulation, South China Sea Warm Current and Kuroshio Intrusion. In: Journal of Oceanography, Vol. 56, pp. 607–624.

KING, I. (2006): A finite element model for stratified flow and cohesive sediment/sand transport – RMA 10S Users Guide. Version 3.5E.

KRAMER, J. (1989): Kein Deich, kein Land, kein Leben – Geschichte des Küstenschutzes an der Nordsee. Leer, Verlag Gerhard Rautenberg.

LIEBERMAN, N. VON, SCHWARZE, H., ZIMMERMANN, C. (1998): Aufgabe und Wirkungsweise von Lahnungen. Die Küste, H. 60, Boyens, Heide in Holstein, Germany.

MIGNIOT, C., BOULOC (1981): Étude des propriétés physique de différents sédiments très fins et de leur comportement sous des actions hydrodynamiques.

MOSELEY, J.C., SHINER, J.A., CALNAN, T. (2000): Habitat Enhancement and Protection Shamrock Island, Corpus Christi Bay, Texas. In: Tait , L.S. (Ed.): Proceedings of the 13th Annual National Conference on Beach Preservation Technology, Florida Shore & Beach Presentation Association.

NIELSEN, C., APELT, C., (2003): Parameters Affecting the Performance of Wetting and Drying in a Two-Dimensional Finite Element Long Wave Hydrodynamic Model. In: Journal of Hydraulic Engineering, ASCE, Volume 128-8, 628 – 636.

NGUYEN, T.T. (2009): Surface sediment characteristics and sediment transport from Bassac River mouths to Ca Mau Peninsula (Mekong Delta), Institute of Geosciences, University of Kiel, Germany.

NRC (1990): Managing coastal erosion. Committee on Coastal Erosion Zone Management, Water Science and Technology Board, Marine Board, Commission on Engineering and Technical System, National Research Council. Washington, DC, National Academy Press. 182 pp.

PARKER, R.P. (1986): On the observation of cohesive sediment behaviour for engineering purposes. In: A.J. Mehta (Editor): *Estuarine cohesive sediment dynamics*, Springer-Verlag, New York (1986), pp. 270–289.

PILARCZYK, K.W. (2003): Alternative Systems for Coastal Protection – An Overview. In: Han, Z. (ed.): Proceedings of the International Conference on Estuaries and Coasts, Zhejiang Institute of Hydraulics and Estuary, Hangzhou, China, pp. 409-419.

PILARCZYK, K. (1999): Geosynthetics and geosystems in hydraulic and coastal engineering. Taylor & Francis, USA.

PRATESYA, G. (2007): Protection from Coastal Erosion. In: *Proceedings of the Regional Technical Workshop* (S. 103 - 131). Khao Lak, Thailand: FAO.

PROBST, B. (1996): Deichvorlandbewirtschaftung im Wandel der Zeit. In. Die Küste, Heft 58, Boyens, Heide in Holstein.

REIMERS, H.-C., RICKLEFS, K., THOMAS, B., GRENZER, E. (1998): Optimierung von Küstensicherungsarbeiten im Küstenvorfeld der Nordseeküste. Projektbericht Bundesministerium für Bildung, Forschung und Wissenschaft.

RIJN, L.C. VAN (1993): Principles of Sediment Transport in Rivers, Estuaries and Coastal Seas. Aqua Publications, The Netherlands.

SCHRAGE, N., ANTANASKOVIC, D., JUNG, T., PASCHE, E. (2009): KALYPSO – An open source software tool for flood studies in rivers. 8. International Conference on Hydroinformatics, Concepción (Chile).

SORENSEN, R. M. (2001): Basic Coastal Engineering. Kluwer Academic Publishers.

SOUTHERN SUB INSTITUTE OF FOREST INVENTORY AND PLANNING (2009): Mangroves of Soc Trang 1965 - 2008. Vietnam: GTZ Project Management of Natural Resources in the Coastal Zone of Soc Trang Province.

STADELMANN, R. (1981): Meer - Deiche - Land. Küstenschutz und Landgewinnung an der deutschen Nordseeküste. Karl Wachholtz Verlag, Neumünster, Germany.

U.S. ARMY CORPS OF ENGINEERS (2002): Coastal Engineering Manual (CEM), Engineer Manual 1110-2-1100, U.S. Army Corps of Engineers, Washington, D.C. (6 volumes).

XU, X., QIU, Z., CHEN, H. (1982): The General Description of the Horizontal Circulation in the South China Sea. In: Proceedings of the 1980 Symposium on Hydrometeorology of the Chinese Society of Oceanography and Limnology, pp. 137 - 145. Beijing.

Annex

Failure of the outer slope of the endangered dyke at Vinh Tan in October 2010; Photo GIZ

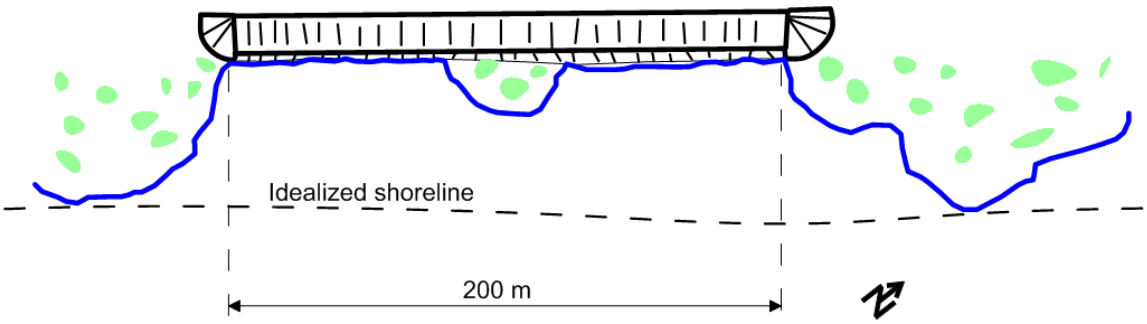

Sketch of the idealised shoreline in the focus area at Vinh Tan

Deutsche Gesellschaft für
Internationale Zusammenarbeit (GIZ) GmbH
Management of Natural Resources in the Coastal Zone
of Soc Trang Province
134 Tran Hung Dao Street,
Soc Trang City, Viet nam

T + 84 79 3622164
F + 84 79 3622125
I www.giz.de
I www.czm-soctrang.org.vn